TREE RINGS AND CLIMATE IN THE GREAT LAKES REGION—PAST, PRESENT, AND FUTURE

By

Scott Matthew Warner

A DISSERTATION

Submitted to
Michigan State University
in partial fulfillment of the requirements
for the degree of

Plant Biology – Doctor of Philosophy
Ecology, Evolution, and Behavior Program – Dual Major

2021

ABSTRACT

TREE RINGS AND CLIMATE IN THE GREAT LAKES REGION—PAST, PRESENT, AND FUTURE

By

Scott Matthew Warner

As climate change unfolds it is necessary to gain a better understanding of how tree growth is affected by contemporary climate. This can provide information about both prerecorded climate and future growth responses to climate change. Yet, tree growth and its relationship with climate remains understudied in one section of the northeastern United States, the Great Lakes Region. Here, I use dendrochronology to (1) reconstruct 500 years of moisture conditions on South Manitou Island, Lake Michigan, (2) compare growth and growth-climate relationships within/among nine species along a latitudinal gradient from southern Indiana to Upper Michigan, and (3) forecast future growth under climate change. I find that (1) while drought was a regular occurrence since the mid-1500s, the most severe droughts and the most variable conditions overall occurred in the 20th century, (2) the predominant climatic factors associated with growth in the region are summer temperature (negative relationships) and summer precipitation (positive relationships), and that the influence of these factors was strongest in the south, and (3) future growth was projected to decline over the rest of this century as climate change proceeds, independent of latitude.

For Nola, beside me throughout

ACKNOWLEDGMENTS

I thank Frank Telewski, for his advice, support, and patience, and for being an excellent major advisor in general. Andrew M. Jarosz went far beyond the role of a typical guidance committee member providing ample amounts of support, feedback, and ideas. In particular, I thank Dr. Jarosz for helping to conceive the study that comprises Chapter 3. I am also grateful to my other committee members, Jeffrey Andresen and Steve Chhin for their guidance. Specifically, thanks to Dr. Andresen for his advice on modeling and selecting climate projections. Thanks to Dr. Chhin for advice on statistics and dendrochronological methods. Alan Arbogast, Justin Maxwell, and William Lovis also provided substantial advice. Many other persons also provided advice, too many to list.

Many persons provided help in the lab and field, particularly Opal Jain. Thanks also to Alan Arbogast, Jill Grimes, Andrew Jarosz, William Lovis, Jaime Salisbury, Andrew Warner, and Nola Warner for help in the field. Thanks to Hazel Anderson, Gillian Chirillo, Matthew Hadden, and Samantha Jeffries for help in the lab. For help in the field and lab, thanks to Ross Chinavare, Garrett Mullanix, Hunter Salisbury, and Frank Telewski.

Thank you to the landowners/stewards who generously allowed me to sample on their land: The Huron Mountain Club, the Indiana Audubon Society, the Jacobson Family (Tustin, MI), Kalamazoo Nature Center, the Michigan Audubon Society, the Michigan Department of Natural Resources, the National Parks Service (NPS Permit No. 85839), the Peterson Family (Stonington Peninsula, MI), Saginaw County Parks, the United States Forest Service, and the University of Michigan Biological Station.

Several funding agencies provided support. Thank you to the Plant Science Fellowship (Michigan State University [MSU]), the Alfred H. and Jean Goldner Endowment, W.J. Beal Botanical Garden (MSU), the Huron Mountain Wildlife Foundation, the James E. Rodman Endowment, the UAW Cal Rapson Endowment, donors to the William A. Lovis Endowment for Environmental Archaeology, the Department of Geography, Environment and Spatial Sciences (MSU), the Department of Plant Biology (MSU), the Ecology, Evolution, and Behavior Program (MSU), the Paul A. Taylor Endowment, and the Dissertation Completion Fellowship (MSU). For funded internships, thank you to the MSU Herbarium (MSC) and the Natural Science Collections Internship (MSU).

To Justin Maxwell, I am grateful for providing data for *A. saccharum*, *C. ovata*, *L. tulipifera*, *Q. alba*, and *Q. rubra* at Pioneer Mothers Memorial Forest. To Alex Dye, I am grateful for providing data for *T. canadensis* at Huron Mountain Club. Thank you to Edward Cook for providing an unpublished *T. occidentalis* chronology from South Manitou Island.

For hospitality, thank you to the rangers of South Manitou Island, Carl Wilms of Mary Gray Bird Sanctuary, the Kalamazoo Nature Center, and the Huron Mountain Wildlife Foundation.

Thank you to Inter-Research for permitting me to reprint with slight formatting modifications a paper from *Climate Research* which comprises chapter 2 of this document: S.M. Warner, S.J. Jeffries, W.A. Lovis, A.F. Arbogast, & F.W. Telewski. 2021. Tree ring-reconstructed late summer moisture conditions, 1546 to present, northern Lake Michigan, USA. *Climate Research*. 83:43–56. https://doi.org/10.3354/cr01637.

Thank you to those who most inspired me in my undergraduate program, Todd Barkman and Steve Keto. To Ralph Reitz, thanks for being the first person to teach me about botany.

I am thankful to my immediate, original, and in-law family members, particularly my wife, parents, and children for their support.

TABLE OF CONTENTS

LIST OF TABLES

LIST OF FIGURES

CHAPTER ONE

INTRODUCTION

Prehistoric, Historic, and Future Climate Change

Although climate is ever-changing, it has changed at an unprecedented rate for more than a century. Global mean surface temperature increased by 0.85 °C from 1880–2012 (Hartmann et al. 2013). Further, in the mid-latitudes of the northern-hemisphere (NH) increases in precipitation, near-surface specific humidity, and heavy precipitation events were observed (Hartmann et al. 2013). By 2035, mean surface air temperature is projected to increase by 0.3–0.7 °C under any of the four Representative Concentration Pathways (RCPs), i.e., greenhouse-gas emissions scenarios identified by the Intergovernmental Panel on Climate Change (Kirtman et al. 2013). By the end of this century, temperature is expected to increase by another 0.3 to 1.7 °C under the lowest-emissions RCP and, under the highest-emissions RCP, by 2.6 to 4.8 °C (Collins et al. 2013).

However, the earth has been even warmer in the past than what is predicted. The most extreme example of the current geologic era is the Early Eocene Climatic Optimum (52–48 mya), in which temperature was 9–14 °C higher than present, and atmospheric CO_2 concentration was around 1000 ppm (Masson-Delmotte et al. 2013), compared to 391 in 2011 (Hartmann et al. 2013). Indeed, changes to the climate are the rule. Over the last 2.6 million years, the NH was subjected to about 20 cycles of glaciation and deglaciation (Davis 1983). Considering that living things persisted through warm, CO_2-rich periods of the distant past and

through more recent ice ages, life may be resilient to climatic fluctuations including contemporary climate change.

Although warming is nothing new, the *rate* of contemporary warming exceeds anything known. For example, during the most recent deglaciation, the fastest warming rate was 0.010–0.015 °C/decade, but from 1880–2012 it was 0.064 °C/decade (Hartmann et al. 2013, Masson-Delmotte et al. 2013). The extent to which plant life will be resilient to ongoing climate change is uncertain. Due to the importance of plants for shelter, food, fiber, medicine, recreation, and ecosystem services, it is necessary to predict how climate change will affect plants. This is particularly salient for trees, many species of which are long-lived and slow to evolve. In northeastern North America, tree longevity can reach ≈2,000 years in *Thuja occidentalis* (white cedar; Kelly & Larson 2007). Such long-lived organisms must have some degree of resilience to environmental change. A 2,000-year-old white cedar alive today would be one that has experienced both prolonged cool and prolonged warm periods (Fig. 1.1). Most notably, it would have endured the Little Ice Age (ca. 1400–1900) and contemporary warming (ca. 1900–present). However, will such trees be able to cope with the anticipated unprecedented rapidity of further climate change?

Plant Responses to Climate Change

Many tree species were able to cope with climate change of the past. Tree responses to the most recent glacial cycle included continental-scale migration, adaptation, and extinction, and responses were characterized by differences among species. Davis (1983) summarized tree species' retreat from advancing glaciers and later colonization of deglaciated land. Some

species migrated faster than others, resulting in continual novel community formation and dissolution. For example, *Tsuga canadensis* (eastern hemlock) and *Pinus strobus* (eastern white pine) commonly occur together today along with many hardwood tree species in the mesic northern forest community type common in the northern Great Lakes Region (GLR) (Cohen et al. 2014), but in their glacial refugia, *T. canadensis* and *P. strobus* grew on the Atlantic central coastal plain and on the continental shelf, largely absent from the hardwoods, which are believed to have survived in small isolated refugia far to the south.

Some species may not have been able to migrate with sufficient speed, such as the formerly widespread *Picea critchfieldii* (Critchfield's spruce), which went extinct in eastern North America ≈15 kya (Jackson & Weng 1999). Complementing migration, many species underwent substantial adaptation, too. For example, Cheddadi et al. (2016) reconstructed median January temperature throughout the distribution of three European tree species between 10 and 3 kya and compared the reconstruction to modern temperatures. *Fagus sylvatica* (European beech) formerly occurred in areas cooler than its modern range and *Picea abies* (Norway spruce) in areas warmer. The ancient climate of the range of *Abies alba* (European silver fir) was comparable to its modern climate. Tree-ring-based growth projections suggest that tree growth, in addition to tree ranges, will also change heterogeneously in response to climate. This is true within species (e.g., Huang et al. 2013, Chhin 2015, Rimkus et al. 2018), and it is also true among species (e.g., Huang et al. 2013, Su et al. 2015, Rahman et al. 2018).

Not only will tree growth be affected by climate change itself but also likely by increasing atmospheric CO_2. Higher CO_2 levels may ameliorate the additional

evapotranspirative demand that will come with higher summer temperatures, allowing plants to keep their stomata closed more often, reducing moisture loss. This effect, CO_2 fertilization, has been found in greenhouse trials (Bazzaz et al. 1990), and in forest trees growing in nature, but evidence is mixed. In observational studies, no support was found in the tropics (Van der Sleen et al. 2015) or boreal Canada (Girardin et al. 2016). However, support was found in the temperate western and eastern U.S. (Wang et al. 2006 and McMahon et al. 2010, respectively) and the GLR (Cole et al. 2010). This was corroborated in experimental studies (Telewski et al. 1999, Walker et al. 2019). Lamarche et al. (1984) attributed unprecedented recent growth of ancient *Pinus longaeva* (bristlecone pine) in the American southwest to rising CO_2, but Salzer et al. (2009) claimed this was due to rising temperatures. It may be that CO_2 fertilization is sustainable only until nitrogen becomes depleted to the point of being a greater limiting factor (Norby et al. 2010).

Though CO_2 fertilization is equivocal, other effects of nascent climate change are clearer. In some cases, one need not turn to models or theory to understand the effects of climate change but can look at effects already observed. In semi-arid forests of China, climate change has led to increases in drought, fire, plant-pathogen outbreaks, tree mortality and tree-growth reductions (Liu et al. 2013). Increased tree mortality has also been found on the Tibetan Plateau (Liang et al. 2015). In the United States, recent severe droughts led to widespread tree mortality in Texas (Crouchet et al. 2019) and reduced radial growth in Indiana (Kannenberg et al. 2019).

Further, climate change has led to phenological changes. Willis et al. (2008) compared contemporary phenological and abundance data to mid-19th-century data. Those species which

adjusted their phenology in response to climate change over the period increased in abundance, while those that failed to adjust decreased. Hufkens et al. (2012) examined how an early, intense spring warm-up followed by a late-spring frost affected tree canopy development and forest-wide productivity. All three study species leafed out early in response to unseasonably warm weather. *Betula alleghaniensis* (yellow birch) and *Fagus grandifolia* (American beech) were able to endure the subsequent frost with little damage. However, canopy development of *Acer saccharum* (sugar maple) was suppressed, leading to declines in forest productivity.

Phenological changes can result in mismatch between interacting organisms. Well-known are the disruptions to pollination that occur when plants and their animal pollinators differentially respond to climate change (Pyke 2016, Hutchings 2018). Additionally, wildflowers, particularly spring ephemerals, those early emerging forest-understory herbs whose aboveground parts soon senesce after the forest canopy develops, respond differently than do overstorey trees. Heberling et al. (2019) compared 19th century and present-day data and found that, in response to climate change in eastern North America, the leaf-out date of both wildflowers and trees had advanced, but in trees it had advanced at a more rapid rate, shortening the crucial window during which spring wildflowers capture most of their sunlight.

Climate plays a large role in determining the range limit of tree species (Siefert et al. 2015), and thus it is no surprise that the distributions of trees and other plants have changed as climate change has proceeded. Generally, species are moving upward in elevation (Kelly & Goulden 2008, Harsch et al. 2009, Kharuk VI et al. 2010, Kopp & Cleland 2014, Bruening et al. 2017). For example, a resurvey of Whittaker's and Niering's (1964) survey of the vegetation of

the Santa Catalina Mountains, Arizona revealed that the mean lower range limit across species had moved upward, though some individual species were exceptions (Brusca et al. 2013). A wider exception to the trend was found in a large swath of California, where a comparison of mean 1930s and present-day elevation of 64 plant species revealed a significant downhill shift, attributable to a regional decrease in climatic water deficit (Crimmins et al. 2011). Just as species are moving upward in elevation, so too are they thriving in previously marginal habitats (Sturm et al. 2001) and moving upward in latitude (Boisvert-Marsh et al. 2014).

Clearly, plant ranges, including those of trees, are shifting. The question is whether tree migration can keep pace with climate change in the long-term. Recent reports suggest that some species will succeed, and others fail (Chen et al. 2011). Emigration and immigration can have large, cascading effects. For example, Rodriguez-Cabal et al. (2013) found that the local extinction of a mistletoe's host plant in Patagonia led to the extinction of the mistletoe (a keystone species), a hummingbird (important pollinator), and both a marsupial and a bird (important seed dispersers).

Vertical and radial growth of a tree's stem and branches are important for mechanical structure, storage of biochemicals, competing for light with other plants, and transporting water, food, and other substances. In trees, stem growth has already been affected by climate change. Gamache and Payette (2004) studied height growth of *Picea mariana* (black spruce) at and near treeline in northern Quebec. Historically, growth at treeline was lower than growth at more southerly locations, but from the 1970s through the end of the study period there was no difference between the two. Latte et al. (2016) studied the radial growth of *F. sylvatica* that occurred from 1930–2008 in Belgium. They found a marked decrease in overall growth and an

increase variability beginning in the 1950s–1960s and 1970s–1980s, respectively, and persisting through the study period, which they attributed to climate change, soil compaction, and nitrogen deposition. At the southern range limit of *F. sylvatica*, radial growth decline over the most recent three decades examined was observed. The decline was greatest at low elevations (Jump et al. 2006).

By contrast, climate-change-attributable radial growth *increase* was observed at an alpine tree line on the Tibetan plateau. *Abies faxoniana* increased its growth rate 16-fold over 1900–2012 relative to 1764–1899. This was attributed to increases in atmospheric CO_2 and soil moisture (Silva et al. 2016). Pretzsch et al. (2014) found accelerated tree growth and forest development in Europe as climate change proceeded. Along a latitudinal gradient in the central Siberian Taiga, *Larix cajanderi* growth did not change over the growth period studied, but growth of *Picea obovata* (Siberian spruce) and *P. sylvestris* accelerated, especially in *P. obovata.* Consistent with among-species differences in post-glacial recolonization rates, such among-species differences in contemporary climate change responses are the norm. Granda et al. (2013) studied growth of four co-occurring species in a Mediterranean forest. Growth of one species had accelerated, that of another declined, and that of two more did not change.

Not only do climate-change responses differ among species but within species, too. Along gradients of altitude and latitude, growth of populations at low elevation or latitude is generally hindered and that of high-altitude/latitude populations helped, consistent with wider trends in the field of global change biology (Parmesan 2006). Dulamsuren et al. (2017) studied *F. sylvatica* in Germany in the middle of its range. At low elevations, growth had declined since the 1980s, while at high elevations it increased. Similar results were found in *P. abies* in east-

central Europe and in three conifer species in British Columbia (Lo et al. 2010, Ponocna et al. 2016). However, exceptions have been found. Housset et al. (2015) studied *Thuja occidentalis* (white cedar) in boreal Canada over three degrees of latitude. Northerly populations were unable to take advantage of recent warming, and in fact their growth recently declined due to concomitant moisture stress.

Though incipient climate change has been substantial in some regions, it generally is still *relatively* minor and within the range of natural historic variability. Thus, growth trends of many tree populations have not yet been affected. In these cases, one can still use contemporary relationships between growth and climate to anticipate the effects of ongoing climate change. Findings are generally consistent with the expectation that low-altitude/latitude populations will suffer and high-altitude/latitude populations benefit. For example, in a meta-analysis of 378 *P. mariana* tree-ring-width chronologies, D'Orangeville et al. (2016) found that in the southern part of the chronology network, growth-temperature relationships were negative, but they gradually became more positive moving north, until by around 49° N the majority were positive. Similar results were found for *Pinus pinea* in Iberia (Natalini et al. 2016) and for *Sequoia sempervirens* (coast redwood) in California (Carroll et al. 2014), but exceptions are found. No latitudinal trend in growth-climate relationships was found for *Sorbus torminalis* (wild service tree) in Europe (Rasmussen 2007).

As for altitudinal gradients in growth-climate relationships, *Picea schrenkiana* (Schrenk's spruce) in northwest China had negative growth-temperature and positive growth-precipitation relationships at low elevation and positive growth-temperature relationships at high elevation

(Huo et al. 2017). However, no such trend was found in a different part of northwest China in *Juniperus przewalskii* (Przewalski's juniper) (Gao et al. 2017).

Clearly, growth-climate relationships differ within and among species, unsurprising given that each species is physiologically adapted to its environment, and, within species, populations are locally adapted. Robakowski et al. (2011) found, among four broad-leaved tree species of eastern North America, differences in photosynthetic temperature optima and differences among different provenances within species, even when grown in common gardens for more than a decade. Further, tree species differ in how they adjust stomatal conductance as soil and air moisture change (Hinckley et al. 1979, Pataki & Oren 2004).

Thus, species and populations differ in their response to climate, and so too climate change differs from region to region. For example, high latitudes are warming more than low latitudes. Precipitation has increased in eastern North America, and many other places around the globe, but it has decreased in the Sahel Region of Africa and scattered pockets elsewhere (Hartmann et al. 2013). Because each region has its unique climate change prognosis and each tree species its own response, it is necessary to study a variety of species across different regions to understand how each species will respond to climate change in different parts of its range.

Forests and Climate of the Great Lakes Region

The GLR is an area with ample, variable forests which play important ecological and economic roles. In Michigan, the annual state and regional economic impact of the timber industry is $14 billion (Leefers 2017). Further, there are more than 20 million acres of forest in

that state, including 56% of the land area and amounting to 1,400 trees for every person (Dickmann & Leefers 2016). The region has a high concentration of distribution limits of tree species, both northern and southern limits, because of the tension zone—a diffuse region in which the hardwood forests dominant in the south gradually give way to the mixed hardwood-conifer forests of the north (Andersen 2005)—allowing the comparison of southern- and northern-range-margin populations.

Most of the region experienced a cycle of glacial and nonglacial conditions over at least the last 800,000 years, except the southern extreme, which did not experience the two most recent glaciations, although it may have been affected by more ancient ones. The most recent glaciation was the Wisconsin glaciation. It reached peak ice extent ≈24 kya and is responsible for most of the current soil types, topography, and lake levels in the study region (Larson & Kincare 2009). The variation in soils affects modern vegetation, with mesic plants growing in fertile, coarse-textured soils, and xeric plants in dry, sandy soils (Harman 2009).

The contemporary climate of the region is unique due to the temperature-moderating, moisture-influencing Great Lakes. For example, due to the predominantly west-flowing wind, both major peninsulas of Michigan are downwind of a Great Lake, resulting in an overall more wet, cloudy, snowy, and moderate climate than areas upwind (Andresen & Winkler 2009). Recent climate change has resulted in a generally warmer, wetter regime (Andresen 2012), and long-term Great Lakes Region forecasts predict these trends to continue (Hayhoe et al. 2010, Christensen et al. 2013, Byun & Hamlet 2018).

Study Objectives

With the unique climate and diversity of forest types in the Great Lakes Region, it is important to examine relationships between tree growth and climate in the region. This will provide information about both future responses to climate and prerecorded climate (climate preceding the era of widespread instrumentally derived records kept by humans). Yet, the relationship between tree growth and climate has been insufficiently examined in the region with relatively few published tree-ring chronologies coming from there (Zhao et al. 2019). In this dissertation, I use 47 tree-ring chronologies from Indiana and Michigan to accomplish four major objectives. First, I reconstructed 500 years of summer moisture conditions on South Manitou Island in northern Lake Michigan to put current and predicted future climate into a historical perspective (Chapter 2). Second, I quantified relationships between tree growth and climate in nine species along a latitudinal gradient to establish baseline data for this understudied region and facilitate comparisons within and among species (Chapter 3). Third, I examined the temporal stability of growth-climate relationships to determine whether tree rings were an appropriate proxy to use for climate reconstruction in the region (Chapter 3). Finally, I projected growth over the rest of this century in the context of climate change via parsimonious growth-climate models to identify vulnerable species/regions and to identify potentially climate-change-resilient populations (Chapter 4).

APPENDIX

APPENDIX

Figures

Figure 1.1. Global average annual temperature deviations from 1850–1900 reference period. Note that the medieval warm period (Middle Holocene Climatic Optimum) was a predominantly North Atlantic phenomenon and hence does not register on this global scale. Thanks to Ed Hawkins for sharing the figure, which he made from PAGES2k (Neukom et al. 2019) and HadCRUT 4.6 (updated version of Morice et al. 2012).

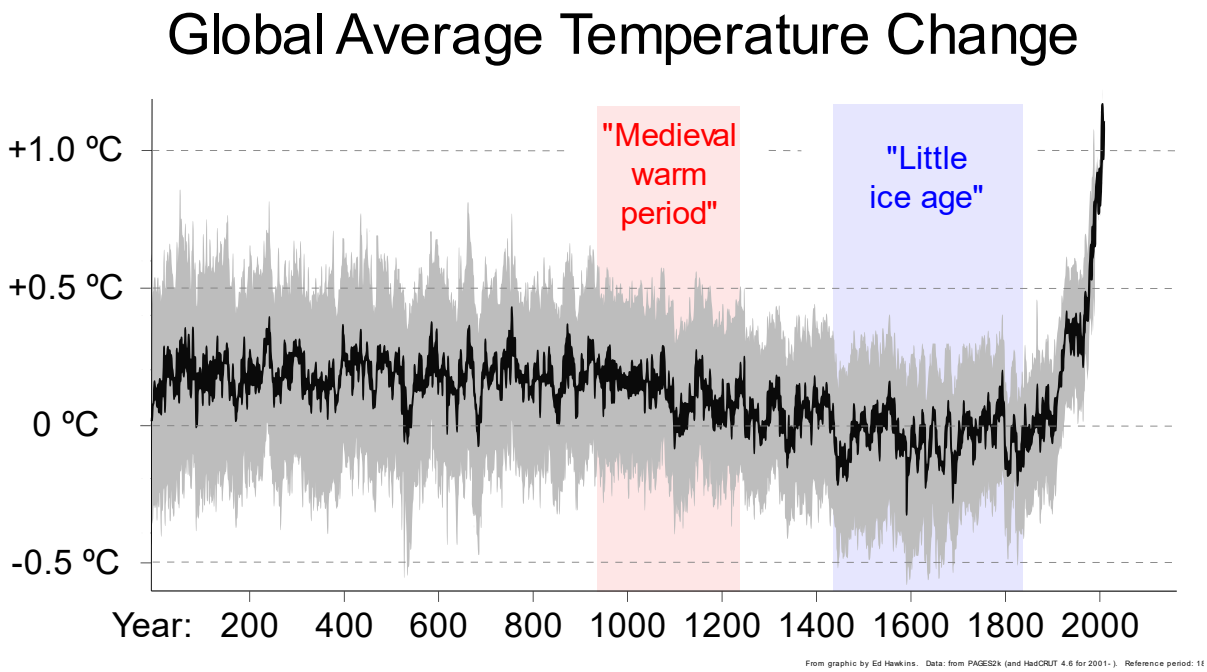

CHAPTER TWO

TREE-RING-RECONSTRUCTED LATE-SUMMER MOISTURE CONDITIONS, 1546 TO PRESENT, SOUTH MANITOU ISLAND, LAKE MICHIGAN, USA

SCOTT M. WARNER[1,*], SAMANTHA J. JEFFRIES[2], WILLIAM A. LOVIS[2,3], ALAN F. ARBOGAST[4], FRANK W. TELEWSKI[1,5]

[1]ECOLOGY, EVOLUTION, AND BEHAVIOR PROGRAM, DEPARTMENT OF PLANT BIOLOGY, MICHIGAN STATE UNIVERSITY, EAST LANSING, MICHIGAN 48824, USA

[2]DEPARTMENT OF ANTHROPOLOGY, MICHIGAN STATE UNIVERSITY, EAST LANSING, MICHIGAN 48824, USA

[3]MICHIGAN STATE UNIVERSITY MUSEUM, MICHIGAN STATE UNIVERSITY, EAST LANSING, MICHIGAN 48824, USA

[4]DEPARTMENT OF GEOGRAPHY, ENVIRONMENT AND SPATIAL SCIENCES, MICHIGAN STATE UNIVERSITY, EAST LANSING, MICHIGAN 48824, USA

[5]W. J. BEAL BOTANICAL GARDEN, MICHIGAN STATE UNIVERSITY, EAST LANSING, MICHIGAN 48824, USA

*Corresponding author: warner91@msu.edu

Acknowledgments

Thank you to Inter-Research for permitting us to reprint with slight formatting modifications a paper from *Climate Research* which comprises this chapter: S.M. Warner, S.J. Jeffries, W.A. Lovis, A.F. Arbogast, & F.W. Telewski. 2021. Tree ring-reconstructed late summer moisture conditions, 1546 to present, northern Lake Michigan, USA. *Climate Research*. 83:43–56. https://doi.org/10.3354/cr01637.

We thank Jill Grimes for assistance with field work, Matthew J. Hadden for assistance with tree ring measuring and dating, and Edward R. Cook for providing an unpublished tree-ring chronology and for advice on crossdating and detrending. We thank the National Park Service for allowing us to sample trees (NPS Permit No. 85839) and the South Manitou Island rangers for their hospitality: providing transportation to and from the island and providing lodging and access to a vehicle while on the island. For accepting our cores into their collection, we thank the Michigan State University Herbarium (MSC). For funding we are grateful to the Alfred H. and Jean Goldner Endowment, donors to the William A. Lovis Endowment for Environmental Archaeology, and the Department of Geography, Environment and Spatial Sciences. To three anonymous reviewers and a journal editor we are grateful for insightful suggestions which helped us to improve our presentation.

Abstract

Drought can affect even humid regions like northeastern North America, which experienced significant, well-documented dry spells in the 1930s, 50s, 60s, and 80s, and proxies

tell us that in the years before instrumentally recorded climate, droughts could be even more severe. To get a more complete picture of pre-recorded climate, the spatial coverage of proxy-based climate reconstructions must be extended. This can better put in context past, current, and future climate, and it can lend anthropological and historical insights. With regard to tree rings as climate proxies, however, there is increasing evidence that relationships between tree growth and climate can be inconsistent over time, in some cases decreasing the utility of tree rings in the representation of climate. We developed a chronology from white cedar *Thuja occidentalis* tree ring widths for the period 1469−2015 C.E. with which we modeled the relationship between growth and July−September moisture conditions (Palmer *Z* index). The relationship was consistent across the period of instrumentally recorded climate, 1895−present, and the model explained 27% of variability. Therefore, we used the model to reconstruct July−September moisture conditions from 1546−2014. We found the most variable century to be the 20th, the least the 18th. The severest decade-scale droughts (≤0.75 SD from mean) occurred in the 1560s, 1600s/10s, 1630s, 1770s/80s, 1840s, and 1910s/20s, the severest pluvials (≥0.75 SD) in the 1610s/20s, 1660s/70s, and the 1970s/80s. The occasional occurrence of severe droughts throughout the reconstruction, increasing variability in the 20th century, and expected climate change-enhanced late summer drought, portend a future punctuated with severe droughts.

KEY WORDS: Great Lakes climate ・ Lake Michigan climate ・ *Thuja occidentalis* dendrochronology ・ White cedar dendrochronology ・ Dendroclimatology ・ Drought reconstruction ・ Moisture reconstruction ・ Tree ring reconstruction

Introduction

In the North American Great Lakes Region (GLR) several episodes of unusual weather have recently occurred, at least from a modern perspective. Anomalously high temperatures have been observed: the warmest March on record across the US Midwest in 2012 (National Oceanic and Atmospheric Administration [NOAA] National Centers for Environmental Information 2012a), the second warmest February in the US Midwest in 2017 (NOAA National Centers for Environmental Information 2017a), and 5 consecutive record-high daily temperatures in Chicago, Illinois, September 2017 (NOAA National Centers for Environmental Information 2017b). August 2012 brought severe to exceptional drought to 40% of the US Midwest (NOAA National Centers for Environmental Information 2012b). Conversely, 2013 was the wettest in the upper GLR since 1900 (Knutson et al. 2014). Recent anomalous cold temperatures have also been observed: the 2013−2014 winter of the North American Midwest was the third coldest since 1920 (Wolter et al. 2015), and February 2015 was the third coldest February on record in Michigan (NOAA National Centers for Environmental Information 2015).

However, the widespread reliable instrumental climate record extends only to 1895 in the region (Andresen 2012), so it is difficult to say how unusual recent events were. Further, climate has been dynamic over the recorded period. From 1895−2019, there was in Michigan an increasing trend for annual (January−December) temperature, amounting to 0.127°C per decade (linear correlation, $r^2 = 0.263$, 2-tailed $p < 0.0001$; http://www.ncdc.noaa.gov/cag/statewide/time-series/20/tavg/ann/9/1895-2019). Throughout the entire record there were 3 distinct periods: 1895−1930 was a moderate period, on average

5.94°C, with no significant temporal trend (p = 0.819). 1931−1980 was a warmer period, on average 6.51°C; it started very warm and had a marginally significant cooling trend overall (p = 0.075). 1981−2019 was warmer still, on average 7.19 °C, with a marginally significant warming trend (p = 0.077).

Precipitation has also been on the rise in Michigan. From 1895−2019, annual (January−December) precipitation values increased by 1.09 cm decade^{-1} (linear correlation, r^2 = 0.224, 2-tailed p < 0.0001; http://www.ncdc.noaa.gov/cag/statewide/time-series/20/pcp/ann/9/1895-2019). Again, there were distinct periods. 1895−1929 was the driest, at 766 mm yr^{-1}, and it was without a trend (p = 0.878). 1930−1999 got continuously wetter, with a trend of 1.27 mm yr−1 (p = 0.006) and a mean of 801 mm yr^{-1}. The most recent period, 2000−2019, was a period of rapid moistening, with a trend of 7.81 mm yr^{-1} (p = 0.012) and a mean of 878 mm yr^{-1}. These moistening trends are consistent with other regions of eastern North America, including Indiana/ Illinois (Mishra & Cherkauer 2010), southeastern New York (Pederson et al. 2013), and Iowa (Ford 2014).

Trends in snowfall are mixed in the GLR, being modulated by location relative to Great Lakes shorelines. Areas near the leeward shore, such as western lower Michigan, receive greater snowfall than inland and windward coastal areas due to the lake effect (Scott & Huff 1996). In lake effect areas alone, snowfall has been increasing since the 1940s. In non-lake effect areas, however, snowfall did not significantly change over the same period (Burnett 2003, Andresen 2012). Consistent with this trend, Suriano et al. (2019) found that from 1960−2009 snow depth had decreased or not changed across the Great Lakes Basin, but snowfall had increased in many areas along the lakes' leeward shores. Further, since 1960

snowmelt is increasing in lake effect areas such as the east coast of the Georgian Bay and decreasing outside these areas such as the north coast of Lake Superior (Suriano & Leathers 2017). Throughout the Great Lakes Basin, a shift toward earlier snowmelt has progressed since 1960 (Suriano & Leathers 2017). As expected by the precipitation trend, cloudiness has increased since at least the 1960s (Andresen 2012). Thus, the GLR is getting warmer, wetter, cloudier, and in some areas snowier.

In the future, additional changes in the regional climatology are anticipated. To account for uncertainty of future anthropogenic contributions to climate change, the Intergovernmental Panel on Climate Change (IPCC) has established 4 potential scenarios called representative concentration pathways (RCPs) that correspond to a range of greenhouse gas concentrations. From lowest to highest concentration, the pathways are RCP 2.6, 4.5, 6.0, and 8.5. Mid-century projections for eastern North America under, for example, RCP 4.5 predict precipitation increases in the northern part of the continent, particularly in winter, but also summer, and for temperature to increase beyond the range of natural variability (Christensen et al. 2013). Projections for the GLR specifically suggest that temperature will increase during all seasons throughout the rest of this century, and precipitation will increase in winter and spring while remaining the same or decreasing in summer and fall (Hayhoe et al. 2010, Byun & Hamlet 2018). Byun & Hamlet (2018) predict a 6.5°C increase by 2100 under RCP 8.5 and 3.3°C under RCP 4.5. Their predictions for precipitation are more equivocal. Under RCP 8.5, there may be a 5−25% increase in annual precipitation by the 2080s, with large increases in winter/spring and perhaps little change in summer/fall. Thus, climate has changed and is expected to continue changing in the GLR. To put this climatic change in a historical perspective, however,

the climate record must be extended into the period preceding reliable records with proxies such as fossilized pollen in lakes/bogs, elemental isotope concentrations, and tree rings. Proxy records reveal that since the last deglaciation of the region between 12−10 kya, several distinct climatic intervals have occurred: the warm, dry Hypsithermal (9−5 kya), the warm, wet Middle Holocene Climatic Optimum (800−1300 C.E.), and the cool, wet Little Ice Age (1400−1900 C.E.). This information is limited spatially to places with lakes and bogs and ancient trees and logs.

Temporally, information about paleoclimates becomes more limited moving backward in time. Here in northeast North America, tree longevity peaks at ≈2000 yr (Kelly & Larson 2007), but even a quarter of that age is rare, and the mesic climate often results in decay of the most ancient wood. Thus, any tree ring chronology dating back further than perhaps 250 yr—about twice the length of recorded data—is a valuable contribution to the understanding of ancient climate. Tree ring chronologies that remain consistently correlated with climate over time are particularly valuable. The field of dendrochronology has traditionally stood on the principle of uniformitarianism, meaning present-day relationships between natural phenomena are like those of the past (Fritts 1976). However, it is increasingly evident that the factors affecting growth in some trees are inconsistent. For example, numerous tree ring chronologies from high northern latitudes have revealed a deteriorating growth−temperature relationship in recent decades (reviewed in D'Arrigo et al. 2008). Further, deteriorating growth−climate relationships have been found occasionally at lower latitudes, including the northeastern US. Maxwell et al. (2016) found across several species in southern Indiana/Illinois a weakening relationship between growth and Palmer drought severity index (PDSI) and attributed it to a

scarcity of droughts in recent decades. Saladyga & Maxwell (2015) found in the central Appalachians weakening relationships between *Tsuga canadensis* growth and both summer precipitation and late winter temperature, and they attributed these changes to infestation by hemlock woody adelgid and a shift in the temperature regime.

Toward a better understanding of both prerecorded climate in the GLR and the temporal stability of using tree rings as climate proxies there, we present a tree ring chronology for the northeastern part of Lake Michigan extending to 1469 C.E. We use it to reconstruct July−September Palmer *Z* index, a drought metric, to 1546 C.E. Our specific objectives were to (1) quantify moisture over the last several centuries, (2) identify significant droughts and pluvials at the 5 to 10 yr scale, (3) put recent droughts and pluvials into historical context by quantifying their return intervals, and (4) examine how the strength of the relationship between tree growth and moisture changes over time. This complements other studies in the region (Cook et al. 1999, Buckley et al. 2004, Pederson et al. 2013, Ford 2014) to present a more complete picture of ancient climate in the greater GLR.

Methods

In May 2016, we used increment borers to take 101 cores from 43 white cedars *Thuja occidentalis* on South Manitou Island, Michigan, located in northern Lake Michigan 11 km west of mainland lower Michigan (Fig. 2.1). The area has warm, wet summers and cold, dry winters, with annual precipitation at 791 mm and annual temperature at 6.0 °C. February, the coldest, driest month, is on average −7.7 °C with 39 mm of precipitation. July, the hottest month, and among the wetter months, averages 19.4 °C and 73 mm (1895−2010 meteorological normals,

ftp://ftp.ncdc.noaa.gov/pub/data/cirs/climdiv/). We focused our sampling on two subsites: first, the Valley of the Giants (45.0035°, −86.1481°), a stand of old-growth mesic northern forest and, second, among the dunes just to the north of this stand (45.0127°, −86.1520°). In the Valley of the Giants, we selected a variety of trees representing what appeared to be large old-growth specimens as well as some younger trees in order to create a cross-dated chronology from the living grove, for a total of 57 cores from 27 trees and logs. The dunes are peppered with ghost forests—stands of dead trees and logs; these trees and logs were presumably covered and uncovered by the movement of sand over the decades and centuries, with their preservation aided by sand cover (Fig. 2.2). We took 44 cores from 16 trees and logs scattered about the dunes.

We glued the cores to wooden mounts (Frame and Trim Molding) and surfaced them with sandpaper up to a grit of 400. We skeleton-plotted each core, that is, made graphical representations of the relative narrowness of each tree ring (Stokes & Smiley 1968), focusing first on the cores from the Valley of the Giants. We cross-dated across skeleton plots, first on cores within the same tree to build tree-level composite plots, and then across composites to build a stand-level master composite. For individual-core plots which did not match well against the master, we checked the wood for potential false rings, and identified potential missing rings, years for which a tree does not lay down xylem along part of its cambial surface due to stress. From this, we had tentative dates for each tree ring from the Valley of the Giants, and then used the same strategy for the trees from the dunes. As an additional check, we cross-dated our skeleton plots against an independently derived, unpublished *T. occidentalis* chronology from South Manitou Island (E. R. Cook pers. comm.).

We used a scanner to generate images of the cores for computerized ring width analysis, at a resolution of 1600−3200 dots per inch, depending on core length. With the program CooRecorder (version 9.0.1, Cybis Elektronik & DATA AB), we measured the width of each tree ring to the nearest hundredth of a millimeter. To test our tentative dates, we ran the ring measurements through the program COFECHA (Holmes 1983), which compares each individual series of ring measurements to the mean of all measurements and identifies any cores which do not correlate well against the rest. These problems were addressed through an examination of the wood and a review of the measurements. If there were no ambiguous cracks in the wood, ring boundaries that looked suspiciously false, or measurement errors, potential false and missing rings were identified through skeleton plot cross-dating and then re-tested in COFECHA until all measurement series were accurately dated. At the conclusion of the dating process, cores were prepared for permanent storage in a natural history collection. These are being accessioned into the Michigan State University Herbarium (MSC).

Ring width series for individual cores were standardized and detrended using program ARSTAN (Cook 1985). We focused on extracting a climatic signal from the ring-width series. To do so, we fit to each ring-width series a cubic smoothing spline with a length equal to 67% of the total length of the ring width series. Year by year ring width indices (RWI) were calculated by dividing the observed ring width by that expected according to the fitted spline. This process attenuates long-term confounding trends, and accentuates interannual and interdecadal variation caused by climate fluctuation. To ameliorate unstable variance due to inconsistent sample depth over time, we used Briffa r-bar-weighted stabilization in ARSTAN (Osborne et al. 1997, Pederson et al. 2012). The bi-weight robust mean of all trees' RWI series was calculated

in ARSTAN, which yielded three composite chronologies, 'standard', 'residual', and 'ARSTAN'. We selected the 'ARSTAN' chronology for further analysis. It retains the pooled variance at the site level, which is hypothesized to be due to climate, and therefore is skilled at examining long-term climate variability (Cook 1985). The quality of the chronology was assessed with the expressed population signal (EPS) statistic, which expresses how well a finite sample represents a theoretical infinite population (Wigley et al. 1984), and has been used widely in dendrochronological climate reconstructions (e.g., Buckley et al. 2004, Pederson et al. 2012, Maxwell et al. 2016; but see critique from Buras 2017; see Fig. 2.3). We calculated EPS using 50 yr segments overlapping 49 yr, i.e., each 50 yr window represented by at least two trees was assessed. Our predetermined EPS minimum for chronology quality was 0.80 (D'Orangeville et al. 2018).

To quantify the influence of climate on our RWI chronology, we took the common period—the interval shared by both the RWI and climate-observation datasets—and used ordinary least- squares (OLS) regression on one-half of the data, 1896−1955, the calibration period. To find the climate variable best correlated with growth and that could thus provide the most information on prerecorded climate, we tested several variables related to moisture balance, including precipitation, mean temperature, PDSI, Palmer hydrological drought index (PHDI), and Palmer *Z* index. Pilot analyses revealed the best source for climate data to be US Climate Division data from NOAA (ftp://ftp.ncdc.noaa.gov/pub/data/cirs/climdiv/). Our site falls within Michigan Division 3 (Fig. 2.1). With each tested variable, we determined the influence of the most influential month(s). Because tree growth can be affected by both current- and prior-year conditions, the window of months considered ran from the May preceding the year of ring

formation to the September of the year of ring formation (Fritts 1976). We examined growth−climate relationships at the 1-, 2-, 3- and 4-month scales. To clarify, this included for example prior-November through current-February, current-August−September, and prior-August alone. We selected the final variable based on r^2 and the consistency of r^2 when comparing the same model across the calibration period and the verification period (1956−2015). According to standard dendrochronological procedure, we further verified the final model with the reduction of error (RE) and coefficient of efficiency statistics (CE), which both compare the ability of the model to predict observed values within the verification period. RE compares the model's predictive ability relative to the calibration period mean's predictive ability. CE does the same relative to the verification period mean (Fritts 1976, Cook et al. 1999).

To confirm that the model was consistent throughout the period, not in only the two specific 60 yr windows chosen for the calibration and verification periods, we quantified the r^2 value in each 60 yr window of the common period, i.e., 1896−1955, 1897−1956, . . ., 1956−2015. This value was plotted, and the stability of the correlation inspected visually (Harvey et al. 2020). After finding similar results across each window, the calibration and verification periods were combined into a single period across which the relationship between the selected climate variable and RWI was quantified. To reconstruct climate, we applied this regression equation on the RWI chronology preceding the observed climate record.

Results

Our final ring width chronology cross-dated well, with an intercorrelation among all cores of 0.547 (Grissino-Mayer 2001). The chronology is based off 101 cores and spans

1469−2015; however, from 1469−1546 the sample is limited to a single tree, one from which three cores were extracted. For further analysis, we therefore used only the period 1547−2015, the interval in which the sample included at least two trees (four cores). After 1547, the sample size increased rapidly, from 9 cores in 1560 to 14 in 1580 and 17 in 1600. It remained robust thereafter (Fig. 2.3). Despite the low sample size early in the chronology, EPS was high throughout, with a mean of 0.944 and no 50 yr segments falling below our predetermined threshold of 0.80 (D'Orangeville et al. 2018; Fig. 2.3).

The detrended, standardized ring width chronology—the RWI chronology—was modeled against several moisture-balance-related climate variables. The climate variable most associated with RWI was prior-year July−September Palmer *Z* index. It was consistent across the 1896−1955 calibration and 1956−2015 verification periods, with an r^2 of 0.239 and 0.301, respectively (Table 2.1). Additionally, it was relatively stable in each of the 60 yr windows overlapping the calibration and verification periods (Fig. 2.4). As an additional model-quality check, RE and CE were calculated. These statistics assess the predictive skill of a model and can range from $-\infty$ to 1. Any number higher than zero indicates a model with skill (Fritts 1976, Cook et al. 1999), a threshold which our model met (Table 2.1). Prior-year July−September Palmer *Z* index was directly correlated with RWI, that is, a wetter summer resulted in a wider ring the following year. For every unit increase in Palmer *Z* index there was a 9.6 and 8.2% increase in RWI during the calibration and verification periods, respectively (Table 2.1).

Because we obtained similar results across the calibration and verification periods, we combined them into a full model (Pederson et al. 2012; Table 2.1) which was used to reconstruct 1546−2014 Palmer *Z* index. Because of the lagged effect, we used RWI at year$_{t+1}$

to predict Palmer *Z* index at year$_t$. Additionally, we tried a model in which both year$_t$ and year$_{t+1}$ RWI were used as predictors, but this improved r^2 only mildly (0.266 for the single predictor vs. 0.271 for the double), and the Akaike information criterion (AIC) suffered (373 for the single vs. 374 for the double). AIC is a model-quality metric that assesses the goodness of fit while penalizing for having too many parameters; a lower value is better (Akaike 1974). We checked reconstructed 1896−2015 Palmer *Z* against observed values; the datasets were significantly correlated ($r^2 = 0.266$, $p < 0.0001$), but reconstructed Palmer *Z* was less variable than observed values (standard deviation [SD] = 0.58 vs. 1.31). Therefore, both reconstructed and observed Palmer *Z* indices were standardized to a mean of zero and SD of 1. This was done by subtracting from each value the dataset's mean and dividing by the dataset's SD (Quiring 2004, Ford 2014). The standardized reconstructed data correlated well with the standardized observed data, with a few notable exceptions: early 1900s decades, late 1910s/early 1920s, and late 1960s/early 1970s (Fig. 2.5).

Additionally, our reconstructed summer drought index agreed with that of a previous study from a nearby site. Cook et al. (1999) conducted gridded reconstructions of summer moisture throughout the continental USA. Although none of their grid points were on South Manitou Island or any of the nearby islands, there were reconstructions in adjacent mainland Michigan. The nearest reconstruction was on mainland northwest lower Michigan, Grid Point 225 in their study. Despite their use of a different drought index (PDSI) over a different time window (June−August), there is reasonable agreement throughout common period 1546−2003, after standardizing their data in the same manner as ours ($r = 0.498$, $p < 0.0001$).

Over the entire reconstruction there is no trend in moisture over time ($p = 0.82$), but there are multidecadal, even centennial, trends (Fig. 2.6). For example, there was a rapid moistening trend from 1560−1599 ($p = 0.0003$, slope = 0.0468 yr^{-1}) and more modest trends from 1560−1678 ($p = 0.001$, slope = 0.008 yr^{-1}) and 1916−1986 ($p = 0.006$, slope = 0.019 yr^{-1}). Rapid drying trends were found for 1663−1701 ($p < 0.0001$, slope = 0.050 yr^{-1}) and 1882−1922 ($p = 0.0008$, slope = 0.054 yr^{-1}). The driest periods in our reconstruction, either especially intense or long-duration, were 1560−1565 (mean = −1.52), 1574−1579 (−1.15), 1604−1615 (−1.04), 1634−1638 (−1.74), 1683− 1701 (−0.55), 1715− 1724 (−0.63), 1767− 1782 (−0.69), 1804−1812 (−0.74), 1842−1849 (−1.25), 1916−1922 (−1.86), 1966−1970 (−1.86), and 1987−1991 (−1.08). The wettest were 1551−1559 (0.84), 1592−1600 (0.83), 1616−1623 (1.12), 1663−1678 (0.77), 1726−1733 (0.73), 1745−1749 (1.00), 1757−1765 (0.50), 1824−1835 (0.60), 1850−1861 (0.71), 1877−1885 (0.85), 1900−1904 (1.41), 1934−1939 (0.67), 1950−1954 (1.19), 1956−1965 (0.68), and 1971−1986 (0.79). For easier visualization, some of the above information is reflected in Fig. 2.7. The most extreme decades (≥ 0.50 SD from mean) were graphically depicted. Of these decades, the most extreme pluvials were 1616−1625, 1666−1675, and 1977−1986, the most extreme droughts 1559−1568, 1604−1613, 1631−40, 1773−1782, 1840−1849, and 1916− 1925.

Toward putting climate of the modern era into a historical perspective, we more closely examined the most extreme non-overlapping half-decades from 1895−2014 according to the reconstruction (Fig. 2.8a), quantifying the return intervals of these extreme events relative to the 1546−2014 reconstruction (Fig. 2.8b). The most extreme 5 yr pluvials were 1900−1904, 1950−1954, 1960−1964, and 1982− 1986 (Fig. 2.8a). If one were to look only at the last 120 yr,

one would think these intervals were more common than they were from a historical perspective. Extreme 5 yr pluvials such as these four occurred every 116, 29, 23, and 58 yr within the 1895−2014 period, while they occurred just every 155, 47, 33, and 93 yr from 1546−2014 (Fig. 2.8b). The most extreme 5 yr droughts were 1906−1910, 1917−1921, 1966−1970, and 1987−1991. From 1895−2014, these extreme half-decades occurred once every 10, 116, 58, and 13 yr, while from 1546−2014 they occurred only once every 15, 465, 233, and 19 yr. This tendency, for extremes to be more frequent in the most recent 120 yr than in the rest of the reconstruction, held for the less extreme 5 yr pluvials and droughts too (Fig. 2.8b).

From the perspective of human-delineated centuries, the driest were the 17th (mean = −0.035 ± 0.101 SE) and the 21st (mean = −0.098 ± 0.221 SE) (Fig. 2.9a). The wettest were the 16th (mean = 0.032 ± 0.152 SE) and the 20th (mean = 0.031 ± 0.122 SE). However, these differences were not significant; there were no among-century differences in the mean (1-way ANOVA; F = 0.091, df = 5463, p = 0.994). The most variable centuries were the 16th and 20th (SD = 1.12, 1.22), the least the 18th (SD = 0.79). These variability differences are corroborated by the number of extreme events per century (Fig. 2.9b). The 16th century was one in which extreme drought years (−1 SD) occurred about once every four yr (frequency = 0.278), extreme pluvials (1 SD) about every fifth year (frequency = 0.222). In the 20th century, extreme drought years occurred about once in 5 yr (0.220 frequency), extreme pluvial years about every fourth year (0.260 frequency), whereas over the reconstruction at large the frequency of extreme droughts and pluvials was about every 6 yr (0.168 and 0.164, respectively). Additionally, the 20th century contained the only −3 SD year. By contrast, the least variable century, the 18th, had frequencies

for drought and pluvial years of 0.110 and 0.080, respectively. For pluvial years, there was a significant deviation from the null hypothesis of equivalent frequencies per century (chi-squared goodness-of-fit χ^2 =12.62, df = 5, p = 0.027). However, there was no significant difference in frequency of extreme drought years among centuries (chi-squared goodness-of-fit χ^2 = 8.94, df = 5, p = 0.111).

Discussion

Our reconstruction model explained 26.6% of the variability in prior-July–September Palmer Z index. Doubtless, this relatively low number is due in part to a paucity of weather station data near our island site (http://www.ncdc.noaa.gov/cdo-web/datatools/findstation). Although we relied on a regionally coarse estimate for all northwest lower Michigan (Fig. 2.1), pilot analysis revealed it worked better than any single station in isolation. The low variance explained may also reflect the relatively benign, cool and moist climate of northeastern North America, especially since our island site is buffered from extreme summer heat by Lake Michigan. Benign climates lead to low correlations between tree ring chronologies and climate (Fritts 1976). Cook et al. (1999) reconstructed summer drought throughout the continental USA, and their tree ring-climate verification statistics were lowest in the upper Midwest and New England. Finally, it could be specific to white cedar *Thuja occidentalis*. In using that species to reconstruct precipitation in adjacent Ontario, Canada, Buckley et al. (2004) found r^2 = 0.36 in their calibration period and lower values in each of their verification periods, with the growth-climate relationship in the more recent of the two verifications largely deteriorating.

The phenomenon of growth-climate relationships deteriorating in recent decades has been found in many tree ring chronologies (D'Arrigo et al. 2008, Saladyga & Maxwell 2015, Maxwell et al. 2016), but it was not observed in this dataset. Our growth-climate relationship was consistent across each half of the dataset (Table 2.1), as well as in each 60 yr window overlapping with those halves (Fig. 2.4). There was variability, but overall there was no great difference between the minimum $r^2 = 0.239$ and maximum $r^2 = 0.415$. Numerous hypotheses have been put forth to explain the phenomenon in which tree growth-climate relationships have deteriorated, especially for high northern latitudes, where it is posited that global warming has rendered tree growth less limited by insufficient heat, thereby weakening the growth-temperature relationship over time (D'Arrigo et al. 2008). At our site, the study variable, Palmer Z index, did not have a significant trend over the modeled period, 1895− 2014; this was true of the reconstruction (linear correlation, $p = 0.52$) and observational record (linear correlation, $p = 0.16$). The lack of change in the study variable may explain why tree growth relationships with it did not deteriorate. Additionally, Maxwell et al (2016) found that the deteriorating growth-precipitation relationships he observed were due to a lack of droughts in the calibration period, but our calibration period did contain significant droughts (Figs. 2.6, 2.7, & 2.8a).

Though our r^2 was relatively low, we are confident in the model and reconstruction because the RE and CE values exceeded zero, a rigorous quality check. Other tree ring-based reconstructions have reported similar r^2, RE, and CE values for all or part of their study period for all or some of their tree ring chronologies, mostly in humid eastern North America (Cook et al. 1999, Maxwell et al. 2011, 2012, Ford 2014), but sometimes even in the drier North

American Great Plains (Cook et al. 1999). Our finding that summer moisture is most important to growth is consistent with other similar studies in temperate North America. Palmer Z index incorporates both incoming and outgoing moisture, i.e., precipitation and evapotranspiration. This is consistent with the wealth of literature that has found temperate tree growth consistently correlated negatively with temperature, and positively with precipitation (e.g., Martin-Benito & Pederson 2015, D'Orangeville et al. 2018, LeBlanc & Berland 2019, Harvey et al. 2020). In agreement with our results, *T. occidentalis* in adjacent Ontario was most strongly correlated (inversely) with prior-July/August maximum temperature (Kelly et al. 1994). Conversely, inverse correlations with current June temperature were the most consistent along a 3-degree latitudinal gradient in Quebec, though that is far to the north of our site (47–50° vs. 45°) (Housset et al. 2015). It may be counterintuitive that prior-year, not current-year, conditions can most influence radial growth, but this is not anomalous. Favorable weather at $year_{t-1}$ leads to strong root growth, starch storage, budset, and leaf production, which can boost radial growth at $year_t$, particularly in evergreen trees, which will still have leaves from $year_{t-1}$, the boon year, at $year_t$. Palmer Z index was better correlated with growth than were other moisture indices. Unlike PDSI and PHDI, the Z index has no memory. It reflects conditions in the current month(s) only (Heim 2002). Our Z index-based model performed better than the PDSI- and PHDI-based models because *T. occidentalis* growth is correlated primarily with mid- to late summer conditions of either the prior or current year (Kelly et al. 1994, Housset et al. 2015). In early summer months, the magnitude is weaker, and in spring correlations are either weaker or the inverse of the summer. Growth relationships with spring temperature are often positive (Kelly et al. 1994, Housset et al. 2015) and with precipitation negative (Kelly et al. 1994,

Housset et al. 2015). This would potentially confound the reconstruction of an index which incorporates conditions from several preceding months. To repel confusion, it should be reiterated that while the Palmer Z index has no memory, tree growth does have memory and can thus be affected by prior-year Palmer Z.

Our reconstructed moisture conditions did not reveal the most recent several decades to be remarkably wet, either in the reconstruction or the observed record, and this contrasts with a recent moistening trend found in the instrumental record for Indiana/ Illinois (Mishra & Cherkauer 2010) and Michigan (Andresen 2012, http://www.ncdc.noaa.gov/cag/statewide/time-series/20/pcp/ann/9/1895-2019) and with some other dendroclimatic reconstructions in northeastern North America. Ford (2014) found a moistening trend in Iowa from about 1940 to present, with the most recent 20 yr of recorded annual precipitation, 1984−2013, greater than any other 20 yr period, recorded or tree ring-reconstructed, back to 1640. However, the results for Michigan and Iowa were based on precipitation alone, not a drought index like Palmer Z, which incorporates both incoming and outgoing moisture. Pederson et al. (2013) did reconstruct a moisture index, May−August PDSI, in southeastern New York back to 1531 and found the most recent 43 yr period to be uniquely moist and an overall moistening trend extending back to about 1800. Cook et al. (1999), too, reconstructed a moisture trend. At their studied geographic point nearest to our site, in northwest mainland lower Michigan, over the period common to our study, 1546−2003, they found a slight but significant moistening trend in June−August PDSI (linear correlation, $r = 0.107$, $p = 0.026$). We found neither the 20th nor 21st century to be particularly moist but did find a 5 yr and two other 10 yr pluvials in the second half of the 1900s (Fig. 2.7). In agreement

with our study, Buckley et al. (2004) did not find a moistening trend in adjacent Ontario, with none of their most moist decades occurring after the 1830s. Differences among studies may reflect different variables and time windows examined, as well as local-scale climatic differences.

We found three severe 6 yr droughts in the late 1500s: 1560−1565 (mean = −1.52 SD), 1574−1579 (−1.15), and 1586−1591 (−0.73) (Fig. 2.6). Signatures of drought during this time—the Late 16th-Century Megadrought—have been found widely in North America, including in the mid-Atlantic (Stahle et al. 1998, Maxwell et al. 2011), Southwest (Grissino-Mayer 1996), throughout the West (Fritts 1965), Arkansas (Stahle et al. 1985), and elsewhere (Woodhouse & Overpeck 1998). This dry episode has been implicated for being potentially causal to several important events of human history, including the abandonment of pueblos in New Mexico by indigenous people (Douglass 1935, Schroeder 1968, Burns 1983), the disappearance of the Lost Colony of Roanoke Island, Virginia (Stahle et al. 1998), conflict between American Indians and the Spanish, and abandonment of the Santa Elena colony on Parris Island, South Carolina (Anderson et al. 1995), and perhaps even the Chichimeca War in Central Mexico (Stahle et al. 2000). Future research in our group will focus on the effects of prerecorded climate on the indigenous peoples of the upper GLR, particularly their degree of reliance on maize horticulture.

We also found correlation with the nearby reconstruction of Cook et al. (1999) and with Buckley et al. (2004), the latter working just across Lake Huron from northern lower Michigan. They and we found droughts in the 1600s decade, the 1770s, the 1840s, and the 1910s, and a

pluvial in the 1830s, though there were also periods both dry and wet which did not coincide. Unlike us, they did not find the Late 16th-Century Megadrought.

Although drought conditions dominated the late 16th century, we also found that century to include pluvials in the 1550s, 1580s, and 1590s (Fig. 2.6). The late 16th century was a variable time (SD = 1.12), though not to the same extent as the 20th century (SD = 1.22) (Fig. 2.9b). This is consistent with the observation and expectation that climate change has made and will continue to make climate more variable (Medvigy & Beaulieu 2012, Christensen et al. 2013). Additionally, Maxwell et al. (2012) found the 20th century to contain both the most extreme wet and dry decades in an 800 yr May precipitation reconstruction in the mid-Atlantic Region.

Indeed, some of the events in the 20th century were unusual in their extremity. The year 1921 was the only year of the entire reconstruction 3 SD from the mean, −3.01, and 1917−1921 was the worst 5 yr drought of the entire reconstruction (Fig. 2.9). There was a general tendency for the extreme 20th century events to be more common in that century than in the reconstruction at large. For example, the 1966−1970 drought had a 20th-century return interval of 58 yr and for the entire reconstruction a return interval of 233 yr. It was the same for pluvials. The 1900−1904 and 1982−1986 wet events had 20th-century return intervals of 116 and 58 yr, respectively, and entire reconstruction return intervals of 155 and 93 yr. The high prevalence of extreme droughts in the 20th century, coupled with predictions of increased temperature without significant increases in summer/fall precipitation (Hayhoe et al. 2010, Byun & Hamlet 2018), suggest that extreme droughts will be more common in the coming century than in the last several.

In future research, we will use our climate reconstruction to better understand the history of human habitation and use of South Manitou Island, proximal islands, and the nearby mainland (Lovis et al. 1976, 2017, 2020). Further, additional climate reconstructions must also be conducted in the GLR. The region has lost the great majority of its old-growth forest, but significant remaining pockets present a trove of uncollected data. There are numerous long-lived species in the region (Rocky Mountain Tree-Ring Research, Inc. & the Tree Ring Laboratory of Lamont-Doherty Earth Observatory and Columbia University 2013), with tree rings known to reflect climate in the region (Graumlich 1993), including *Tsuga canadensis*, *Pinus strobus*, *P. resinosa*, *Acer saccharum*, *Quercus alba*, and *Betula alleghaniensis*. When it is desirable to avoid coring living trees, alternatives should be sought such as dead trees, fallen logs, stumps, and structures with beams of a known geographical source (Larson & Rawling 2016). The unfortunate imminent decline of the long-lived *T. canadensis* to hemlock woody adelgid could provide an opportunity to obtain more data. To preserve data sources, park policies banning backcountry campfires, and wood collection even in the front-country, are needed, such as the policy of Bruce Peninsula National Park, Ontario, in the heart of ancient *T. occidentalis* country.

Conclusion

We derived a composite ring width index chronology from a living old-growth stand and from ghost forest stands of white cedar *Thuja occidentalis* in northern Lake Michigan and modeled it against observations of late summer moisture conditions (Palmer Z index). The model was consistent throughout the observational record and was used to reconstruct moisture conditions back to 1546 C.E. The first half-century of the reconstruction included

three 6 yr droughts, each with moisture levels ≤0.73 SD from the mean. This corroborates a body of literature documenting a widespread severe drought in late 1500s North America. Other extreme droughts (≤0.75 SD) were found throughout the record including 10 yr episodes in the 1600s/10s, 1630s,1770s 80s, 1840s, and 1910s/20s. Ten-year pluvials (≥0.75 SD) were found in the 1610s/20s, 1660s/70s, and the 1970s/80s. The 20th century was the most variable century of the reconstruction and was a period during which both pluvials and droughts occurred with a greater frequency than in the reconstruction at large. As climate variability and late summer heat continue to increase, society should prepare to cope with extreme drought even in humid regions.

APPENDIX

APPENDIX

Figures

Figure 2.1. Study site, South Manitou Island, is indicated by a red square off northwest lower Michigan. The subsites Dunes and Valley of the Giants are indicated, respectively, with blue and red pins. Boundaries within Michigan are counties; counties with an asterisk represent US Climate Michigan Division 3.

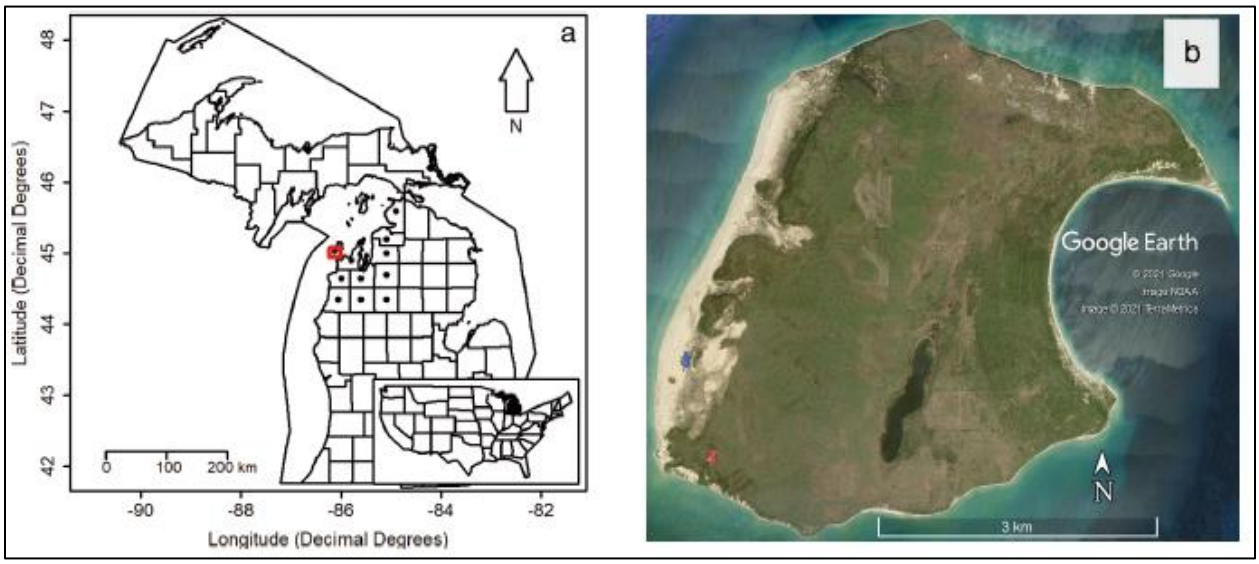

Figure 2.2. Rooted tree in paleosol in the dune field on South Manitou Island (photo credit: Alan Arbogast).

Figure 2.3. Ring width index (purple), sample size (green), expressed population signal (EPS; dark blue) over time, and year at which our chronology was truncated due to insufficient sample size (<1 tree [<3 cores]; black vertical line). EPS measures how well a finite sample represents a theoretical infinite population (Wigley et al. 1984) and was calculated in 50 yr windows, overlapping by 49 yr. The first plotted value in 1565 represents the window 1516−1565. Before 1516, sample size is 1; thus, there are no EPS values prior to the window beginning at that year. Our predetermined EPS minimum was 0.80 (D'Orangeville et al. 2018), a threshold which each of our 50 yr windows exceeded. Ring width index and EPS, both unitless, are plotted on the same axis.

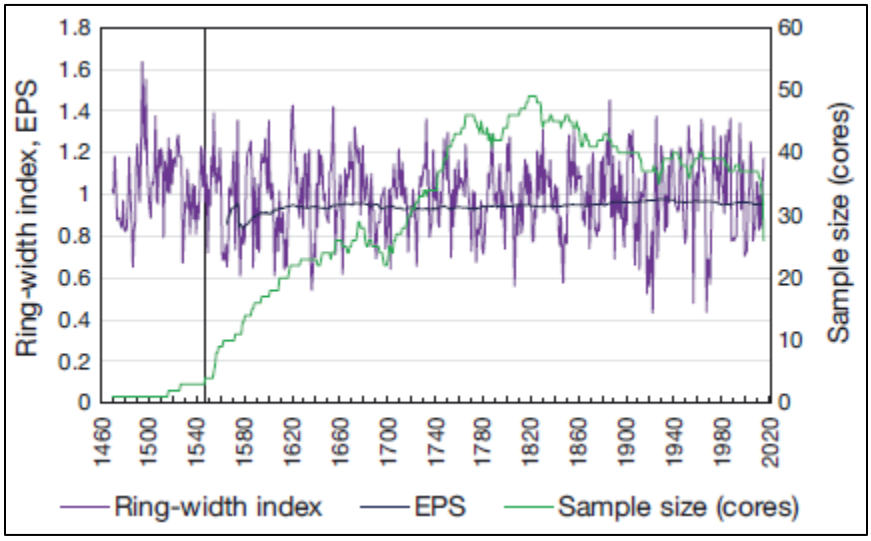

Figure 2.4. Evolution of the relationship between observed year$_t$ July−September Palmer Z index and year$_{t+1}$ *Thuja occidentalis* ring width index. The relationship was modeled over 60 yr windows overlapping 59 yr, i.e., 1896−1955, 1897−1956, . . ., 1956−2015.

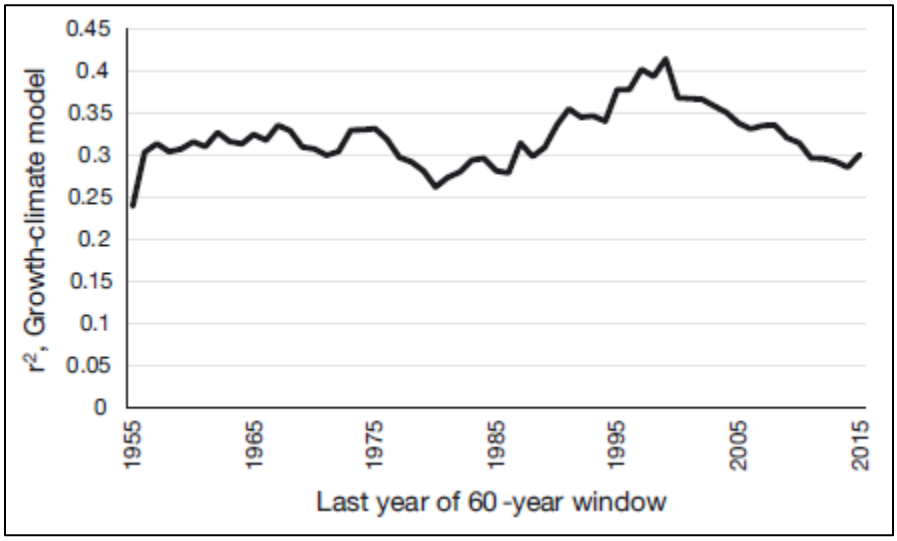

Figure 2.5. Standardized observed vs. reconstructed Palmer Z index (a) and standardized observed, reconstructed Palmer Z Index vs. time (b). Dashed black line in (a) is the best fit estimated by linear regression.

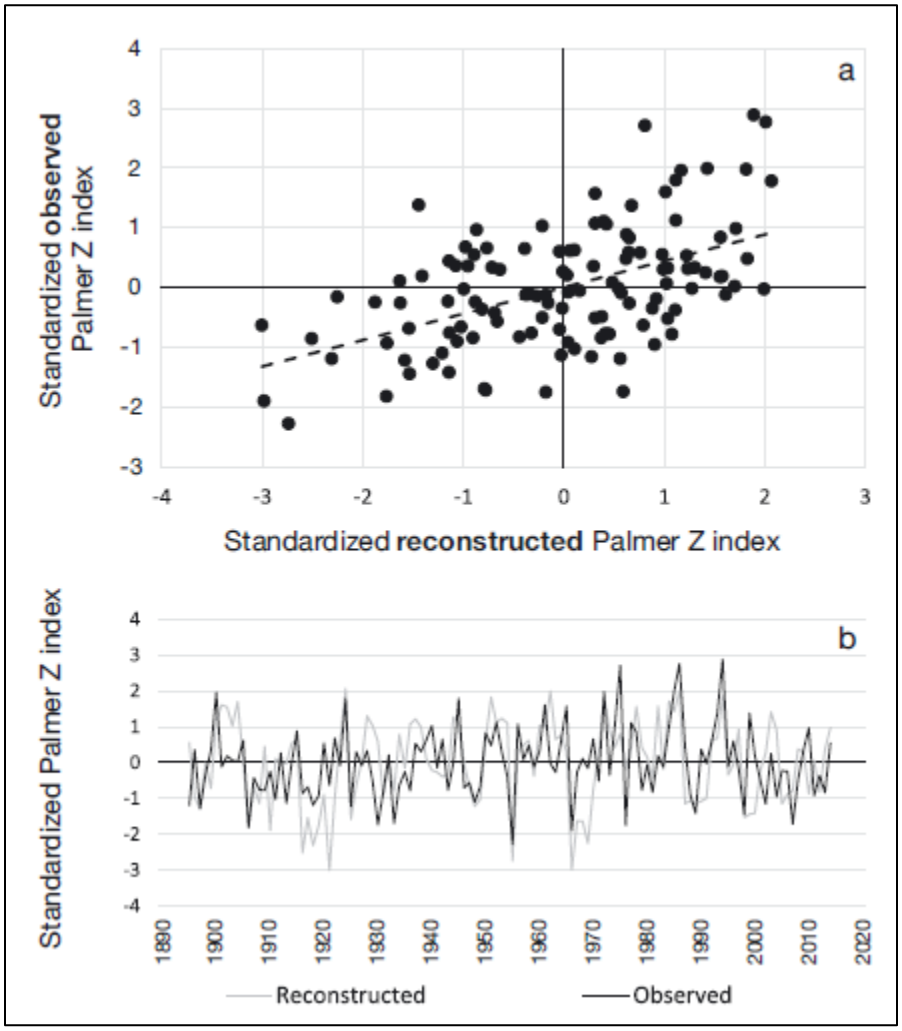

Figure 2.6. Reconstructed annual (gray) and 9 yr moving average (black) of standardized July–September Palmer *Z* index, 1546–2014. The year at which the moving average is plotted is the middle year of the 9 yr window.

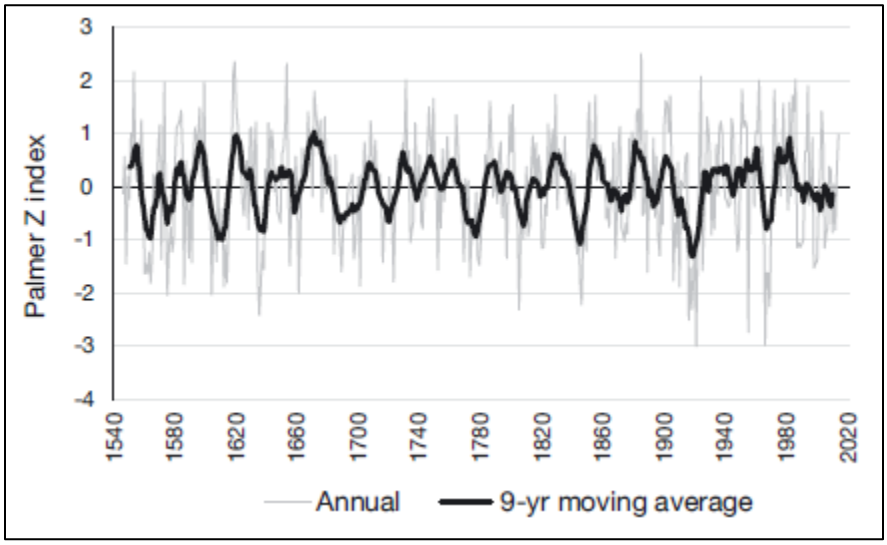

Figure 2.7. The most extreme 10 yr non-overlapping pluvial and non-overlapping drought events, defined here as having a mean standardized reconstructed Palmer Z index ≥|0.50|, over the entire reconstruction. Year on the *x*-axis is the last year of the decade, for example, 1559 represents 1550–1559.

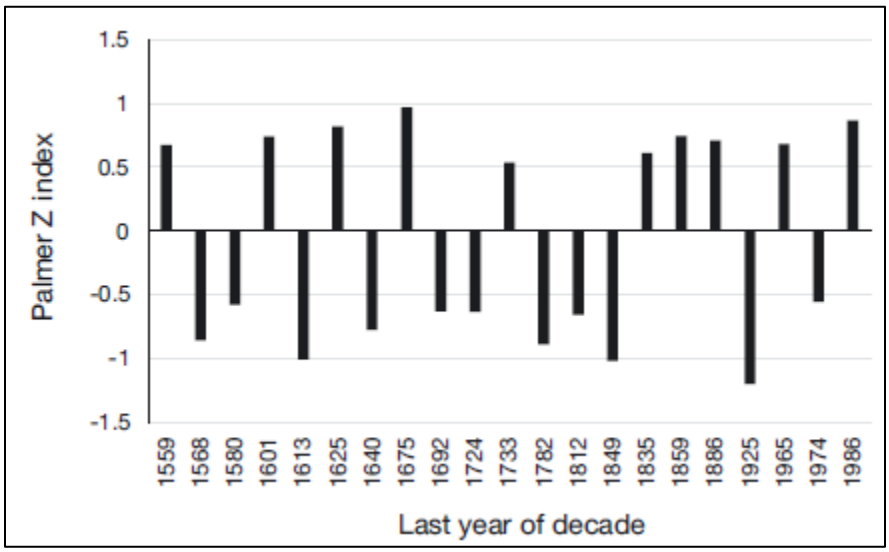

Figure 2.8. Reconstructed extreme 5 yr non-overlapping events over 1895−2014, the common period of the reconstruction and observational record (a) and the return interval of extreme 5 yr periods over 1895−2014 and 1546−2014 (b). Extreme events are here defined as having a mean standardized Palmer Z index ≥ 0.50. Year on the *x*-axes is the last year of the 5 yr period, for example, 1904 represents 1900−1904. All extreme events of the observational record corresponded to extreme reconstructed events. In cases where an extreme event was reconstructed but not reflected in the observational record, the corresponding mean over the observational record is still displayed. Numbers above the bars are the return intervals in years.

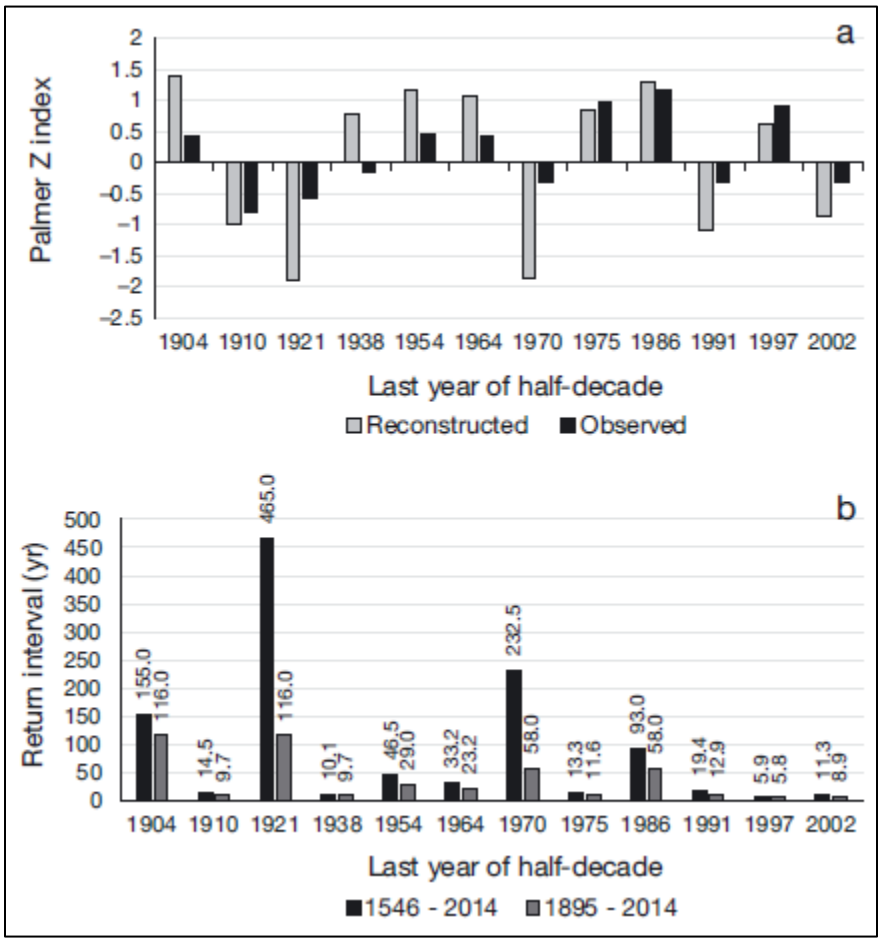

Figure 2.9. Mean and SD of standardized reconstructed Palmer *Z* index per century (a) and number of extreme years and their frequency throughout each century and the entire reconstructed period (b). In (a) the error bars on the gray columns are the standard error of the mean; there were no significant differences in the mean among centuries (1-way ANOVA, p-value >0.05). In (b) the number above each bar is the frequency of extreme years within each period.

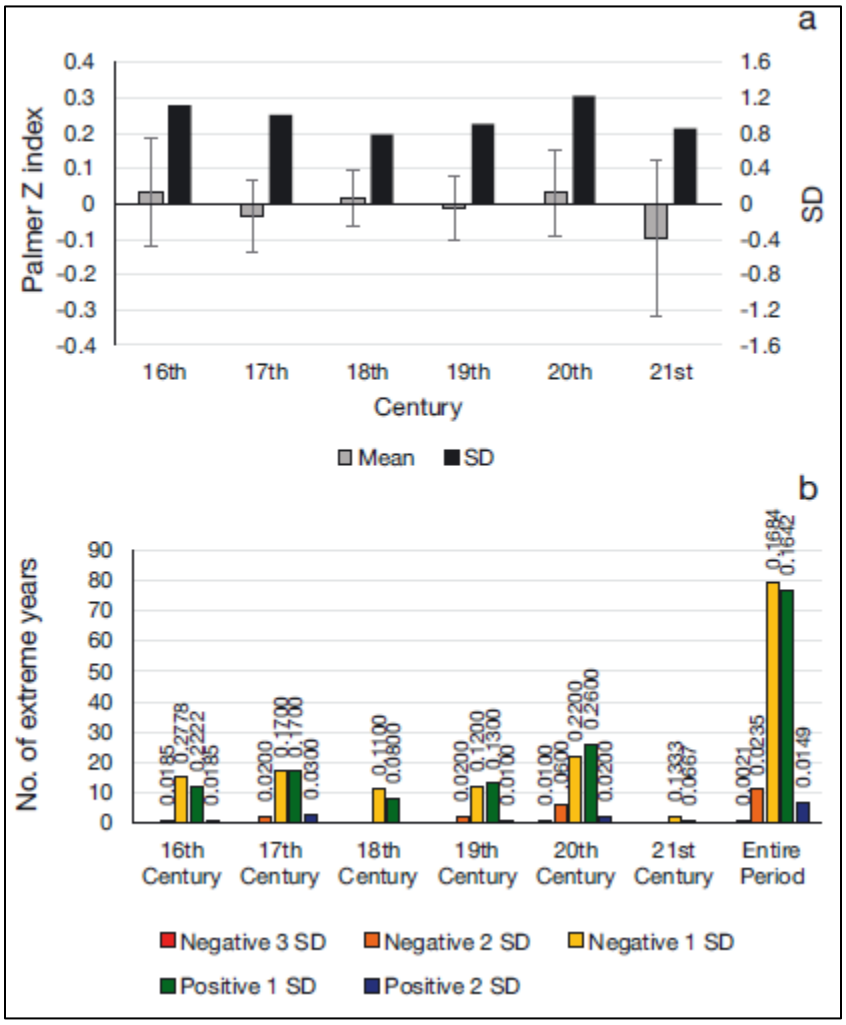

Tables

Table 2.1. Statistics and coefficients for models relating $year_t$ July–September Palmer Z index and $year_{t+1}$ *Thuja occidentalis* ring width index. RE: reduction of error; CE: coefficient of efficiency—see Methods section for more details (Fritts 1976, Cook et al. 1999). NA: not applicable.

Period	July–Sep Palmer Z Coefficient	r^2	RE	CE
Calibration (1896–1955)	0.0960	0.239	NA	NA
Verification (1956–2015)	0.0818	0.301	0.259	0.202
Full Model (1896–2015)	0.0855	0.266	NA	NA

CHAPTER THREE

IN GREAT LAKES REGION MESIC FORESTS, CONTEMPORARY GROWTH-CLIMATE RELATIONSHIPS SUGGEST THAT SOUTHERLY TREE POPULATIONS ARE MOST VULNERABLE TO CLIMATE CHANGE

Abstract

The North American Great Lakes Region is forest-rich and ecologically important, yet relationships between tree growth and climate there have been insufficiently quantified and the temporal consistency of those relationships insufficiently assessed. A network of 46 tree-ring-width chronologies, 35 previously unpublished was established. The network included nine species from 12 sites along an eight-degree latitudinal gradient in Indiana and Michigan. I sought to compare growth and growth-climate relationships within and among tree species and to examine how temporally consistent those relationships were.

Relationships between tree-ring widths and monthly temperature and precipitation were quantified and compared among species and sites. Principal components analysis was conducted to identify patterns in ring-width anomalies and growth-climate relationships within and among species. The temporal consistency of growth-climate relationships was examined along moving intervals with bootstrapped correlation analysis.

The most consistent growth-temperature relationship was a negative association with current-June mean temperature. The most consistent growth-precipitation relationship was also in the current-June month; in this case, the relationships were positive. This was true throughout the gradient but especially in the south, and this held when species were pooled or

considered individually. Relationships with some climate variables were inconsistent. For example, the relationship between growth and prior-September precipitation went from r = 0.226 in the first interval examined, 1904–1937, to r = -0.030 in the final interval, 1971–2004. However, the strongest growth-climate relationships were stable over time.

Strongly and temporally consistent negative growth-June-temperature and positive growth-June-precipitation relationships portend a future of reduced radial growth as climate change proceeds. Further, the temporal consistency suggests that growth-climate modeling is a reliable method for reconstructing past climate and predicting future growth in the region, when the most growth-influencing variables are used in the model.

Introduction

The Great Lakes Region (GLR) of North America contains ample, diverse forests which play important ecological and economic roles. In Michigan, the annual state and regional economic impact of the timber industry is $14 billion (Leefers 2017). There are more than 20 million acres of forest, including 56% of the land area and amounting to 1,400 trees for every person (Dickmann & Leefers 2016). The region has a high concentration of tree species' distribution limits, both northern and southern, because of the tension zone—a diffuse region in which the hardwood forests dominant in the south gradually give way to the mixed hardwood-conifer forests of the north (Andersen 2005)—allowing the comparison of southern- and northern-range-margin populations.

Most of the region experienced alternating cycles of glacial and interglacial conditions over the last 800,000 years, the most recent being the Wisconsin glaciation, the peak of which

was ≈24 kya. This glaciation is responsible for most of the current soil types, topography, and lake levels (Larson and Kincare 2009). The variation in soils affects modern vegetation, with mesic plants growing in fertile, coarse-textured soils and xeric plants in dry, sandy soils (Harman 2009).

The contemporary climate of the region is unique due to the temperature-moderating, moisture-influencing Great Lakes. Due to the predominantly west-flowing wind, both major peninsulas of Michigan are downwind of a Great Lake, resulting in an overall more wet, cloudy, snowy, and moderate climate than areas upwind (Andresen & Winkler 2009). Recent climate change has resulted in a generally warmer, wetter regime. Widespread reliable weather data collection began in 1895 in Michigan. From then through 2019, mean annual temperature increased by 0.127 °C/decade and total annual precipitation by 1.09 cm/decade (http://www.ncdc.noaa.gov/cag/statewide/time-series/20/tavg/ann/9/1895-2019, http://www.ncdc.noaa.gov/cag/statewide/time-series/20/pcp/ann/9/1895-2019).

Long-term forecasts for North America predict further increasing precipitation and temperature. Mid-century projections under Representative Concentration Pathway (RCP) 4.5 predict precipitation increases in the northern part of the continent, particularly in winter, but also summer, and for temperature to increase beyond the range of natural variability for all the continent (Christensen et al. 2013). For the GLR, Byun & Hamlet (2018) predict a 6.5 °C increase by 2100 under RCP 8.5 and 3.3 °C under RCP 4.5. Their predictions for precipitation are more equivocal. Under RCP 8.5, the GLR may experience a 5–25% increase in annual precipitation by the 2080s, with large increases in winter/spring and perhaps little change in summer/fall. This is consistent with a previous prediction, as well (Hayhoe et al. 2010).

With the unique climate and diversity of forest types, climate change responses among tree species may be unique in the GLR. In any case, it is important to anticipate how the major tree species will be affected to inform conservation and forest management. For example, will tree growth responses to climate change in the region be more species-specific or site-specific? In some studies of the tree growth-climate relationships in Eastern North America, growth-climate relationships are more similar within species across sites than within sites across species. In the Hudson River Valley, Pederson et al. (2004), found that species-specific differences in growth-climate relationships were bigger than site-specific differences, suggesting that the species at a given site will not respond uniformly to climate change. Similar results were found by Gruamlich (1993) in the Western Great Lakes Region and by Cook et al. (2001) in the U.S. West Gulf Coast, at least at the more environmentally benign sites. By contrast, growth-climate relationships were more similar across sites than across species along a latitudinal gradient in the eastern United States (Martin-Benito & Pederson 2015).

In this regard, the GLR remains understudied. There does exist a latitudinal comparison of growth-climate relationships among several species in Wisconsin and the Western Upper Peninsula of Michigan (Graumlich 1993), a model predicting how different trees will migrate under ongoing climate change (Walker et al. 2002), a model of climate change vulnerability for 11 Michigan tree species (Penskar & Derosier 2013), and work on the growth-climate relationships of trees in the Lower Great Lakes Region (Maxwell et al. 2016, Au et al. 2020), but a better understanding of how the major tree species are affected by climate is required. Further, there is evidence that growth-precipitation relationships are weakening over time in Indiana (Maxwell et al. 2015). The potential temporal inconsistency in growth-climate

relationships has implications both for tree-ring-based climate reconstruction and forecasts of future growth and productivity. Is the deteriorating growth-precipitation relationship a wider trend in the GLR?

Below I present a study on the growth-climate relationships of nine major tree species in Indiana and Michigan. My objectives were to (1) quantify growth-climate relationships, (2) compare relationships within species, (3) among species, and (4) among groups based on position relative to the species' overall range, and (5) test the temporal stability of those relationships.

Methods

The Study Region

The study region includes 12 sites along a latitudinal gradient from southern Indiana at 38.54 °N to the Upper Peninsula of Michigan at 46.88 °N (Fig. 3.1, Table 3.1). According to one estimate, this 8.34° gradient would be equivalent, in terms of temperature lapse, to an altitudinal gradient of 1668 m (Montgomery 2006). In selecting sites, mature forests were sought with the aim of finding trees old enough that their growth could be compared against the regional climate record which generally extends from 1895 to the present. To control somewhat for site conditions, forests of the mesic type were selected, a common, important type in the region (Cohen et al. 2014). Overall, site selection was a balance of including a wide latitudinal gradient while efficiently using limited resources.

The Study Species

Ecologically and economically important species that occur commonly as canopy dominants in the region's mesic forests were selected, including the southerly beech-maple type and northerly northern-hardwoods type (Table 3.1). Additionally, species with long lifespans were preferred, again to maximize the length of the dataset. Some of the species' ranges span the entire study region: *Acer saccharum* Marshall (sugar maple), *Fagus grandifolia* Ehrh. (American beech), and *Quercus rubra* L. (red oak). Others find a northern limit in the region, *Carya ovata* (Mill.) K. Koch (shagbark hickory), *Liriodendron tulipifera* L. (tulip poplar), and *Quercus alba* L. (white oak), and others a southern limit, *Betula alleghaniensis* Britton (yellow birch), *Pinus strobus* L. (eastern white pine), and *Tsuga canadensis* (L.) Carrière (eastern hemlock). Chronologies derived for *A. saccharum* and *Q. alba* from Price Nature Center (PNC) and from Voorhees (Vrh) and Warner (War) Audubon Sanctuaries were published previously (Au et al. 2020). Chronologies for *A. saccharum* (Au et al. 2020), *L. tulipifera*, Q*. alba*, and *Q. rubra* from Pioneer Mothers Memorial Forest (PMF) (Maxwell et al. 2015), *C. ovata* from PMF (Maxwell & Harley 2017), and *T. canadensis* from Huron Mountain Club at Rush Lake (HMC) (Dye & Woods 2019) also were published previously.

Field Methods

Of the 46 populations that ultimately went into this study, 40 were selected *a priori*. These included all but *T. canadensis* at HMC and *A. saccharum*, *C. ovata*, *L. tulipifera*, *Q. alba*, and *Q. rubra* at PMF. For those 40 populations, field work was conducted from 2016–2018 at 12 sites, sampling between one and five species per site, from nine species. Upon arrival at a site, a

general reconnaissance was performed to identify suitable stands. Suitable stands were defined as ones with at least ten trees per focal species which appeared to be mature. Trees then were selected from throughout these suitable stands to minimize within-stand differences, targeting mature trees. Making the most of limited resources, between 10 and 27 trees were sampled per species per site, obtaining generally two cores per tree but occasionally only one or up to four. According to stipulations from landowners/managers, for some populations only living trees were cored and from others both living and dead trees. In the case of standing trees, all cores were taken at breast height (1.37 ± 0.5 m) or the equivalent position along a downed tree.

For the other six populations, data were obtained from other researchers. For *A. saccharum*, C*. ovata*, *Q. alba*, *L. tulipifera*, and *Q. rubra* at PMF, field work was done in 2012–2014, using methods consistent with those described above, except the sample size for *C. ovata* was six trees (Maxwell & Harley 2017, Au et al. 2020). For *T. canadensis* at HMC, field work was done in 2016; all trees with diameter at breast height greater than 10 cm were sampled within two 16-m radius plots, for a total of 52 *T. canadensis* trees which were suitable to my study based on temporal coverage (Dye & Woods 2019).

Core Processing, Cross-Dating, and Detrending

Cores were air dried and glued to wooden mounts, then sanded with a palm sander using progressively finer grades of sandpaper beginning with 120- or 150-grit and ending with 400- or 600-grit, depending on species. The 120-grit grade was used only for hardwoods. With the conifers, 150-grit was the first grade used. For some *A. saccharum* populations, 600-grit was

the final grade used because that species often had quite narrow rings that were difficult to see. For all other species, 400-grit was the final grade used. To ensure the calendar date of each tree ring was known, cross-dating was performed across the cores of each population. Cross-dating was accomplished according to either the list (Yamaguchi 1991) or skeleton plot method (Stokes & Smiley 1996), depending on species. The list method is a simpler, less conservative approach that was used only for some populations of the most easy-to-date species (i.e., *L. tulipifera*, *Quercus spp.*, and *C. ovata*. Methods applied to cores in previous studies are reported in their respective publications (Maxwell & Harley 2017, Dye & Woods 2019, Au et al. 2020).

Depending on the chronology, tree-ring widths were measured either to a resolution of .001 millimeters using a Velmex measuring system (Velmex, Bloomfield, NY, USA) or to .01 millimeters in the computer program CooRecorder (version 9.0.1, Cybis Elektronik & DATA AB, Saltsjöbaden, Sweden) or in some cases the program WinDendro (Regent Instruments, Sainte-Foy, Quebec, CN). In the case of computerized ring-width measuring, digital images were generated for each core by scanning them with a flatbed computer scanner at a resolution of 1200–3200 dpi, depending on core length. Initial cross-dating was confirmed by running for each population all the ring-width measurement series through program Cofecha (Holmes 1983). Potential cross-dating issues were flagged by the program, and these issues were troubleshot by checking for measurement errors or misplaced missing or false rings. Revised ring-width series were re-run through Cofecha until successfully cross-dated or eliminated due to failure in the cross-dating process. In total, fewer than 5% of cores were discarded, either due to severe rot or failure to cross-date.

Non-climatic trends due to endogenous stand dynamics or tree age/size were dampened through standardization and detrending in program ARSTAN version 44 (Cook 1985). First, all pre-1895 years were excised from ring-width series because they were not relevant to this dendroclimatological study due to the absence of meteorological data prior to 1895. Further, sample sizes tended to be low that far in the past, rendering cross-dating less reliable. In ARSTAN, indices were calculated by dividing observed ring widths by expected widths based on a fitted curve. The fitted curves were cubic smoothing splines, with a rigidity typically 40–70% the length of the cores in years, but occasionally as low as 20% or 30% to cope with isolated extremely exaggerated ring-width indices. Among the three detrended chronologies ARSTAN provides, I selected the Residual Chronology for further analysis because it was stripped of autocorrelation and is therefore suitable for regression analysis (Speer 2009), and it is frequently used in similar studies (e.g., Huang et al. 2010, Harvey et al. 2020, LeBlanc et al. 2020).

Quantifying and Comparing Growth-Climate Relationships

To quantify growth-climate relationships (Objective 1), the residual chronologies were run in program DENDROCLIM2002 (Franco & Biondi 2004) against monthly mean temperature and total precipitation data. For meteorological data, gridded 4 km × 4 km interpolations were obtained from the PRISM Climate Group (Daly et al. 2008). In a bootstrapping procedure, DENDROCLIM2002 randomly selects one ring-width index from the dataset, replaces it, randomly selects another, and so on, until 1000 ring-width indices are randomly selected and linearly regressed against the corresponding meteorological data. I used the interval common

to all 46 ring-width-index chronologies, 1903–2004. The climatological window ran from the May preceding the year of ring formation through the September of the year of ring formation.

To compare growth-climate relationships within and among species (Objectives 2 & 3), a combination of principal components analysis (PCA) and linear regression was employed. A correlation matrix was constructed consisting of 46 rows, one for each population, and 34 columns, one for each climate variable (17 months × 2 types of climate variables). Each cell corresponded to the correlation coefficient between a population's ring-width indices and a climate variable, as calculated in DENDROCLIM2002. Rather than focusing intensely on so many variables, the two most influential variables, one for temperature, one for precipitation, were retained for in-depth analysis and a handful of others for brief interpretation. The most influential variables were determined by calculating the absolute value of the mean across all populations. For each of the two retained climate variables, all species were pooled and linear regression of the 46 growth-climate coefficients vs. latitude was conducted. To compare growth-climate relationships within species (Objective 2), a subset of species, *A. saccharum*, *F. grandifolia*, and *Q. rubra* was selected, the three species for which at least seven populations were sampled in this study, enough to make a meaningful comparison along the latitudinal gradient. A similar approach was then taken, in that linear regression of the growth-climate coefficients for the two most influential climate variables vs. latitude was conducted (Martin-Benito & Pederson 2015, Harvey et al. 2020). To determine whether trends in growth-climate relationships were influenced by species' relative position within their overall distributions (Objective 4), species were also pooled according into the categories of 'Northerly', 'Southerly',

and ‘Trans-Gradient’ (Chapter 3 Methods, Subsection “Study Species); linear regression was employed within these categories as above.

Further, to identify general patterns within and among species in overall growth-climate relationships (Objectives 2 and 3), a wider subset of the 34 climate variables was retained. Because all growth-climate coefficients with a p-value < 0.05 were considered significant, 2.3 of 46 correlation coefficients for a given climate variable would be expected to turn out significant just by chance. I therefore retained only those climate variables for which 5 of 46 populations turned out significant, about double the number expected by chance (modified from Huang et al. 2010). Those climate variables were retained in a separate correlation matrix, and PCA was conducted on that matrix. Two biplots, one for principal components (PCs) 1 and 2 and one for PCs 3 and 4, were generated for visualization of patterns in growth-climate relationships.

To test the temporal stability of growth-climate relationships (Objective 5), DENDROCLIM2002 was again used, but instead of the 1903–2004 single-interval analysis, moving-interval analysis was conducted. The intervals were equal to 34 years, twice the number of predictors (17 months) for both mean temperature and total precipitation. Thus, the first interval was 1904–1937, the second 1905–1938, and so on up to 1971–2004. Rather than focusing on such a large number of variables (17 months × 2 classes of climate variables), the two climate variables which among all 46 populations changed the most over time, both the most dynamic temperature and precipitation variable, were retained for further analysis and interpretation (Harvey et al. 2020).

Results

General Chronology Characteristics

For 46 tree populations across nine species and 12 sites, I collected tree cores, established calendar dates for each tree ring, measured tree-ring widths, and detrended and standardized tree-ring-width series resulting in 46 ring-width-index chronologies (Table 3.2, Fig. 3.2). All chronologies extended back to 1895 except *B. alleghaniensis* at Beaver Island which extended to 1903. All chronologies extended up to at least 2011 except *F. grandifolia* at Colonial Point. That chronology was truncated after 2004, because the population developed symptoms of beech-bark disease, a potentially confounding factor, around 2005 (Adam Schubel pers. comm.). Sample size for each population ranged from 6 trees/12 cores to 52 trees/84 cores. Sample quality was assessed with the expressed population signal (EPS), which measures how well a finite sample represents the total population (Wigley et al. 1984 but see Buras 2017). My predetermined minimum EPS value of 0.80 was met by all populations (Table 3.2; D'Orangeville et al. 2018).

Comparing Tree-Ring Chronologies Across Populations

To identify general patterns in overall ring-width-index chronologies, PCA was conducted on a correlation matrix in which each row was a year and each column a tree population. Of the 46 PCs, one for each dependent variable (population), four were retained for interpretation, those which accounted for at least 5% of the variation (Legendre & Legendre 1998). The first four PCs together explained 55.6% of the variation in ring-width indices, the first 32.8%, the second 10.3%, the third 7.0%, and the fourth 5.5% (Fig. 3.3).

On the first PC, all populations loaded positively, with a general trend that the hardwoods loaded higher than the conifers and the southerly populations higher than the northerly ones (Fig. 3.3a). Loadings on this PC were correlated significantly and negatively with latitude (r = -0.552; Table 3.3). The second PC separated even more clearly the northerly and southerly populations. Loadings were significantly and positively correlated with latitude (r = 0.912; Table 3.3), with all populations north of the site at 43.3° N loading positively and 23/24 to the south of it, negatively (Fig. 3.3a). Taking the first two PC's together, which collectively explain 42.8% of the variability, both species and site are important for determining ring-width anomalies. Generally, populations cluster together within sites, i.e., they have similar loadings on both PCs. This is particularly evident at PMF (38.5 °N), Mary Gray Bird Sanctuary (MGB, 39.6°), and Vrh (42.4°), all of which were sites where hardwoods alone were sampled. At sites where both conifers and hardwoods were sampled, there is still within-site clustering, but only when hardwoods and conifers are separated, particularly for the proximal sites of Maywood History Trail/Peterson Hemlock Grove (Mwd/Pet, 45.8°). Within subregions, i.e., latitudinal bands spanning 1–3°, there was within-species clustering, too. This was particularly evident with northerly populations of *T. canadensis*, *P. strobus*, *B. alleghaniensis*, and *A. saccharum*.

The third PC explained 7.0% of the variation, and it was not associated with latitude according to linear regression (r^2 = -0.242, p = 0.106). The mid-latitude populations tended to load negatively, and the high-latitude populations, other than the hemlocks, to load around zero (Fig. 3.3b). The high-loading populations included two classes: populations from the two most southerly sites and the hemlocks (all northerly). The fourth PC explained 5.5% of the variability. Along this component, *T. canadensis* was well separated from the other species,

loading quite positively. Taking these PCs together, the hemlocks clustered together, and the white pines also clustered together. Other than that, site was more important for determining growth anomalies. Within-site clustering was particularly evident at PMF (38.5° N), MGB (39.6° N), Vrh (42.4° N), and PNC (43.3° N).

The Strongest Growth-Climate Relationships, 1903–2004 Single-Interval

Relationships between radial growth and climate were estimated using bootstrapped correlation analysis in DENCROCLIM2002 over the common interval 1903–2004. Among the 17 months over which mean temperature (T_{mean}) was considered, the most important month was June of the current year, the year the ring was formed. The mean of the growth-JunT_{mean} correlation coefficient across all 46 populations was r = -0.268. It was also the most consistent T_{mean} variable, significant in 31 populations and virtually always negative (42/46 populations). Pooling all species, I regressed all 46 correlation coefficients against latitude; the lower the latitude, the more that June heat dampened growth ($r^2 = 0.588$, $p < 0.00001$; Table 3.4, Fig. 3.4a). To illustrate, this variable was significant in just one of ten populations at the three most northerly sites and fifteen of fifteen populations at the three most southerly (Table 3.4, Fig. 3.4a). This phenomenon held true within species, too. Considering the well-replicated species in isolation, the amount of variability in growth-Jun$_{Tmean}$ relationships explained by latitude was r^2 = 0.908 for *A. saccharum*, r^2 = 0.652 for *F. grandifolia*, and r^2 = 0.827 for *Q. rubra* (Table 3.4, Fig. 3.4a). The phenomenon also held true within the pooled trans-gradient species and the pooled southerly species (r^2 = 0.343 for southerly and r^2 = 0.815 for trans-gradient species, Fig. 3.4a). However, northerly species did not follow this pattern (r^2 = 0.016, Fig. 3.4a).

Among all months considered, the most important for precipitation-growth relationships was again current-June (Fig. 3.4b, Table 3.5). It was the most consistently significant across populations (33/46) and had the highest magnitude (mean growth-Jun_{Ppt} correlation coefficient = 0.283). For all populations, the relationship was positive, significantly for the 24 most southerly populations. Latitude and growth-Jun_{Ppt} correlation coefficients were inversely correlated: the lower the latitude, the more precipitation boosted growth ($r^2 = 0.521$, $p < 0.0001$). As with T_{mean}, species-specific results for the three well-replicated species were similar to the pooled-species results. The amount of variability in growth-Jun_{Ppt} relationships explained by latitude was $r^2 = 0.467$ for *A. saccharum*, $r^2 = 0.372$ for *F. grandifolia*, and $r^2 = 0.643$ for *Q. rubra* (Table 3.5, Fig. 3.4b). This was also true within the pooled trans-gradient species and the pooled southerly species ($r^2 = 0.451$ for southerly and $r^2 = 0.468$ for trans-gradient species, Fig. 3.4b). However, northerly species showed a slight trend in the opposite direction, i.e., growth-$June_{Ppt}$ relationships were slightly stronger at the most northern site ($r^2 = 0.161$, Fig. 3.4b).

Other Growth-Climate Relationships, 1903–2004 Single-Interval

Among all climate variables considered, 18/34 were significant in at least five populations (Tables 3.4 & 3.5). Five is about double what is expected by chance alone with a significance threshold of $p = 0.05$. Briefly, some of the variables other than Jun_{Tmean} and $_{Ppt}$ which were often important were Jul_{Ppt} (significant in 32/46 populations), Jul_{Tmean} (28/46), Jan_{Ppt} (18/46), May_{Ppt} (16/46), prior-Aug_{Tmean} (15/46), and prior-Aug_{Ppt} (12/46) (Tables 3.4 & 3.5). For each of these variables, except prior-Aug_{Ppt}, there was a significant association between

latitude and the growth-climate relationship, when species were pooled. Relationships with Jan, May, Jun, and Jul_{Ppt} were generally positive, and they became more positive moving south. Relationships with Jun and Jul_{Tmean} were generally negative and became more negative moving south. Relationships with prior-Aug_{Tmean}, too, were generally negative, but here they became *less* negative moving south. Overall, 18/34 growth-climate relationships were significantly associated with latitude (Tables 3.4 & 3.5).

Comparing Growth-Climate Relationships Across Populations, 1904–2004 Single Interval

PCA was conducted on a correlation matrix of growth-climate coefficients. Only coefficients significant in at least 5 of 46 tree populations were retained in the matrix. Each column was a climate variable, each row a population, and each cell a correlation coefficient. A biplot of the two most important PCs was generated (Fig. 3.5), this for visualization of patterns in growth-climate relationships, to interpret on a single figure a prodigious amount of information. The biplot was duplicated to highlight both within-site clustering (Fig. 3.5a) and within-species clustering (Fig. 3.5b). The first two PCs explained 68.4% and 11.9% of the variation, respectively.

There was much overlap in how populations clustered, both by species and site, but it was clear that, within latitudinal bands, populations clustered according to species more than site (Fig. 3.5). For example, at each of the most northerly sites at which at least three species were sampled, latitudes 44.1, 45.6, 45.8, and 46.9 °N, there was not close clustering among species. There was tighter within-site clustering at southerly sites, but also much overlap among sites. Within species, there was tight clustering within most of the narrowly sampled

taxa: *B. alleghaniensis*, *T. canadensis*, *L. tulipifera*, *Q. alba*, and *P. strobus*. However, for the widely sampled species, *A. saccharum*, *F. grandifolia*, and *Q. rubra*, there was wide separation within species. For *Q. rubra* and *A. saccharum*, a latitudinal gradient was apparent. Northerly populations tended to load more negatively on PC 1. However, within subregions, both *A. saccharum* and *Q. rubra*, did cluster well within species. Together, these results suggest that both species and site are important for determining growth-climate relationships, but that species is more important than site at small spatial scales.

Additionally, the biplot allows approximation of the importance of each climate variable and the relationship of each population with each climate variable. The longer the vector arrow, the more important the climate variable. For example, Jun and Jul_{Ppt} and Jun and Jul_{Tmean} are quite important. May and prior-Dec_{Tmean} are less important. The relationship between climate variables and populations' growth is approximated by the angle between them. A 180° angle indicates a perfect inverse relationship (r = -1), 0° a perfect direct relationship (r = 1), and 90° no relationship (r = 0). In this way one can, for example, determine what sets apart *T. canadensis* from the other species. Those populations had relatively weak relationships with current-summer conditions and relatively strong relationships with prior-July conditions. Additionally, each of the four *T. canadensis* populations were among the few to have a significant affinity for current-Mar_{Tmean}. Similar comparisons could be made by studying the growth-climate correlation matrix (Tables 3.4 & 3.5), but it is easier to study the biplot (Fig. 3.5). That was the purpose of conducting this PCA.

Changes in Growth-Climate Relationships, 1903–2004 Moving-Intervals

The moving-interval correlation analysis showed that the monthly T_{mean} variable that changed the most was prior-July (Table 3.6). For 8/46 populations, the slope was steepest for this month, with relationships moving from positive to negative among all eight. This was most prevalent in the south but also occurred at two more-northern sites. All eight of the populations for which prior-July was the *largest*-changing month were *A. saccharum* or *F. grandifolia*, but the positive to negative trend was also observed among most populations of other species, too (Fig. 3.6a).

The monthly precipitation variable that was most variable across the timeline was prior-September (Table 3.6). For 13/46 populations, the slope was steepest for this month, with relationships moving from positive to negative in more recent years, among all 13. This was most prevalent at the sites Vrh and Kalamazoo Nature Center (KNC), in the middle of the latitudinal gradient, in southern Michigan, but it was found also at more northerly sites. It was not clustered among a few species but was found in seven species, six hardwoods and *P. strobus*. Even for most of the other populations, those for which prior-September was not the largest-changing month, a similar trend was still observed (Fig. 3.6b). By contrast, growth relationships with the strongest growth-related variables, Jun_{Tmean} and Jun_{Ppt} changed little over the interval (Fig. 3.6c,d).

Discussion

Comparing Tree-Ring Chronologies Across Populations

In a PCA of all 46 ring-width-index chronologies, the first PC, explaining 32.8% of the variation, was one on which all populations loaded positively (Fig. 3.3a). The shared sign indicates a direct relationship among populations regarding growth anomalies (variations from the mean). Thus, along the first PC, a good growth year in southern Indiana also meant a good year as far away as the northern Upper Peninsula (Brubaker 1980). Other studies, also examining many tree-ring chronologies over large areas, have found all (or nearly all) populations to load in the same direction on the first principal component: in the Great Lakes Region (Graumlich 1993), eastern boreal Canada (Huang et al. 2010), the southeastern U.S. (Pederson et al. 2012), and the U.S. Pacific Northwest (PNW) (Brubaker 1980, Peterson & Peterson 1994). It is believed that this represents a shared response to a coherent regional climate signal. Though my study area covered eight degrees latitude (940 km), a 6.7-°C difference between the warmest and coolest site, and a 473-mm/year difference between the driest and wettest (Table 3.1), annual weather was correlated among sites. For common period 1903–2004, mean annual temperature of the most southerly sites was well correlated even with that of most northerly sites (lowest Pearson r among all pairwise comparisons = 0.555; Table 3.7). Correlations for total annual precipitation were not as strong, but there was still a clear relationship (lowest r = 0.160; Table 3.8).

Although all populations loaded positively on PC 1, there were differences in magnitude. The PCA does not examine growth-climate relationships directly, but for two reasons it is likely that different loadings among populations are due largely to climate (Cook et al. 2001). First is

because of the prodigious influence of climate on tree growth (Fritts 1976). Second, much of the non-climatic influence on growth was removed in the detrending process (Cook et al. 2001). The conifers, in this study sampled only at northern sites, all loaded on PC 1 only slightly negatively, whereas the hardwoods loaded with a higher magnitude, even in the north. This may be due to the conifers' relatively weak relationships with current-summer conditions and with Jan_{Ppt}, as all those factors were strongly correlated with latitude, along with PC 1 loadings. That could also explain the lower loadings of northerly populations, as the northerly hardwoods tended to have weaker relationships with those variables than did southerly hardwoods.

PC 2 revealed an even more clear-cut distinction between northerly and southerly populations, with each population north of the site at 43.3 °N loading negatively and virtually all to the south of south of it, positively. Indeed, PC 2 loadings were highly correlated with latitude ($r = 0.928$). However, this PC accounted for only 10.3% of the variation. Thus, in a small number of years, a good growth year in the north is opposed by a poor year in the south and vice versa. Geographical-gradient thresholds across which PC loadings flip sign have been found in other studies. Brubaker (1980) studied conifer tree rings at 38 sites in the PNW. On the second PC, all sites west of the crest of the Cascade Mountains loaded positively and all but two east of the crest negatively. Littell et al. (2008) studied *Pseudotsuga menziesii* (Douglas fir) tree rings at four mountain ranges in the Pacific Northwest. In a PCA of the tree-ring chronologies, along the second PC, nearly all populations from the two eastern ranges loaded positively and all from the western ranges, negatively. In contrast, no threshold was found across wide swaths of the West Gulf Coast, USA (Cook et al. 2001) eastern boreal Canada (Huang et al. 2010), or the GLR (Graumlich 1993).

PC 3 explained 7.0% of the variation, and on that PC *T. canadensis* loaded strongly positively, together with the hardwoods at the two most southerly sites. These two classes exhibited quite different suites of growth-climate relationships; thus, it is unclear why they would share this common loading along PC 3. PC 4 explained just 5.5% of the variation, but that was higher than the 5% threshold selected (Legendre & Legendre 1998). Along this PC, *T. canadensis* was well separated from the other species, loading quite positively. That species had many atypical relationships with climate variables. All four of its populations had significantly positive relationships with Mar_{Tmean}, a phenomenon exhibited by another species in just one case, and relationships usually being negative among all other populations. Beyond just March, *T. canadensis* tended to be positively correlated with temperatures outside of the growing season with atypically high correlations November through March (Table 3.4). This may be due to the ability of evergreen trees to photosynthesize over the winter given sufficiently high temperatures (Schaberg et al. 1998), however the other conifer, *P. strobus*, did not at all show the same phenomenon. Additionally, *T. canadensis* showed an unusually strong aversion to prior-summer heat (Jun–Sep), which again may be attributable to its evergreen habit; the effects of poor leaf production at $year_t$ will carry over to $year_{t+1}$ (Fritts 1976). However, again *P. strobus* did not share this signature. Radial growth of *T. canadensis* was also found to be unique by Pederson et al. (2012), separating from the growth of several hardwood species along one PC.

Though the two most important PCs were associated with latitude, species was also important. The narrowly sampled species especially tended to load similarly to their conspecifics, especially on the first PC, but on that PC the widely sampled species also loaded

similarly with their conspecifics at least among nearby sites. Overall, it was concluded that both species and site were important for separating ring-width-index chronologies. By contrast, Pederson et al. (2012) found species to be more important than site, as did Cook et al. (2001) and Graumlich (1993). However, though Graumlich was also working in the GLR, the latitudinal gradient studied was four degrees, narrower than that of the present study. Huang et al. (2010) found both site and species to be important, with the first PC separating populations by site and the second, third, and fourth by species.

The Strongest Growth-Climate Relationships, 1903–2004 Single-Interval

By far, the most important growth-climate relationships were in the current-summer months, especially June and July. Growth-temperature relationships were quite negative, -precipitation relationships, quite positive. This was also true of August, but to a lesser extent. Negative growth-temperature and positive -precipitation relationships are a signature of moisture stress (e.g., Martin-Benito & Pederson 2015).

Summer moisture stress leads to leaf senescence (Marchin et al. 2010), fine-root mortality (Gaul et al. 2008), and stomatal closure (Panek & Goldstein 2001). The dominant signature of summer moisture stress is nearly ubiquitous in the wood of temperate trees, and it bodes ominously with the ongoing acceleration of climate change. To list a few examples, this signature was found across several hardwood species along a Georgia-to-Vermont latitudinal gradient in the eastern U.S. (Martin-Benito & Pederson 2015), *Pseudotsuga menziesii* in the montane PNW (Littell et al. 2008), several hardwood and *Pinus* species in Louisiana and east Texas (Cook et al. 2001), across a suite of hardwood and conifer species along a latitudinal

gradient from southern Wisconsin to northern Michigan (Graumlich 1993), and across several oak species and in *L. tulipifera* throughout the eastern United States (LeBlanc & Berland 2019, LeBlanc et al. 2020).

It is generally only at the far northern end of the temperate world, and further to the north, that there is little signature of summer moisture stress in tree rings. Across a 46–54° N latitudinal gradient, there were few stands exhibiting negative summer temperature or positive summer precipitation relationships, especially in the current summer, and in fact positive growth-summer-temperature relationships were more common than negative in the north (Huang et al. 2010). Babst et al. (2013) studied 1000 tree-ring chronologies from the major European tree species in north Africa and throughout Europe (30–70° N) and found predominantly positive growth-precipitation and negative growth-temperature relationships at low-latitude/altitude sites and the inverse at high sites. Harvey et al. (2020) worked on *Fagus sylvatica* (European beech), *Quercus robur* (English oak), and *Pinus sylvestris* (Scots pine) at European sites between the 51st and 59th parallels. Positive current-June precipitation relationships were quite important in the hardwoods, but few other summer variables were consequential, and in the conifers current-*March* temperature was most important. In *Picea mariana* (black spruce) chronologies throughout northeastern North America above the 60th parallel, current-summer-temperature relationships were mostly positive and -precipitation relationships negative (D'Orangeville et al. 2016).

In the present study, the signature of summer moisture stress was nearly ubiquitous, but it was strongest in the south (Fig. 3.4). This is consistent with other studies in temperate eastern North America (e.g., Martin-Benito & Pederson 2015, LeBlanc & Berland 2019, Au et al.

2020). By contrast, LeBlanc et al. (2020) found no such latitudinal trend in *L. tulipifera* across the eastern U.S. In the present study, the latitudinal trend in the strength of the summer-moisture stress signal held for both trans-gradient and southerly species. Thus, as the southerly species, *C. ovata*, *Q. alba*, and *L. tulipifera*, approached their northern limit, the strength of the summer-moisture stress weakened, but it was still present, and it was not lower than that of co-occurring species that were not near their northern limit. Thus, the southerly species were not relieved of the negative effects of high temperatures and insufficient precipitation near their northern limit (Fig. 3.4). This is consistent with other dendrochronological work at and near northern range limits in the temperate world (e.g., LeBlanc & Berland 2019, LeBlanc et al. 2020) and with the hypothesis that in benign environments, such as temperate eastern North America, range limits are determined by abiotic not biotic factors (e.g., Darwin 1859, MacArthur 1972). No clear latitudinal trend in the summer moisture stress signal was found in the present study for the northerly species (Fig. 3.4). However, caution should be exercised in the interpretation because the sample size was low (n = 10) and the latitudinal gradient narrow (2.76°).

Other Growth-Climate Relationships, 1904–2004 Single-Interval

Aside from the signature of current-summer moisture stress, relatively few variables were consistently important. Jan_{Ppt} was one of these few, being significantly positive in 18 populations. This precipitation would most often fall as snow in the GLR. Winter snow insulates and protects soil from freezing temperature (Zhang 2005). Without this protection, fine-root mortality increases, and trees must devote more resources to fine-root production the

following growing season (Tierney et al. 2001). Further, lack of snow leads to roots taking up less nitrogen and to more nitrogen leaching out of the soil (Campbell et al. 2014). Though winter snow accumulation can also boost tree growth by melting and providing moisture in the spring (Wu et al. 2019), that is unlikely a factor here because growth in this network was not limited by insufficient moisture in early spring (Table 3.5).

The next-most-important additional variable was May_{Ppt}, significant in 16 populations. Relationships with May_{Ppt} were generally positive, more so in the south. Interpretation is like that of Jun and Jul_{Ppt}. Relationships with prior-Aug_{Tmean} were significant in 15 populations. These relationships were generally negative, but unlike relationships with current-summer temperature, these relationships became *less* negative moving south. Rather than directly affecting radial growth as with current-summer temperatures, this is a lagged effect caused by decreased root production, bud set, carbon assimilation, and in the conifers leaf production in the previous year (Fritts 1976).

Some of these relationships and others could offset the enhanced summer moisture stress that ongoing climate change will bring. Winter/spring precipitation and temperature are likely to increase (Byun & Hamlet 2018). Significantly positive relationships with prior-Nov_{Ppt}, Jan/Feb_{Ppt}, and prior-Dec_{Tmean} (Fig. 3.5, Tables 3.4 & 3.5) could ameliorate the effects of summer drought, but this is complicated by the conversion of winter precipitation from snow to rain, which would not necessarily have the same effect. Further, warmer winter temperatures will increase winter respiration (Wibbe et al. 1994). Modeling the combined effects of a variety of climate variables on future growth, and comparing this within and among species, will be the subject of future research the next chapter.

Changes in Growth-Climate Relationships, 1903–2004 Moving-Intervals

Moving-interval growth-climate analysis was conducted for 34-year windows overlapping by one year, and changes in growth-climate relationships were quantified. Dendrochronology has stood traditionally on the premise that growth-climate relationships are stable over time, allowing the use of observed relationships to reconstruct centuries or millennia of unrecorded climate. This premise will need to be reworked, as more studies have revealed the dynamic nature of growth-climate relationships (reviewed by D'Arrigo et al. 2008). Changes in growth-climate relationships have been found chiefly at high latitudes where the historically well-linked variables of tree-growth and heat have diverged from each other as climate change has proceeded (e.g., Jacoby & D'Arrigo 1995, Briffa et al. 1998, D'Arrigo et al. 2004). Further, the phenomenon is not limited to recent decades, as it has also occurred during a period of early-20th-century warming in Fennoscandia (Schneider et al. 2014), nor is it limited to high latitudes as Maxwell et al. (2015) found a recent weakening between tree growth and moisture stress in southern Indiana, and Marquardt et al. (2019) found a shift in the seasonality of growth-climate sensitivity in *Pinus* of sky islands in Arizona. However, growth-climate divergence is not universal, even at high latitudes. For example, among 64 *Larix* and *Picea* tree-ring chronologies from the Alps, no divergence was found (Buntgen et al. 2008).

The present study found evolving growth-climate relationships, most dramatically for prior-Jul_{Tmean} and prior-Sep_{Ppt}, but relationships evolved in other months, too (Table 3.6). However, it is unlikely that recent shifts in growth-climate relationships in the GLR will impede climate reconstruction because reconstruction is usually done with the most-growth-correlated climate variables. The most frequently evolving growth-climate relationships (Table 3.6) were

not the ones that most influenced growth (Fig. 3.6, Tables 3.4, 3.5, & 3.6). Similar results were found in *L. tulipifera* in the eastern U.S. (LeBlanc et al. 2020). However, caution should still be exercised because even with the two most influential climate variables, JuneT_{mean} and June$_{Ppt}$, with which growth was relatively consistently correlated across time, there were stray populations for which the relationship was unstable (Fig. 3.6c,d).

Several hypotheses to explain high-latitude divergence exist, including global dimming (e.g., Stine & Huybers 2014), changes in non-focal variables (Vaganov et al. 1999), non-linear growth-climate relationships (e.g., D'Arrigo et al. 2004), and moisture stress (e.g., Barber et al. 2000). In the GLR, the fading drought signal was attributed to a lack of droughts in recent decades (Maxwell et al. 2015). This is consistent with the finding that in the eastern U.S., growth-precipitation relationships are weak when there is ample precipitation (LeBlanc and Berland 2019). However, the changes to growth-prior-Jul$_{Tmean}$ and -prior-Sep$_{Ppt}$ observed in this study were not due to changes to the climate variables over time, as they changed little according to the PRISM-derived data (data for individual months not shown). It may be that a different climate variable, one that influenced the growth-climate relationships considered, changed (Vaganov et al. 1999). This topic deserves further research.

Conclusion

Among 46 tree populations from nine species across an eight-degree latitudinal gradient in the Great Lakes Region, annual ring-width anomalies are determined by latitude more than by species. Within narrow latitudinal bands, species becomes more important than site, however. Across all populations except *T. canadensis* in the north, current-Jun/Jul$_{Tmean}$ and $_{Ppt}$

are the most growth-limiting variables. The negative growth-temperature and positive growth-precipitation relationships suggest sensitivity to moisture stress, and this portends a future of reduced productivity as climate change continues. The growth-summer-climate relationships were strongest in the south, and thus the north may be temporarily buffered from the negative effects of climate change. Across most sites and species, some of the minor growth-climate relationships changed over time considerably, in a consistent direction, however the most limiting factors were stable over time. Projected changes to the most limiting variables can thus likely be used to predict future growth changes.

APPENDIX

APPENDIX

Figures

Figure 3.1. The study sites and their latitude. Sites sharing a latitude are further differentiated with the first letter of their name (Table 3.1).

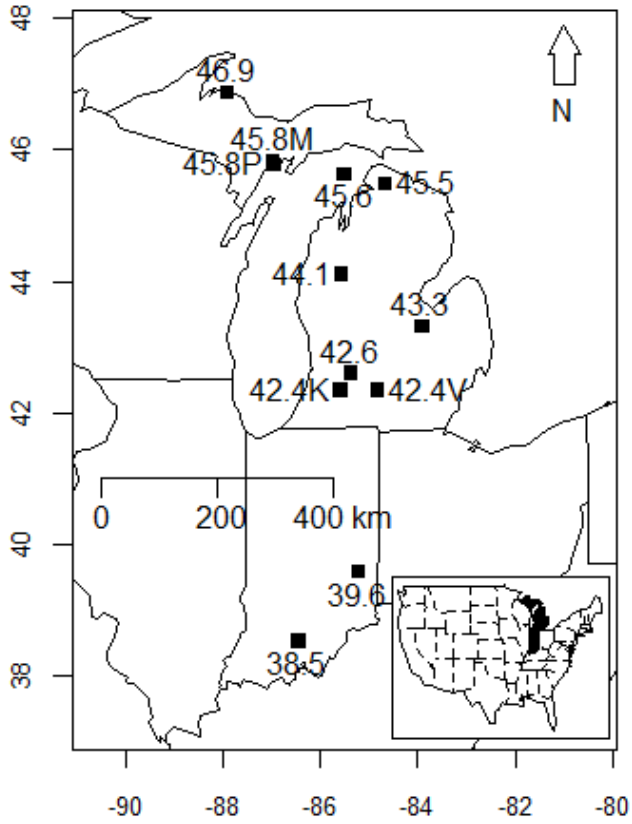

Figure 3.2. Detrended, standardized residual ring-width-index chronologies. Two-letter species codes: are in Table 3.1. Species codes: As = sugar maple *Acer saccharum*, Ba = yellow *birch Betula alleghaniensis*, Co = shagbark hickory *Carya ovata*, Fg = American beech *Fagus grandifolia*, Lt = tulip poplar *Liriodendron tulipifera*, Ps = white pine *Pinus strobus*, Qa = white oak *Quercus alba*, Qr = red oak *Quercus rubra*, Tc = eastern hemlock *Tsuga canadensis*. Sites are depicted by their latitude; when two sites share a latitude, they are disambiguated with a one-letter code: K = Kalamazoo Nature Center, V = Voorhees Audubon Sanctuary.

Figure 3.3. Loadings of each stand on principal components (PCs) 1 & 2 (a) and on PCs 3 & 4 (b). Loadings were calculated with a PC analysis on a correlation matrix in which each stand was a column, each row a year, and each cell a given stand's mean ring-width index in a given year. Species codes: As = sugar maple *Acer saccharum*, Ba = yellow birch *Betula alleghaniensis*, Co = shagbark hickory *Carya ovata*, Fg = American beech *Fagus grandifolia*, Lt = tulip poplar *Liriodendron tulipifera*, Ps = white pine *Pinus strobus*, Qa = white oak *Quercus alba*, Qr = red oak *Quercus rubra*, Tc = eastern hemlock *Tsuga canadensis*.

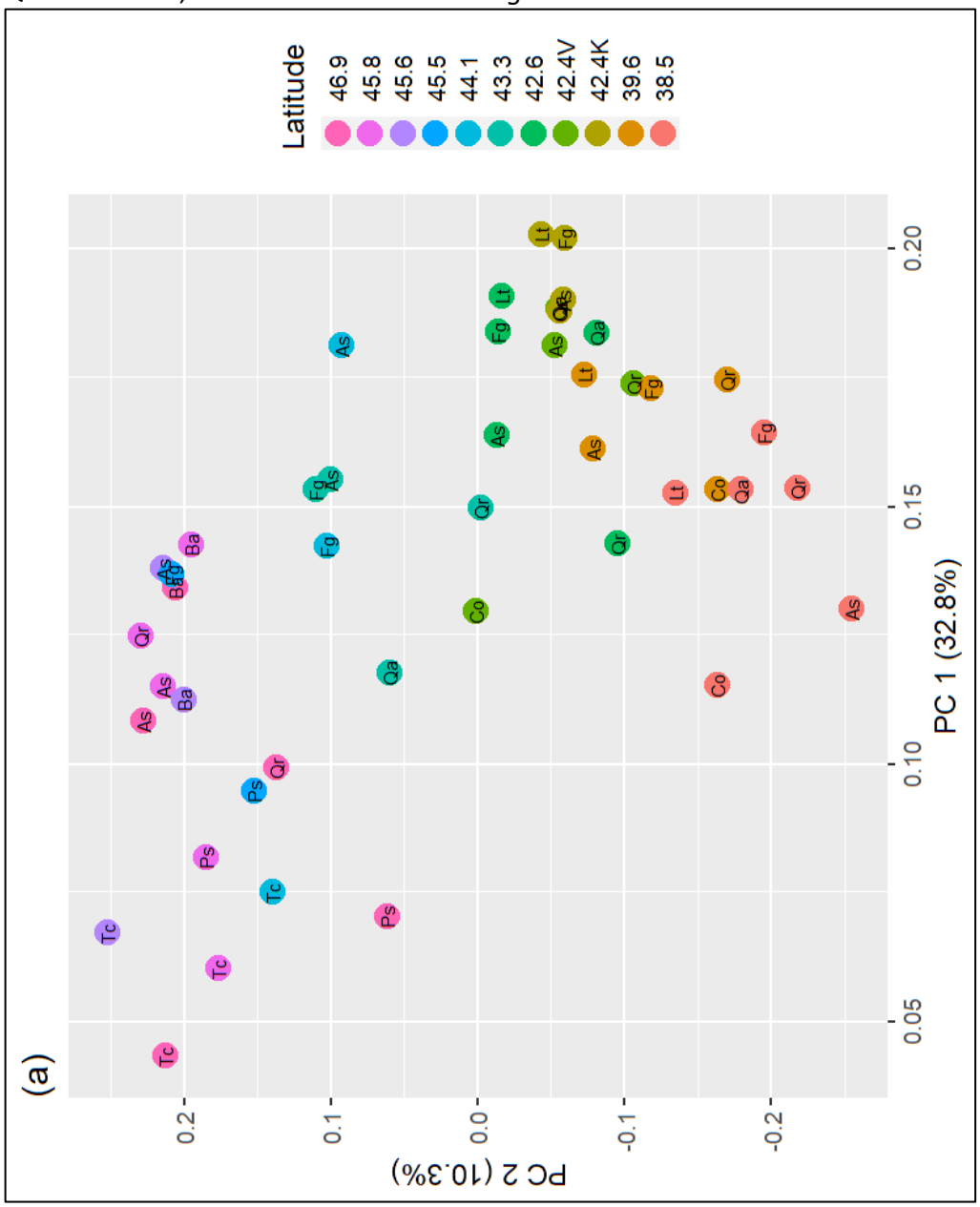

Figure 3.3 Cont'd

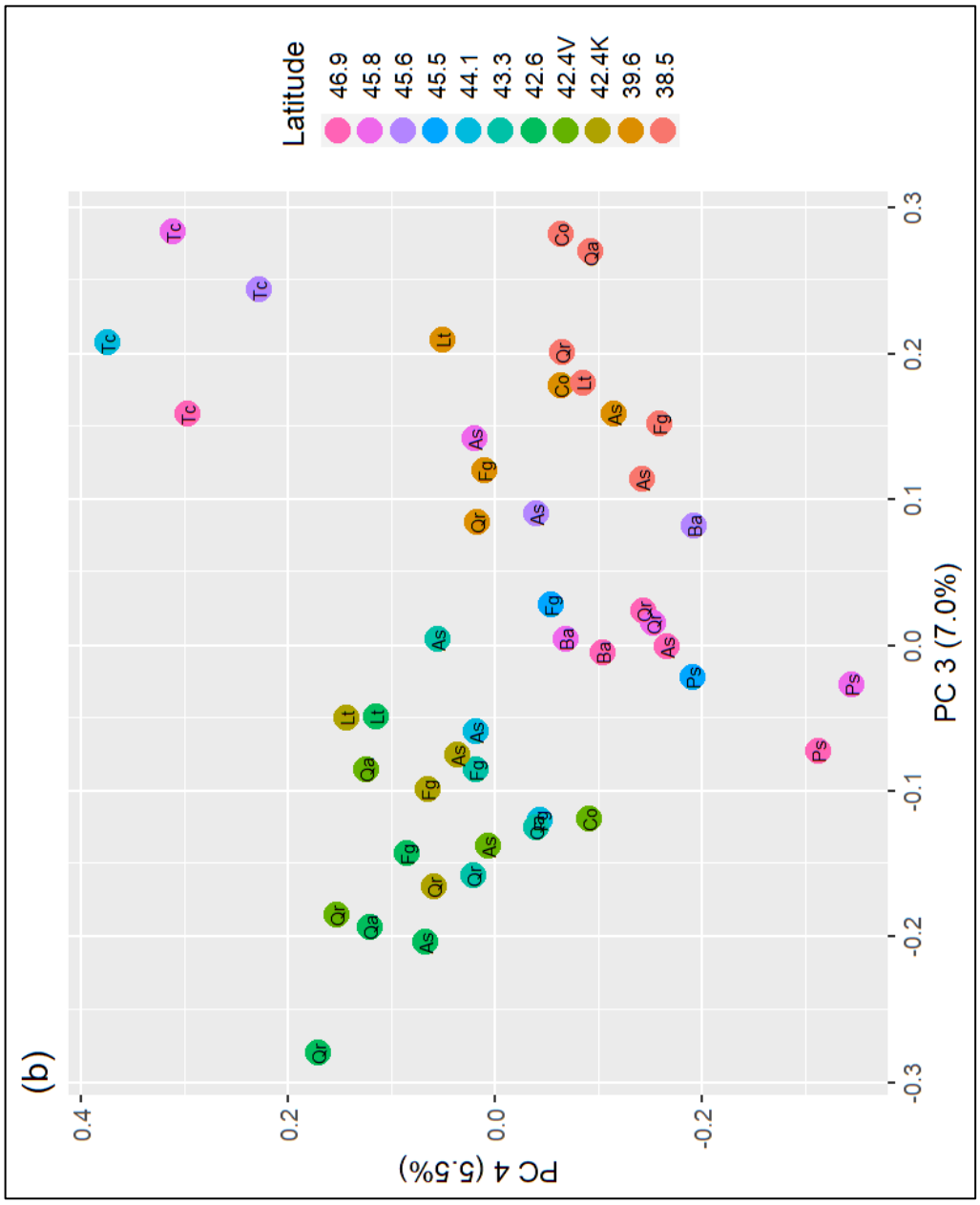

Figure 3.4. Latitude vs. (a) growth-Jun$_{Tmean}$ and (b) growth-Jun$_{Ppt}$ correlation coefficients (Pearson r). Species are grouped according to distribution within the study gradient: circles represent trans-gradient, triangles northerly, and squares southerly species.

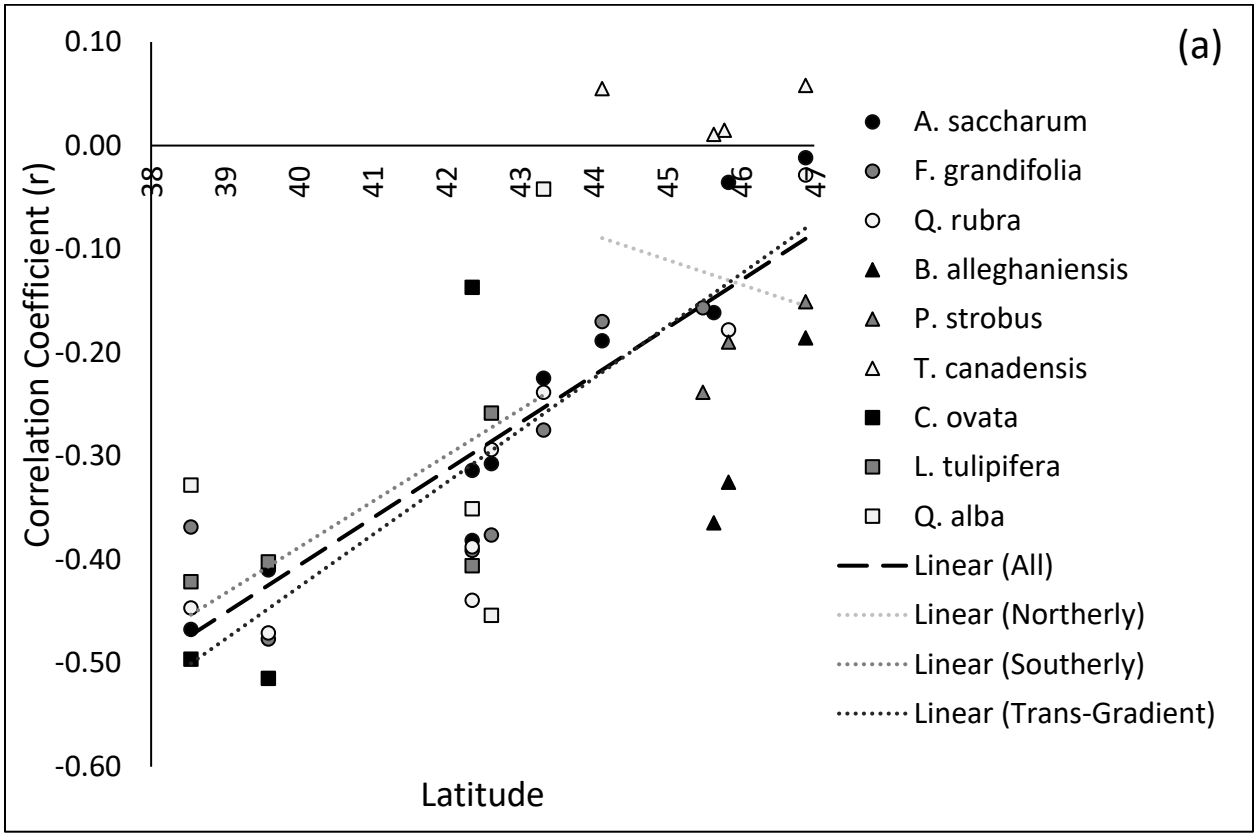

Figure 3.4 Cont'd

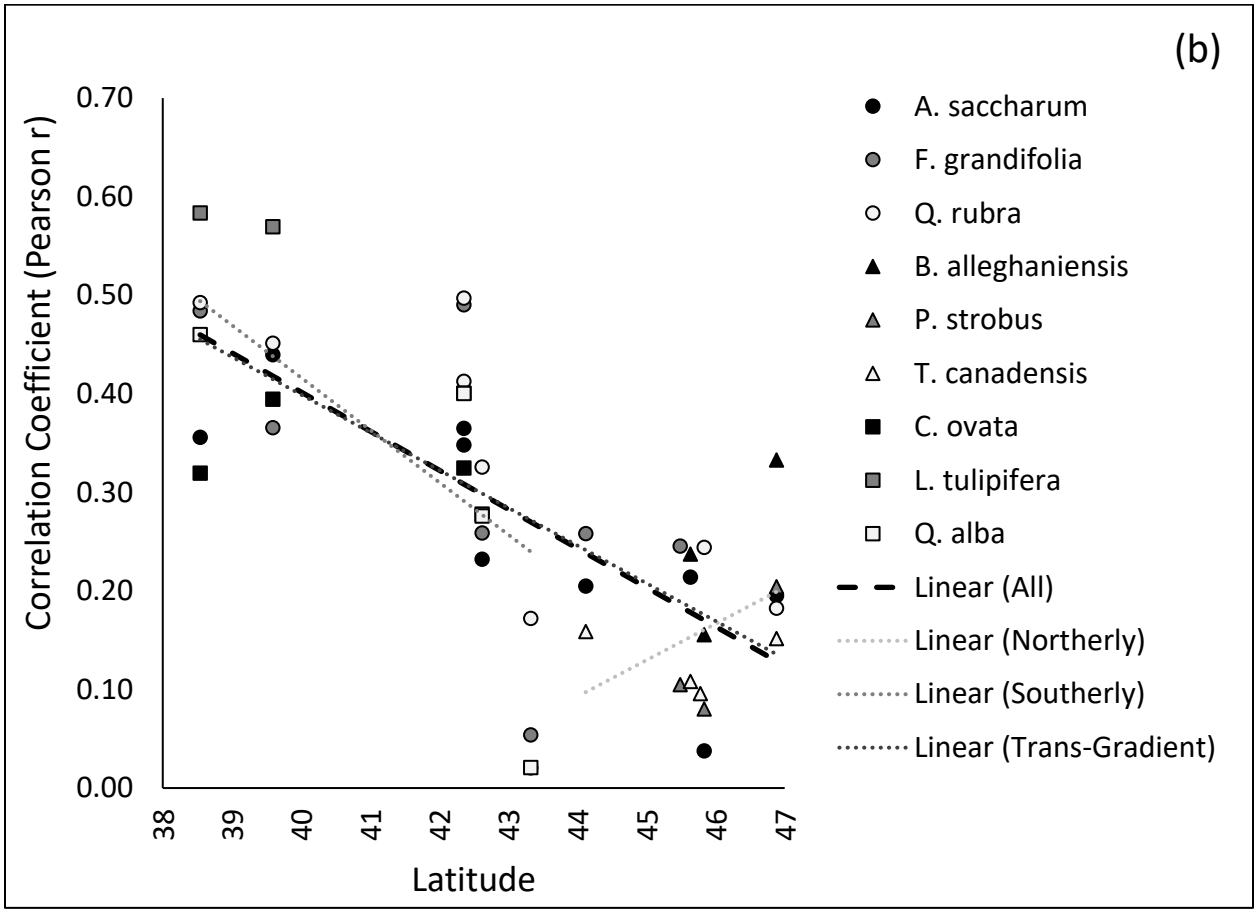

Figure 3.5. Growth vs. climate principal component analysis biplots with colors selected to highlight (a) clustering among sites and (b) species. Note that the subfigures are identical other than the color scheme. Each colored label represents a population, each vector a climate variable. Climate variables are labeled with numbers corresponding to months (month 1 = Jan., 12 = Dec.). The letters preceding the months indicate whether the month occurred in the year prior to ring formation ("p") or in the year of ring formation, the current year ("c"). Species codes: As = sugar maple *Acer saccharum*, Ba = yellow birch *Betula alleghaniensis*, Co = shagbark hickory *Carya ovata*, Fg = American beech *Fagus grandifolia*, Lt = tulip poplar *Liriodendron tulipifera*, Ps = white pine *Pinus strobus*, Qa = white oak *Quercus alba*, Qr = red oak *Quercus rubra*, Tc = eastern hemlock *Tsuga canadensis*. Sites are denoted by their latitude; when two sites share a latitude, they are disambiguated with a one-letter code: K = Kalamazoo Nature Center, V = Voorhees Audubon Sanctuary.

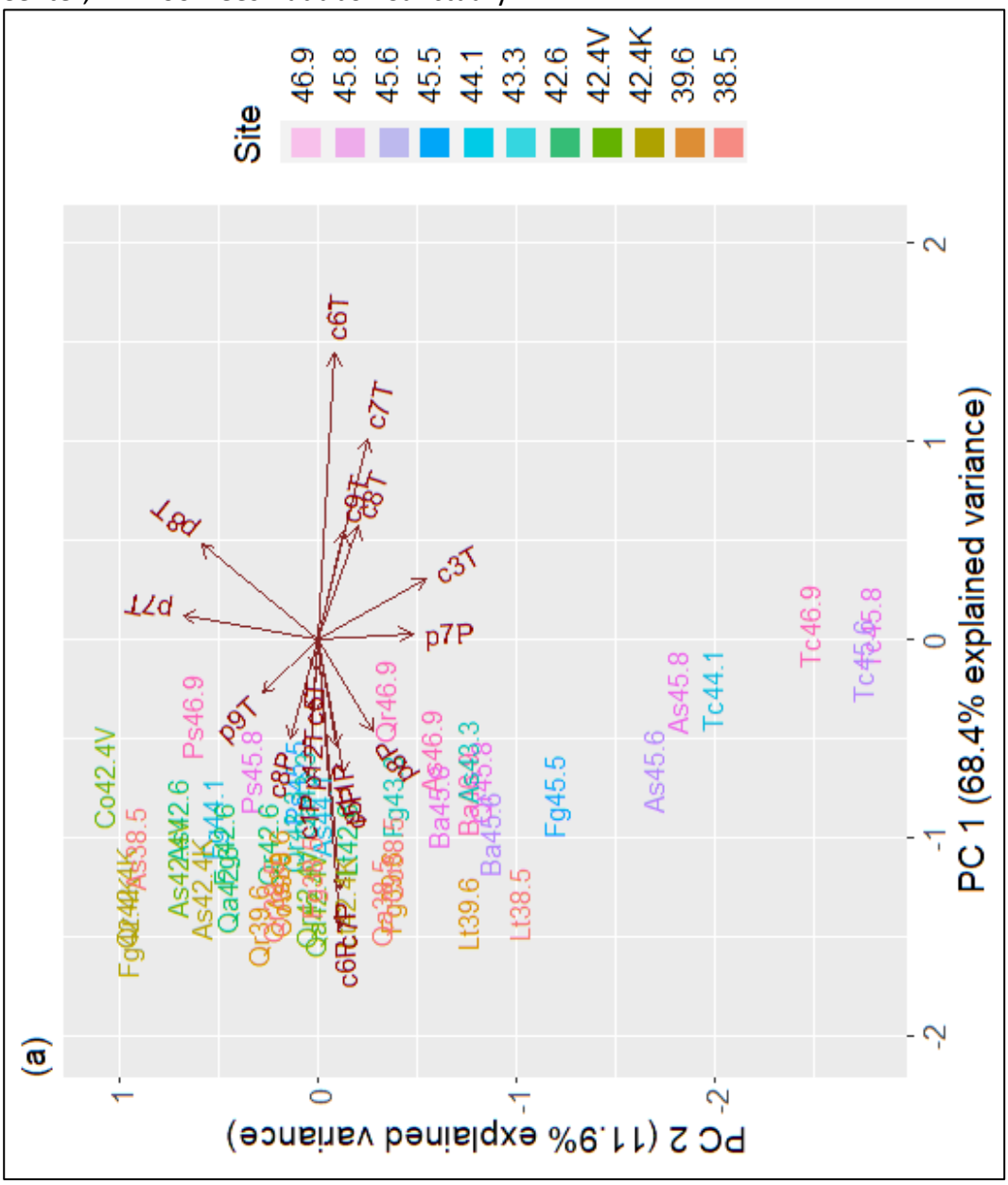

Figure 3.5 Cont'd

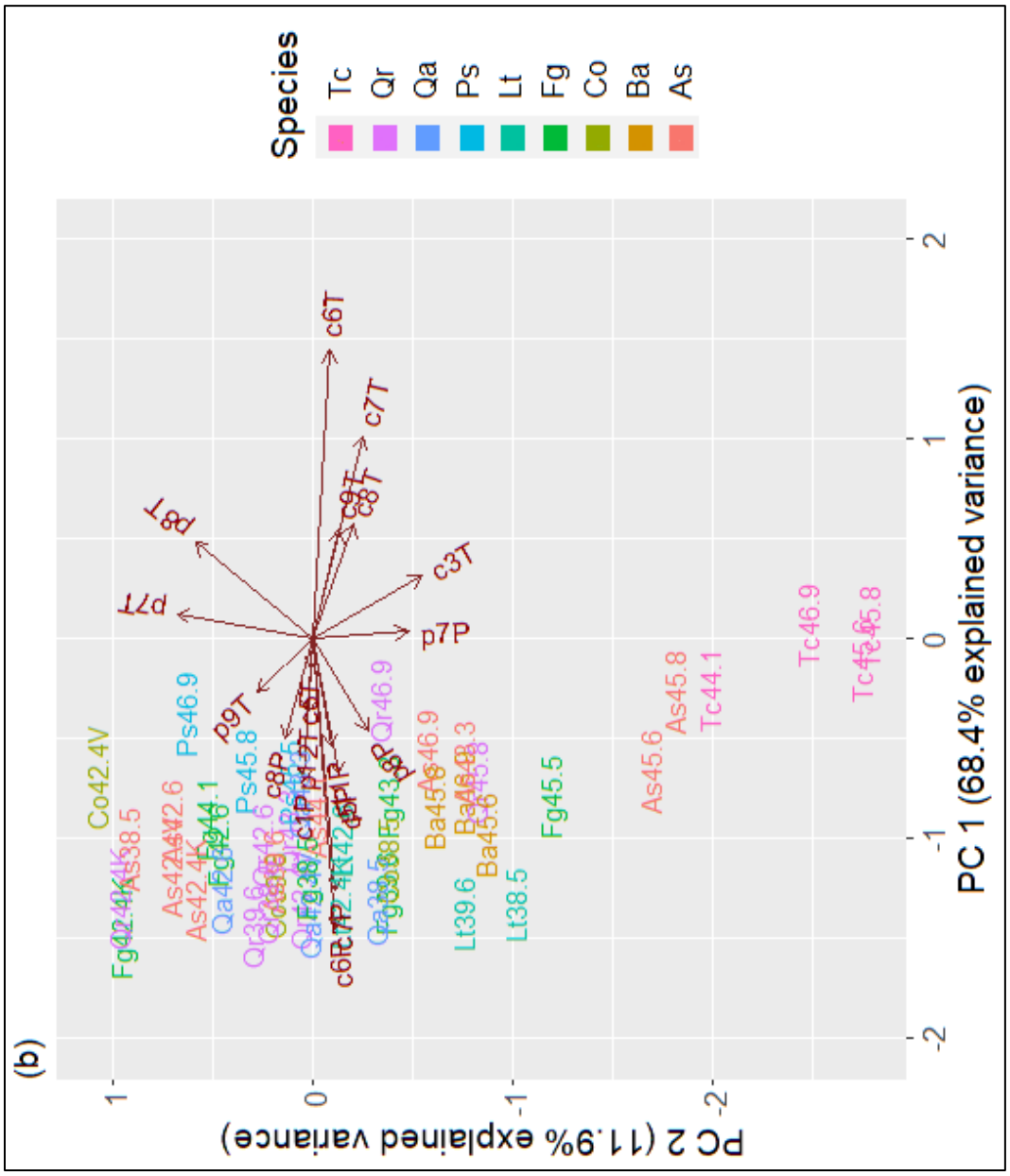

Figure 3.6. Growth-climate coefficients (Pearson r) vs. time for (a) prior-Jul$_{Tmean}$, (b) prior-Sep$_{Ppt}$, (c) Jun$_{Tmean}$, and (d) Jun$_{Ppt}$. The year is the final year of a 34-year window, for example, the final year, 2004, corresponds to the 1971–2004 window. Aside from the mean, each curve represents an individual population.

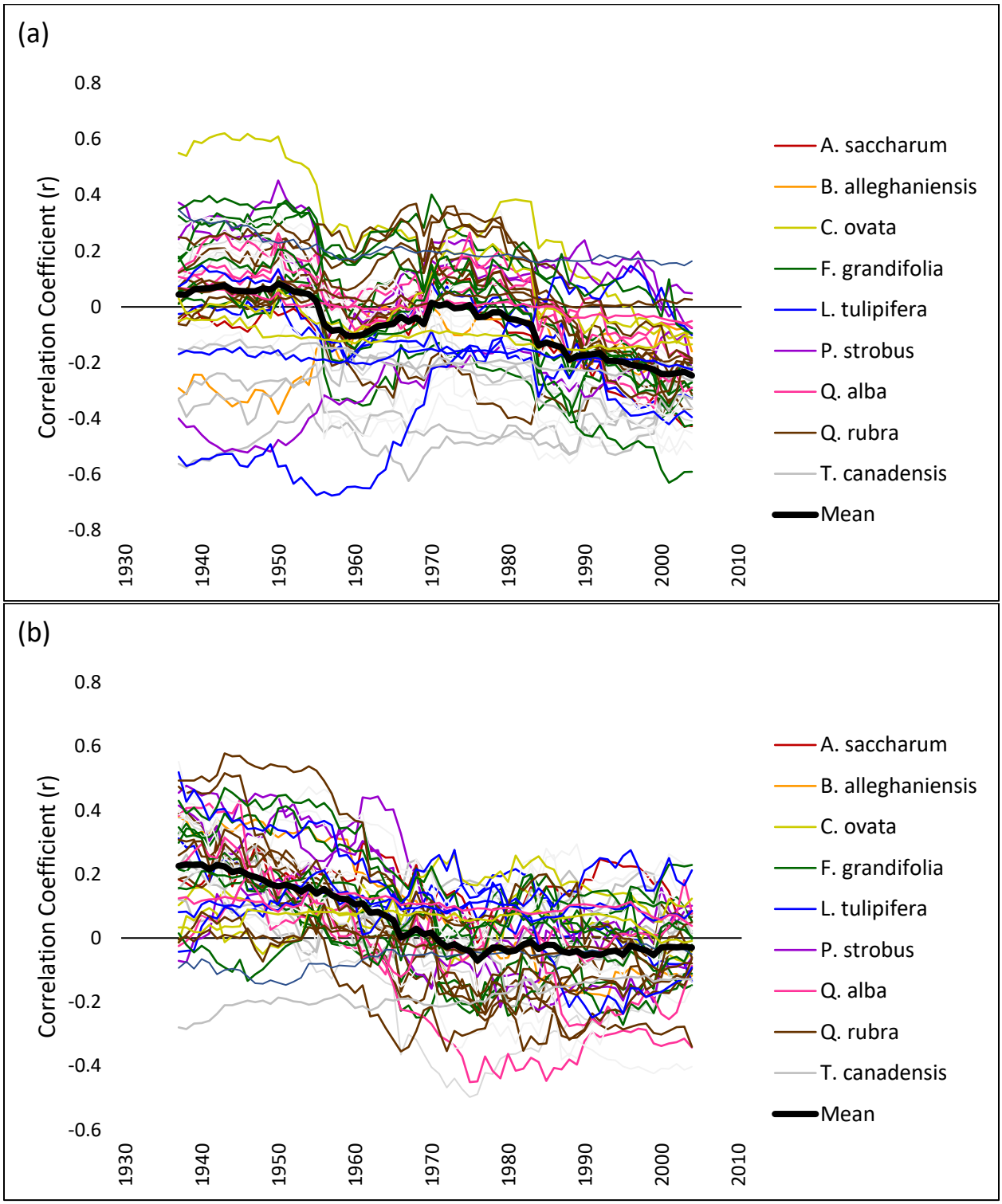

Figure 3.6 Cont'd

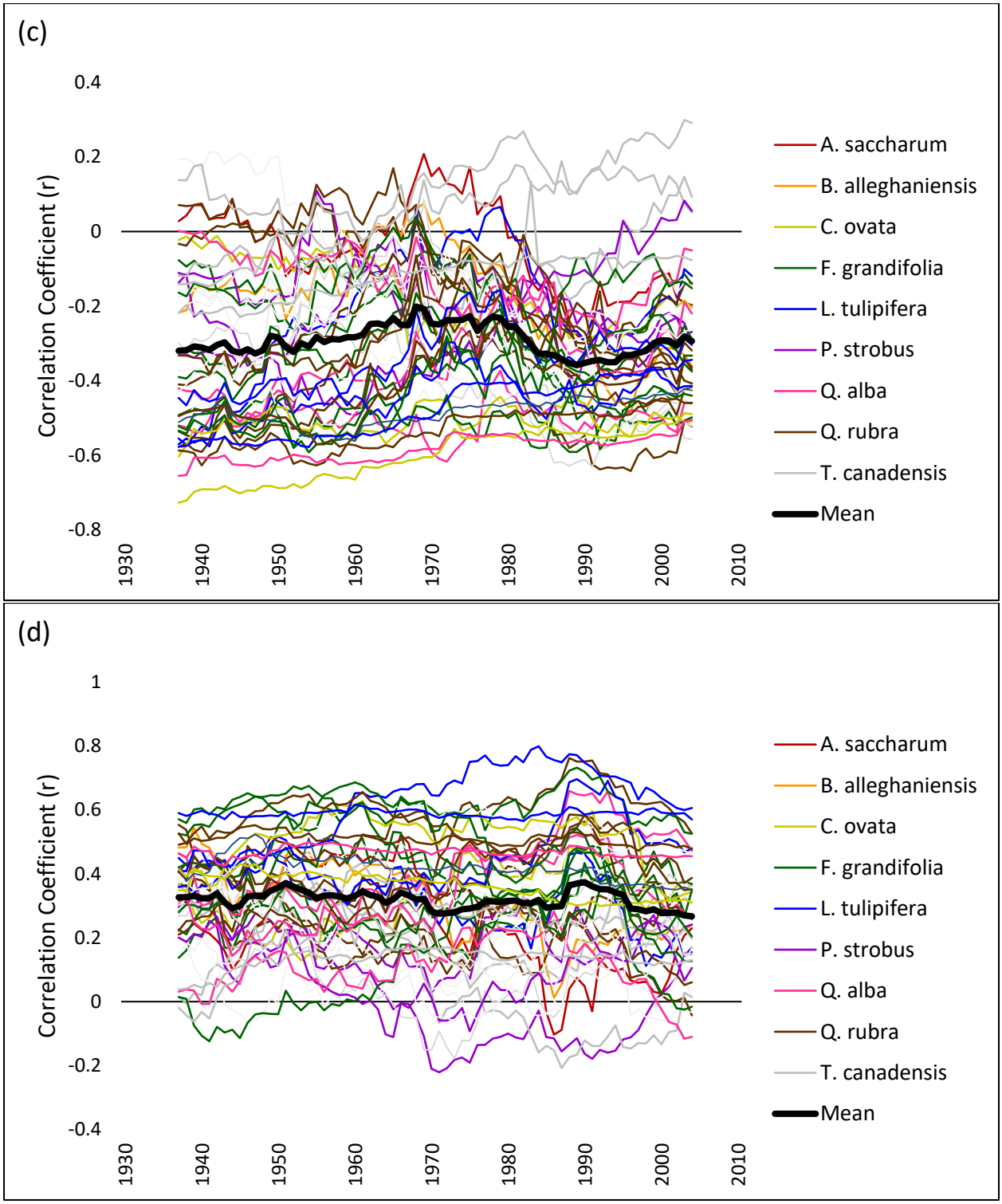

Tables

Table 3.1. Site characteristics. Meteorological data are 1981–2010 normals (https://prism.oregonstate.edu/). Species codes: As = sugar maple *Acer saccharum*, Ba = yellow birch *Betula alleghaniensis*, Co = shagbark hickory *Carya ovata*, Fg = American beech *Fagus grandifolia*, Lt = tulip poplar *Liriodendron tulipifera*, Ps = white pine *Pinus strobus*, Qa = white oak *Quercus alba*, Qr = red oak *Quercus rubra*, Tc = eastern hemlock *Tsuga canadensis.*

Site	Species	Latitude (decimal degrees)	Longitude (decimal degrees)	Mean Annual Temperature (°C)	Mean Annual Ppt. (mm)
Huron Mountain Club (HMC)	As, Ba, Ps Qr, Tc	46.88070	-87.91703	5.7	766.2
Maywood History Trail (Mwd)	As, Ba, Qr, Ps, WP	45.83690	-86.98482	5.8	738.5
Petersons' Hemlock Grove (Pet)	Tc	45.78080	-86.96793	5.7	732.3
Beaver Island (BvI)	As, Ba Tc,	45.63522	-85.51808	6.8	800.2
Colonial Point (CoP)	Fg, Ps	45.48848	-84.68538	6.4	779.6
Jacobson Sugar Bush (JSB)	Fg, Tc, As	44.11998	-85.56775	6.6	857.2
Price Nature Center (PNC)	As, Fg, Qa Qr	43.32607	-83.92752	8.8	828.5
Warner Audubon Sanctuary (War)	As, Fg, Lt, Qa, Qr	42.61938	-85.38603	9.0	938.9
Voorhees Audubon Sanctuary (Vrh)	As, Co, Qa, Qr	42.35675	-84.83425	9.0	907.9
Kalamazoo Nature Center (KNC)	As, Fg, Qr, Lt,	42.35583	-85.59538	9.5	982.5
Mary Gray Bird Sanctuary (MGB)	As, Co, Fg, Lt, Qr	39.59205	-85.22300	10.9	1085.1
Pioneer Mothers Memorial Forest (PMF)	As, Co, Fg, Lt, Qa, Qr	38.54017	-86.45593	12.4	1204.2

Table 3.2. General chronology characteristics. EPS = expressed population signal (Wigley et al. 1984). Site codes: BvI = Beaver Island, CoP = Colonial Point, HMC = Huron Mountain Club, JSB = Jacobsons' Sugar Bush, KNC = Kalamazoo Nature Center, MGB = Mary Gray Bird Sanctuary, Mwd = Maywood History Trail, Pet = Petersons' Hemlock Grove, PMF = Pioneer Mothers Memorial Forest, PNC = Price Nature Center, Vrh = Voorhees Audubon Sanctuary, Warner = Warner Audubon Sanctuary. Species codes: As = sugar maple *Acer saccharum*, Ba = yellow birch *Betula alleghaniensis*, Co = shagbark hickory *Carya ovata*, Fg = American beech *Fagus grandifolia*, Lt = tulip poplar *Liriodendron tulipifera*, Ps = white pine *Pinus strobus*, Qa = white oak *Quercus alba*, Qr = red oak *Quercus rubra*, Tc = eastern hemlock *Tsuga canadensis*.

Population (three-letter site and two-letter species codes)	Latitude	Longitude	Timespan	Number of trees (cores)	Series intercorrelation	Mean ring width (SD) in mm	Mean EPS (lowest 50-y segment)	Original publication (if different from the present)
HMC Ac	45.83690	-86.98482	1895–2017	18 (35)	0.502	0.86 (0.539)	.927 (.918)	
HMC Ba	45.83690	-86.98482	1895–2017	21 (49)	0.574	0.92 (0.553)	0.954 (0.952)	
HMC Qr	45.83690	-86.98482	1895–2017	12 (24)	0.611	2.35 (0.710)	.939 (.924)	
HMC Ps	45.83690	-86.98482	1895–2017	14 (26)	0.526	2.89 (1.052)	0.912 (0.898)	
HMC Tc	46.88070	-87.91703	1895–2015	52 (84)	0.672	0.81 (0.361)	.986 (.985)	Dye & Woods 2019 (Rush Lake)
Mwd As	45.83690	-86.98482	1895–2016	10 (18)	0.571	2.03 (1.082)	0.894 (0.843)	
Mwd Ba	45.83690	-86.98482	1895–2015	9 (20)	0.579	1.25 (0.757)	.906 (.901)	
Mwd Ps	45.83690	-86.98482	1895–2015	10 (22)	0.575	1.82 (0.949)	0.916 (0.887)	

Table 3.2 Cont'd

Mwd Qr	45.83690	-86.98482	1895–2015	10 (20)	0.527	2.27 (0.820)	0.902 (0.901)	
Pet Tc	45.78080	-86.96793	1895–2015	10 (20)	0.685	1.87 (0.772)	0.916 (0.906)	
Bvl As	45.63522	-85.51808	1895–2017	12 (22)	0.622	1.59 (0.842)	0.917 (0.865)	
Bvl Ba	45.63522	-85.51808	1903–2017	10 (20)	0.608	1.57 (0.803)	0.920 (0.903)	
Bvl Tc	45.63522	-85.51808	1895–2016	12 (24)	0.634	1.64 (0.882)	0.958 (0.956)	
CoP Fg	45.48848	-84.68538	1895–2004	17 (34)	0.615	1.62 (0.651)	0.948 (0.935)	
CoP Ps	45.48848	-84.68538	1895–2017	14 (27)	0.562	2.16 (0.940)	0.906 (0.892)	
JSB As	44.11998	-85.56775	1895–2015	13 (26)	0.574	2.02 (0.996)	0.927 (0.917)	
JSB Fg	44.11998	-85.56775	1895–2015	10 (20)	0.603	1.69 (0.900)	0.905 (0.856)	
JSB Tc	44.11998	-85.56775	1895–2016	11 (22)	0.598	1.71 (1.170)	0.924 (0.909)	
PNC As	43.32607	-83.92752	1895–2015	11 (21)	0.558	1.57 (0.878)	0.902 (0.889)	Au et al. 2020
PNC Fg	43.32607	-83.92752	1895–2015	11 (22)	0.633	1.66 (0.747)	0.925 (0.916)	
PNC Qa	43.32607	-83.92752	1895–2015	9 (18)	0.523	2.22 (0.931)	0.879 (0.827)	Au et al. 2020
PNC Qr	43.32607	-83.92752	1895–2015	10 (20)	0.566	2.66 (0.932)	0.928 (0.908)	
War As	42.61938	-85.38603	1895–2015	10 (20)	0.509	1.85 (0.420)	0.8715 (0.8344)	Au et al. 2020
War Fg	42.61938	-85.38603	1895–2015	12 (23)	0.537	1.61 (0.440)	0.9096 (0.8828)	
War Lt	42.61938	-85.38603	1895–2015	10 (19)	0.647	2.71 (0.460)	0.9297 (0.9079)	
War Qa	42.61938	-85.38603	1895–2015	10 (20)	0.64	1.93 (0.460)	0.9453 (0.9397)	Au et al. 2020
War Qr	42.61938	-85.38603	1895–2015	11 (22)	0.6	2.70 (0.446)	0.9478 (0.9367)	
Vrh As	42.35675	-84.83425	1895–2015	10 (20)	0.598	1.81 (0.429)	0.9253 (0.9164)	Au et al. 2020

Table 3.2 Cont'd

Vrh Co	42.35675	-84.83425	1895–2015	10 (20)	0.578	1.59 (0.504)	0.9209 (0.9022)	
Vrh Qa	42.35675	-84.83425	1895–2015	10 (20)	0.64	2.03 (0.462)	0.9468 (0.9402)	Au et al. 2020
Vrh Qr	42.35675	-84.83425	1895–2015	14 (26)	0.699	2.91 (0.488)	0.9711 (0.9694)	
KNC As	42.35583	-85.59538	1895–2015	10 (20)	0.552	2.23 (0.430)	0.9279 (0.8934)	
KNC Fg	42.35583	-85.59538	1895–2015	10 (19)	0.604	2.26 (0.482)	0.9220 (0.9118)	
KNC Lt	42.35583	-85.59538	1895–2015	10 (20)	0.663	2.89 (0.436)	0.9318 (0.8963)	
KNC Qr	42.35583	-85.59538	1895–2015	10 (20)	0.604	3.40 (0.474)	0.9440 (0.9242)	
MGB As	39.59205	-85.22300	1895–2016	14 (27)	0.526	2.54 (1.212)	0.918 (0.914)	
MGB Co	39.59205	-85.22300	1895–2016	14 (28)	0.603	1.98 (0.821)	0.931 (0.915)	
MGB Lt	39.59205	-85.22300	1895–2016	15 (30)	0.630	3.61 (1.676)	0.936 (0.898)	
MGB Fg	39.59205	-85.22300	1895–2016	13 (27)	0.517	1.93 (0.455)	0.8838 (0.8474)	
MGB Qr	39.59205	-85.22300	1895–2016	14 (28)	0.549	2.83 (1.042)	0.930 (0.928)	
PMF As	38.54017	-86.45593	1895–2013	10 (19)	0.501	1.62 (0.853)	.881 (.831)	Au et al. 2020
PMF Co	38.54017	-86.45593	1895–2012	6 (12)	0.580	1.54 (.702)	.891 (.877)	Maxwell & Harley 2017
PMF Fg	38.54017	-86.45593	1895–2016	16 (31)	0.575	2.13 (1.062)	0.940 (0.926)	
PMF Lt	38.54017	-86.45593	1895–2012	20 (22)	0.643	2.12 (1.081)	.937 (.931)	Maxwell et al. 2015
PMF Qa	38.54017	-86.45593	1895–2011	22 (38)	0.605	2.39 (0.869)	.942 (.935)	Maxwell et al. 2015
PMF Qr	38.54017	-86.45593	1895–2012	25 (44)	0.598	3.34 (1.173)	0.954 (.947)	Maxwell et al. 2015

Table 3.3 Correlations (Pearson r) between loadings on each principal component (PC) vs. latitude. The PC loadings were derived from a PC analysis of the ring-width-index chronologies (Fig. 3.3). '*' indicates a significant relationship ($p < 0.05$).

	PC 1	**PC 2**	**PC 3**	**PC 4**
Variance explained	32.8%	10.3%	7.2%	5.5%
Correlation (Pearson r) with latitude	-0.552*	0.928*	-0.242	-0.002

Table 3.4. Partial correlation matrix (T_{mean} only) for the growth-climate coefficient (Pearson r) for each of 34 climate variables for each population. 'Tmean' = mean temperature. Months with a 'p' preceding their abbreviation indicate that they occurred in the year prior to the year of ring formation. Cells in bold are significant ($p < 0.05$). Sites are arranged from north (top) to south (Table 3.1). Site codes: BvI = Beaver Island, CoP = Colonial Point, HMC = Huron Mountain Club, JSB = Jacobsons' Sugar Bush, KNC = Kalamazoo Nature Center, MGB = Mary Gray Bird Sanctuary, Mwd = Maywood History Trail, Pet = Petersons' Hemlock Grove, PMF = Pioneer Mothers Memorial Forest, PNC = Price Nature Center, Vrh = Voorhees Audubon Sanctuary, Warner = Warner Audubon Sanctuary. Species codes: As = sugar maple *Acer saccharum*, Ba = yellow birch *Betula alleghaniensis*, Co = shagbark hickory *Carya ovata*, Fg = American beech *Fagus grandifolia*, Lt = tulip poplar *Liriodendron tulipifera*, Ps = white pine *Pinus strobus*, Qa = white oak *Quercus alba*, Qr = red oak *Quercus rubra*, Tc = eastern hemlock *Tsuga canadensis*.

Population	pMay Tmean	pJun Tmean	pJul Tmean	pAug Tmean	pSep Tmean	pOct Tmean	pNov Tmean	pDec Tmean	Jan Tmean	Feb Tmean	Mar Tmean	Apr Tmean	May Tmean	Jun Tmean	Jul Tmean	Aug Tmean	Sep Tmean
HMC As	.15	.07	-.14	**-.22**	.07	.03	.04	.04	-.03	-.04	-.11	-.06	**.19**	-.01	-.08	.00	**-.21**
HMC Ba	-.01	-.09	-.17	**-.20**	-.05	-.07	-.17	-.04	-.04	-.09	-.09	-.04	.11	-.19	-.16	-.06	-.07
HMC Qr	-.03	.14	.00	-.11	**.20**	.07	.14	.05	.14	.12	.12	.13	**.20**	-.03	.05	**.18**	-.13
HMC Ps	.05	.13	**.21**	-.02	**.24**	-.06	-.07	-.06	.08	.15	.08	**.19**	.18	-.15	-.08	.10	-.04
HMC Tc	.14	**-.22**	**-.32**	**-.33**	**-.26**	-.19	.13	.08	-.07	.12	**.34**	**.29**	.03	.06	.17	.14	.11
Mwd As	-.02	-.15	**-.29**	**-.37**	.09	-.05	-.05	-.04	.05	.02	**.19**	.07	**.23**	-.04	-.04	.04	.04
Mwd Ba	-.02	-.11	-.13	**-.25**	-.05	-.03	-.18	-.08	-.14	-.20	-.06	.04	**.20**	**-.33**	**-.22**	-.09	-.18
Mwd Ps	-.01	**.23**	.16	-.09	.12	.02	.07	-.01	-.09	-.06	**-.17**	.04	**.21**	-.19	**-.19**	-.05	-.13
Mwd Qr	.01	.09	-.11	**-.20**	.05	.06	-.02	.07	-.05	.06	-.07	.16	.11	-.18	-.14	-.02	.08
Pet Tc	.08	**-.30**	**-.42**	**-.30**	**-.23**	-.08	**.23**	.06	.15	.12	**.34**	**.19**	-.04	.02	**.22**	**.20**	-.01
BvI As	.06	-.06	-.20	**-.37**	.04	.00	.10	.07	.03	-.03	.10	-.06	**.20**	-.16	-.03	.07	-.06

Table 3.4 Cont'd

Bvl Ba	.02	.03	-.04	**-.21**	-.04	.11	-.03	-.13	-.14	-.09	.09	.04	.05	**-.36**	**-.27**	-.07	-.03
Bvl Tc	.09	-.17	**-.34**	**-.41**	-.10	-.06	**.23**	.03	.06	.12	**.39**	.16	-.13	.01	.16	**.18**	.12
CoP Fg	-.07	.00	-.10	**-.22**	-.03	.10	-.04	-.03	.10	-.01	.05	.14	**.27**	**-.16**	-.12	-.08	.01
CoP Ps	-.12	.11	.18	-.16	.00	.04	-.05	-.04	-.12	-.07	.03	.15	.15	**-.24**	**-.30**	-.06	-.06
JSB As	.04	.00	-.05	-.15	.12	.05	.07	**.25**	.05	-.05	-.14	-.09	.06	**-.19**	**-.28**	.01	-.14
JSB Fg	.14	.06	.14	-.01	.11	.01	.06	**.20**	.13	.04	-.11	-.20	.14	-.17	**-.26**	-.11	**-.21**
JSB Tc	.10	-.14	**-.30**	**-.26**	-.12	-.05	**.19**	**.24**	**.21**	**.19**	**.35**	.13	**-.31**	.06	.08	-.08	.04
PNC As	**-.23**	-.13	**-.23**	**-.26**	.07	.00	.04	.13	.09	-.05	-.09	.00	.12	**-.23**	-.13	-.01	-.08
PNC Fg	**-.28**	-.06	-.10	**-.17**	.07	-.01	-.04	.08	.03	-.05	-.08	.00	.09	**-.28**	**-.28**	-.14	-.11
PNC Qa	.04	**.22**	.03	-.08	**.20**	**.18**	.18	**.36**	.16	.05	-.12	-.09	.02	-.04	**-.19**	.04	**-.21**
PNC Qr	.06	.07	-.01	-.14	.05	.10	.05	**.23**	.11	-.13	**-.19**	-.07	-.02	**-.24**	**-.19**	-.16	**-.21**
War Fg	.01	.08	-.01	-.08	.12	.00	-.11	.10	-.04	-.16	-.17	-.03	**.22**	**-.38**	**-.22**	-.16	-.05
War Lt	.12	-.12	-.11	-.07	.12	.04	-.07	**.25**	.12	.12	-.05	.11	.02	**-.26**	-.11	-.04	**-.18**
War Qa	.15	.11	.02	-.09	.12	.04	-.01	.18	.04	-.11	-.19	-.06	-.04	**-.45**	**-.36**	-.18	-.10
War Qr	.19	.04	.05	-.13	.07	-.02	-.05	.09	-.04	-.13	**-.22**	-.02	.13	**-.29**	**-.22**	-.16	-.13
Vrh As	-.01	.14	.03	-.10	-.05	.08	-.07	**.26**	.00	-.07	**-.22**	.01	.17	**-.31**	**-.26**	**-.25**	-.16
Vrh Co	.08	.19	**.24**	-.06	.15	.14	-.05	.09	.11	.02	-.14	.03	.16	-.14	-.18	-.13	-.01
Vrh Qa	.11	.07	-.03	-.15	.03	.09	.07	.18	.09	.01	-.06	.02	-.02	**-.35**	**-.33**	**-.19**	-.12
Vrh Qr	.05	.04	.00	-.10	.01	-.01	-.01	.08	.01	-.11	-.15	.07	.04	**-.39**	**-.27**	-.15	-.15
KNC As	.11	.06	.02	-.12	.09	.03	-.06	.14	-.06	-.10	-.09	-.07	.06	**-.38**	**-.29**	**-.21**	**-.27**

Table 3.4 Cont'd

KNC Fg	.16	.12	.12	-.06	**.23**	.03	.06	.09	-.04	-.03	-.10	-.06	-.05	**-.39**	**-.38**	**-.24**	**-.25**
KNC Qr	.10	.02	.10	-.08	.18	.03	-.09	.16	-.01	.01	**-.22**	-.02	.04	**-.44**	**-.33**	-.06	-.16
KNC Lt	.06	-.10	-.13	**-.22**	.07	-.03	-.13	.09	-.01	-.11	-.15	.00	-.04	**-.41**	**-.27**	-.11	-.19
MGB As	.00	.00	-.02	-.07	.08	.17	.02	.09	.02	.06	-.04	-.02	-.02	**-.41**	-.22	-.18	.02
MGB Co	.09	.02	.00	.03	.00	**.18**	.12	-.06	.03	-.03	.04	-.07	-.11	**-.52**	**-.35**	**-.26**	-.13
MGB Fg	-.08	-.01	-.09	-.14	.03	.14	.12	.11	.08	-.02	-.06	.15	-.01	**-.48**	-.19	-.17	-.12
MGB Lt	-.17	-.08	**-.20**	-.10	-.01	.10	-.04	-.03	.09	.09	.09	.02	-.02	**-.40**	**-.30**	**-.20**	-.02
MGB Qr	.05	.02	-.01	-.02	.05	.08	.00	.08	-.01	-.08	-.07	.04	-.01	**-.47**	**-.32**	-.16	-.14
PMF As	.16	.13	.14	.06	.16	-.03	.06	.14	.00	.00	-.09	.08	-.11	**-.42**	**-.22**	-.20	-.11
PMF Co	.15	-.08	-.17	-.07	.00	.03	.16	-.04	.04	.03	.01	-.06	-.21	**-.47**	**-.23**	**-.26**	-.13
PMF Fg	-.01	.10	.03	-.03	.06	.16	.17	.09	-.09	.03	-.02	.07	-.04	**-.37**	-.19	-.14	-.19
PMF Lt	-.06	-.15	**-.26**	-.15	-.03	.08	.05	-.01	-.04	-.12	-.04	-.06	.01	**-.33**	**-.20**	-.20	-.11
PMF Qa	.03	.01	-.07	-.07	-.02	.01	.13	-.02	.12	.05	-.01	-.15	-.13	**-.50**	-.16	**-.21**	-.21
PMF Qr	.01	.14	-.01	.02	.04	.00	.10	.03	.01	.01	.00	.14	-.90	**-.45**	**-.24**	**-.15**	**-.21**
Total significant	2	4	1	15	6	2	3	8	1	1	11	3	11	31	28	11	8
Mean	.03	.01	-.06	-.14	.05	.03	.03	.08	.03	-.01	-.03	.03	.05	-.27	-.18	-.09	-.10
Pearson r, Growth-Climate Correlation v. Latitude	.00	-.12	-.17	**-.62**	-.11	**-.44**	-.16	-.11	-.05	.10	.29	**.30**	**.56**	**.77**	**.50**	**.72**	**.36**

Table 3.5. Partial correlation matrix (Ppt only) for the growth-climate coefficient (Pearson r) for each of 34 climate variables for each population. 'Ppt' = total precipitation. Months with a 'p' preceding their abbreviation indicate they occurred in the year prior to the year of ring formation. Cells in bold are significant ($p < 0.05$). Sites are arranged from north (top) to south (Table 3.1). Site codes: BvI = Beaver Island, CoP = Colonial Point, HMC = Huron Mountain Club, JSB = Jacobsons' Sugar Bush, KNC = Kalamazoo Nature Center, MGB = Mary Gray Bird Sanctuary, Mwd = Maywood History Trail, Pet = Petersons' Hemlock Grove, PMF = Pioneer Mothers Memorial Forest, PNC = Price Nature Center, Vrh = Voorhees Audubon Sanctuary, Warner = Warner Audubon Sanctuary. Species codes: As = sugar maple *Acer saccharum*, Ba = yellow birch *Betula alleghaniensis*, Co = shagbark hickory *Carya ovata*, Fg = American beech *Fagus grandifolia*, Lt = tulip poplar *Liriodendron tulipifera*, Ps = white pine *Pinus strobus*, Qa = white oak *Quercus alba*, Qr = red oak *Quercus rubra*, Tc = eastern hemlock *Tsuga canadensis*.

Population	pMay Ppt	pJun Ppt	pJul Ppt	pAug Ppt	pSep Ppt	pOct Ppt	pNov Ppt	pDec Ppt	Jan Ppt	Feb Ppt	Mar Ppt	Apr Ppt	May Ppt	Jun Ppt	Jul Ppt	Aug Ppt	Sep Ppt
HMC As	-.05	-.07	.12	-.01	.11	.03	-.11	.04	.11	-.12	.04	.06	.06	.20	**.30**	-.01	-.02
HMC Ba	-.12	-.10	.09	.12	.09	.02	-.05	.14	**.20**	.05	-.02	-.04	.08	**.33**	**.24**	-.09	.05
HMC Ps	**-.26**	-.10	-.17	.03	.01	.04	-.03	-.12	-.03	.07	-.01	-.05	-.05	**.20**	.16	.12	.04
HMC Qr	-.13	-.05	-.01	.01	.05	-.02	-.10	-.09	-.04	-.08	.08	-.01	.09	**.18**	.20	.13	.09
HMC Tc	-.07	.18	.09	-.05	-.15	.00	.05	-.08	-.05	.02	-.07	.08	.15	-.06	-.01	-.03	-.07
Mwd As	-.04	-.04	**.20**	.09	.13	-.08	.12	-.03	-.07	.07	.13	-.01	.05	.04	.13	-.01	.07
Mwd Ba	-.01	-.03	.01	.20	.05	.04	.00	-.06	.13	.08	-.15	-.12	.04	.16	**.30**	-.10	.04
Mwd Ps	-.05	-.16	.09	**.24**	.16	.13	.03	-.04	.05	.19	-.11	.03	-.02	.08	**.32**	.02	.07
Mwd Qr	.00	-.10	.11	**.28**	.10	.10	-.03	.09	.04	.00	-.05	.01	.01	**.24**	**.35**	-.01	.11
Pet Tc	.07	.01	**.26**	.08	.15	**-.26**	.13	-.16	-.07	-.17	.00	.01	.09	.10	-.02	-.09	-.02
BvI As	-.08	.02	**.25**	**.21**	.08	-.11	-.01	-.10	.15	-.03	.07	.03	.09	**.21**	.23	.05	.09
BvI Ba	-.06	-.05	.10	**.28**	-.07	.02	-.05	.07	.08	.05	-.04	.03	**.21**	**.24**	**.39**	.05	.11

Table 3.5 Cont'd

BvI Tc	-.01	-.09	.19	.15	.05	**-.27**	.13	.06	.05	.01	-.06	-.14	.12	.11	.09	-.05	-.02
CoP Fg	-.07	.02	**.21**	**.26**	-.02	-.09	.07	.01	**.21**	.13	-.07	.00	.10	**.25**	**.34**	-.04	.00
CoP Ps	.05	-.12	.04	.14	.06	.15	.07	-.08	.06	.08	-.12	.04	.12	.11	**.22**	.16	.08
JSB As	.04	-.05	.00	-.02	-.06	**.24**	.05	-.01	**.15**	.14	-.04	-.04	**.30**	**.21**	**.28**	-.07	-.02
JSB Fg	-.05	**-.19**	.03	.16	.04	.00	**.16**	.03	**.28**	**.21**	-.10	.10	**.20**	**.26**	.11	.07	.04
JSB Tc	.15	.10	.10	.05	.04	-.05	**.22**	.13	.08	.02	-.05	-.06	.13	.16	.08	-.05	.02
PNC As	.01	-.03	**.26**	-.12	.06	.07	.09	-.07	.18	**.20**	-.05	-.10	-.01	.02	**.23**	.15	-.06
PNC Fg	.05	-.03	**.31**	-.02	.04	.03	.17	.00	.15	.16	-.15	-.13	.11	.05	.18	.18	.09
PNC Qa	**-.22**	-.15	.17	.02	**-.17**	-.07	**.21**	.08	**.20**	-.03	-.03	.19	.12	.02	**.47**	.09	-.12
PNC Qr	-.09	**-.17**	.09	.04	**-.14**	.00	.11	.00	**.26**	-.01	-.02	.08	.16	.17	**.29**	.08	.00
War As	-.03	-.10	-.04	-.14	.09	.12	-.02	.07	**.28**	.11	.05	.12	.00	**.23**	.17	**.23**	-.13
War Fg	-.11	.03	-.01	-.01	.12	.12	.09	.05	.12	**.17**	-.06	-.05	.21	**.26**	.19	**.33**	-.07
War Lt	-.16	.12	.00	.01	.06	.16	.17	.15	**.24**	.05	.03	.08	**.24**	**.28**	**.30**	.15	-.16
War Qa	-.14	-.04	.04	.06	.08	-.03	.19	.13	**.18**	.00	.07	.05	**.23**	**.28**	**.28**	.16	.04
War Qr	-.08	-.06	.05	.11	.01	.09	.18	.01	.04	-.10	-.15	.03	**.19**	**.33**	**.22**	.17	-.02
Vrh As	-.12	.03	-.15	.03	.00	.21	.09	.03	**.27**	.10	-.01	-.01	-.02	**.35**	**.29**	.16	-.13
Vrh Co	.00	-.13	**-.20**	-.03	.03	.05	-.06	.13	**.28**	.05	.06	.06	.15	**.33**	.08	-.01	-.03
Vrh Qa	-.08	.01	-.11	.12	.01	.02	.19	.13	**.27**	-.04	.01	.10	**.26**	**.40**	**.37**	.03	-.08
Vrh Qr	-.01	.00	-.03	.15	-.07	.12	**.24**	.06	.09	-.10	-.11	-.01	**.22**	**.50**	**.33**	.06	-.07
KNC As	-.17	.09	-.10	-.01	.18	.15	.12	.10	**.27**	**.21**	-.05	-.07	.02	**.37**	**.30**	**.27**	-.10

Table 3.5 Cont'd

KNC Fg	-.20	.10	-.16	.03	.15	.05	**.22**	.02	**.18**	.15	-.12	-.04	**.19**	**.49**	**.32**	**.24**	-.08
KNC Lt	-.20	.10	-.02	.05	.13	.12	.17	.05	**.21**	.14	-.06	-.04	**.20**	**.40**	**.31**	**.26**	-.01
KNC Qr	-.11	.00	-.10	-.10	.12	.14	**.21**	.01	**.17**	.13	**-.23**	.06	.12	**.41**	**.32**	**.22**	.00
MGB As	**-.19**	.08	-.12	-.02	.07	.13	**.19**	-.05	.13	.06	-.01	-.13	**.18**	**.44**	**.32**	.09	.02
MGB Co	-.14	.07	-.02	**.18**	.08	.12	.12	.07	.15	-.01	.09	-.09	.14	**.40**	**.33**	.12	.03
MGB Fg	-.07	-.03	.04	**.18**	.15	.12	.14	.14	.17	.03	-.04	**-.26**	.20	**.37**	**.35**	.11	-.03
MGB Lt	.03	.12	.01	.15	.12	-.08	.17	.08	.08	.04	.07	-.18	**.26**	**.57**	**.40**	.21	-.03
MGB Qr	-.14	.02	-.15	**.19**	.03	.05	.10	.08	**.18**	-.01	-.03	-.07	**.23**	**.45**	**.45**	.15	.06
PMF As	-.06	-.09	-.07	.12	**.36**	**.28**	.00	-.09	-.06	-.09	-.07	.12	**.36**	**.28**	.00	-.09	-.06
PMF Co	-.07	.13	-.02	**.21**	-.02	-.08	.10	.11	.13	.03	-.01	-.13	**.23**	**.32**	.20	.09	-.02
PMF Fg	-.06	.00	-.07	**.29**	-.02	.11	**.21**	.13	.09	-.02	-.06	-.07	**.23**	**.48**	**.22**	.12	**-.21**
PMF Lt	-.15	.05	-.11	.20	**.58**	**.26**	.13	**-.21**	-.15	.05	-.11	.20	**.58**	**.26**	.13	**-.21**	-.15
PMF Qa	.04	.05	.03	**.21**	**.46**	**.27**	.05	-.06	.04	.05	.03	**.21**	**.46**	**.27**	.05	-.06	.04
PMF Qr	-.08	-.05	-.11	.12	-.07	-.02	.13	.05	.13	.03	.03	-.08	.19	**.49**	**.37**	**.20**	-.11
Total significant	3	2	8	12	2	3	10	1	18	4	1	1	16	**33**	**32**	7	2
Mean	-.07	-.02	.03	.10	.04	.03	.10	.04	.14	.04	-.03	-.02	.14	**.28**	.26	.09	-.02
Pearson r, Growth-Climate Correlation v. Latitude	-.05	-.07	.12	-.01	.11	.03	-.11	.04	.11	-.12	.04	.06	.06	.20	**.30**	-.01	-.02

Table 3.6. The monthly mean temperature (T_{mean}) and total precipitation (Ppt) variables with the steepest slope in a regression of growth-climate coefficient (Pearson r) vs. time. Sites are arranged from north (top) to south. Months in bold indicate the variable which changed most in a column. Site codes: BvI = Beaver Island, CoP = Colonial Point, HMC = Huron Mountain Club, JSB = Jacobsons' Sugar Bush, KNC = Kalamazoo Nature Center, MGB = Mary Gray Bird Sanctuary, Mwd = Maywood History Trail, Pet = Petersons' Hemlock Grove, PMF = Pioneer Mothers Memorial Forest, PNC = Price Nature Center, Vrh = Voorhees Audubon Sanctuary, Warner = Warner Audubon Sanctuary. Species codes: As = sugar maple *Acer saccharum*, Ba = yellow birch *Betula alleghaniensis*, Co = shagbark hickory *Carya ovata*, Fg = American beech *Fagus grandifolia*, Lt = tulip poplar *Liriodendron tulipifera*, Ps = white pine *Pinus strobus*, Qa = white oak *Quercus alba*, Qr = red oak *Quercus rubra*, Tc = eastern hemlock *Tsuga canadensis*.

Population	T_{mean}, biggest changer (direction)	Ppt, biggest changer (direction)
HMC As	prior-Jun (-)	current-Mar (-)
HMC Ba	current-Feb (-)	current-Mar (-)
HMC Ps	current-Feb (-)	current-Apr (+)
HMC Qr	prior-May (-)	current-Mar (-)
HMC Tc	current-Jul (+)	current-Aug (+)
Mwd As	prior-Jun (-)	prior-May (-)
Mwd Ba	current-Feb (-)	**prior-Sep (-)**
Mwd Ps	prior-May (-)	current-Jan (-)
Mwd Qr	current-Jun (-)	prior-Jun (+)
Pet Tc	current-Jul (+)	current-Jan (-)
MaB As	prior-Jun (-)	prior-Oct (-)
MaB Ba	current-Mar (-)	current-Sep (+)
MaB Tc	prior-Jun (-)	current-Jan (-)
CoP Fg	**prior-Jul (-)**	prior-Jun (+)
CoP Ps	current-Jan (+)	**prior-Sep (-)**
JSB As	**prior-Jul (-)**	**prior-Sep (-)**
JSB Fg	prior-May (-)	current-Feb (-)
JSB Tc	current-Jan (+)	prior-May (-)
PNC As	current-Jan (+)	prior-Dec (-)
PNC Fg	current-Jan (+)	prior-Aug (-)
PNC Qa	prior-May (-)	**prior-Sep (-)**
PNC Qr	current-Sep (+)	**prior-Sep (-)**
War As	**prior-Jul (-)**	prior-Oct (-)
War Fg	prior-May (-)	prior-Aug (-)
War Lt	current-Jan (+)	prior-May (+)
War Qa	current-Feb (-)	**prior-Sep (-)**
War Qr	prior-Dec (-)	current-Mar (-)
Vrh As	**prior-Jul (-)**	**prior-Sep (-)**

Table 3.6 Cont'd

Vrh Co	prior-Sep (-)	current-Feb (+)
Vrh Qa	current-Jan (+)	**prior-Sep (-)**
Vrh Qr	current-Sep (+)	**prior-Sep (-)**
KNC As	**prior-Jul (-)**	**prior-Sep (-)**
KNC Fg	**prior-Jul (-)**	**prior-Sep (-)**
KNC Lt	prior-June (+)	**prior-Sep (-)**
KNC Qr	current-Sep (+)	**prior-Sep (-)**
MGB As	**prior-Jul (-)**	current-Jul (-)
MGB Co	current-Jan (+)	current-Apr (-)
MGB Fg	**prior-Jul (-)**	prior-May (+)
MGB Lt	current-Jul (+)	prior-May (+)
MGB Qr	current-May (+)	prior-May (+)
PMF As	current-Jul (+)	current-Sep (+)
PMF Co	current-Jan (+)	prior-Nov (+)
PMF Fg	current-Jul (+)	current-Apr (-)
PMF Lt	prior-May (-)	prior-Dec (-)
PMF Qa	prior-May (-)	prior-May (+)
PMF Qr	prior-May (-)	prior-Dec (-)

Table 3.7. Correlation matrix (Pearson r) for 1903–2004 mean annual temperature among study sites. Site codes: BvI = Beaver Island, CoP = Colonial Point, HMC = Huron Mountain Club, JSB = Jacobsons' Sugar Bush, KNC = Kalamazoo Nature Center, MGB = Mary Gray Bird Sanctuary, Mwd = Maywood History Trail, Pet = Petersons' Hemlock Grove, PMF = Pioneer Mothers Memorial Forest, PNC = Price Nature Center, Vrh = Voorhees Audubon Sanctuary, Warner = Warner Audubon Sanctuary.

	PMF	**MGB**	**KNC**	**Vrh**	**War**	**PNC**	**JSB**	**CoP**	**BvI**	**Pet**	**Mwd**	**HMC**
PMF	1.000	0.949	0.743	0.804	0.801	0.663	0.745	0.642	0.634	0.564	0.555	0.589
MGB		1.000	0.820	0.865	0.876	0.722	0.829	0.717	0.723	0.658	0.650	0.687
KNC			1.000	0.965	0.972	0.928	0.924	0.875	0.887	0.892	0.889	0.869
Vrh				1.000	0.978	0.922	0.925	0.842	0.873	0.859	0.856	0.850
War					1.000	0.910	0.934	0.860	0.890	0.860	0.856	0.850
PNC						1.000	0.902	0.894	0.903	0.895	0.893	0.870
JSB							1.000	0.937	0.933	0.897	0.890	0.903
CoP								1.000	0.959	0.928	0.922	0.913
BvI									1.000	0.942	0.939	0.922
Pet										1.000	0.997	0.969
Mwd											1.000	0.969
HMC												1.000

Table 3.8. Correlation matrix (Pearson r) for 1903–2004 total annual precipitation among study sites. Site codes: BvI = Beaver Island, CoP = Colonial Point, HMC = Huron Mountain Club, JSB = Jacobsons' Sugar Bush, KNC = Kalamazoo Nature Center, MGB = Mary Gray Bird Sanctuary, Mwd = Maywood History Trail, Pet = Petersons' Hemlock Grove, PMF = Pioneer Mothers Memorial Forest, PNC = Price Nature Center, Vrh = Voorhees Audubon Sanctuary, War = Warner Audubon Sanctuary.

	PMF	**MGB**	**KNC**	**Vrh**	**War**	**PNC**	**JSB**	**CoP**	**MaB**	**Pet**	**Mwd**	**HMC**
PMF	1.000	0.810	0.378	0.399	0.334	0.357	0.192	0.280	0.215	0.220	0.229	0.317
MGB		1.000	0.441	0.494	0.417	0.395	0.201	0.219	0.160	0.185	0.180	0.213
KNC			1.000	0.891	0.922	0.676	0.663	0.310	0.269	0.278	0.277	0.244
Vrh				1.000	0.912	0.742	0.604	0.249	0.191	0.211	0.218	0.188
War					1.000	0.732	0.630	0.232	0.174	0.230	0.232	0.171
PNC						1.000	0.662	0.257	0.220	0.232	0.223	0.165
JSB							1.000	0.589	0.519	0.495	0.484	0.335
CoP								1.000	0.885	0.701	0.701	0.614
MaB									1.000	0.684	0.677	0.638
Pet										1.000	0.995	0.722
Mwd											1.000	0.747
HMC												1.000

CHAPTER FOUR

CLIMATE CHANGE IS PROJECTED TO HINDER PRODUCTIVITY OF TREE SPECIES IN INDIANA AND MICHIGAN OVER THE 21st CENTURY

Abstract

Global climate is projected to continue changing over the rest of this century and beyond. Projections of local monthly temperature and precipitation are available through the end of this century based on the models of various meteorological research groups (Taylor et al. 2012). Such projections can be used along with modeled relationships between tree growth and climate to project future growth changes under climate change. Growth-climate models were calibrated over one half of available data for each of 46 tree populations from nine species across Indiana and Michigan. Model verification was then attempted on the other half of each dataset. Successfully verified models were used to project future growth under four climate-change scenarios.

Model verification was successful in 14 of 46 populations. In these populations, the most influential variables were related to summer-moisture stress. A negative association with current-June maximum temperature was the most influential variable in five of these models, followed by a negative association with current-July maximum temperature in three, and a positive association with current-July precipitation in two. Growth was projected to decline significantly in 12/14 populations under the two highest-warming climate-change scenarios and to increase in one population. Under the mildest climate-change scenario, growth was projected to decline in four populations, to increase in one, and to have no significant change in

nine. A preponderance of projected growth decline in all but the mildest scenario suggest that significant management options should be considered including assisted colonization and gene flow.

Introduction

Climate change is expected to have a negative impact on the trees of the eastern United States. Using forest inventories across the eastern U.S. and Canada, Prasad et al. (2020) modeled future habitat suitability and migration potential of 25 tree species. For the U.S., they found that under Representative Concentration Pathway (RCP) 8.5, ≈10,000–500,000 square km of habitat may be lost, depending on species, and much of this will be high-quality habitat. This will be partially offset by gains in potential habitat, however most of the gained potential habitat will be lower quality, and little of it will be realized over this century due to dispersal limitations.

Further, tree-ring-based studies of growth-climate relationships suggest that strong limitations placed on growth by summer-moisture stress are likely to be exacerbated as climate change proceeds. These studies were cited in greater detail in the previous chapter. To recapitulate, this pattern was found for both *Liriodendron tulipifera* (tulip poplar) and *Quercus spp.* (oaks) across their range in eastern North America (LeBlanc & Berland 2019, LeBlanc et al. 2020), for eight hardwood species spanning Georgia to Vermont (Martin-Benito & Pederson 2015), for eleven species in the western Great Lakes Region (Graumlich 1993), and for *Acer saccharum* (sugar maple) and *Q. alba* (white oak) across much of the eastern U.S. (Au et al. 2020).

This pattern was corroborated for Indiana and Michigan in the previous chapter. In a network of tree-ring chronologies from nine species spanning an eight-degree latitudinal gradient, the dominant factor limiting radial growth was summer-moisture stress, i.e., the strongest relationships between growth and climate were negative relationships with June average temperature and positive relationships with June precipitation. This suggests that ongoing climate change in Indiana and Michigan, which is expected to bring increased summer temperature and more erratic precipitation patterns (Hayhoe et al. 2010, Christensen et al. 2013, Byun & Hamlet 2018), will lead to reduced tree growth in the region.

However, the previous chapter also showed that the summer-moisture-stress signal was weaker at the more northerly sites, corroborating other studies (Martin-Benito & Pederson 2015, LeBlanc & Berland 2019, LeBlanc et al. 2020). The weaker signal was particularly apparent in *Tsuga canadensis* (eastern hemlock). Further, other growth-climate relationships found in the previous chapter and elsewhere in the literature suggest that certain aspects of climate change could ameliorate the growth reductions due to anticipated increases in summer moisture stress. Winter temperature, winter precipitation and spring temperature are expected to increase (Hayhoe et al. 2010, Christensen et al. 2013, Byun & Hamlet 2018). Growth of many of the 46 tree populations studied in Chapter 3 was positively correlated with those variables. For example, current-year growth of 18/46 populations was positively correlated with January precipitation (Jan_{Ppt}). For the remaining populations, the relationship was nonsignificant. Growth of eight populations was positively correlated with prior-December mean temperature (prior-Dec_{Tmean}). Similar results were found elsewhere in the northeastern U.S. (Pederson et al. 2004; Martin-Benito and Pederson 2015). Additionally, growth of all four *T. canadensis*

populations studied in Chapter 3 was positively correlated with current-Mar_{Tmean}, which has also been found elsewhere (Cook and Cole 1991, Dye & Woods 2019). Disentangling the potentially positive effects of warmer springs and warmer, wetter winters from the negative effects of warmer, more drought-prone summers requires mathematical modeling.

This has been done to some extent in trees around the world, including in Mexico (Brienen et al. 2010, Pompa-Garcia et al. 2017), Australia (Nitschke et al. 2017), Bangladesh (Rahman et al. 2018), China (Su et al. 2015), western North America (Chhin et al. 2008; Chen et al. 2010; Charney et al. 2016), Spain (Sanchez-Salguero et al. 2017), Lithuania (Rimkus et al. 2018), and eastern North America (Huang et al. 2010, Charney et al. 2016, Chhin 2015, Chhin 2016, Tei et al. 2016). However, little work has been done on the native species of temperate eastern North America, outside of conifers and oaks (Charney et al. 2016). Here, I select the most parsimonious growth-climate models for each of the 46 tree populations discussed above. I then attempt to verify the statistical skill of those models. Finally, I employ all models which have sufficient predictive skill, together with projections of future climate, to project future growth over the rest of this century. I hypothesized that growth will generally decline over this century, but that the decline will be milder at more northerly sites especially for *T. canadensis*.

Methods

Field Methods and Tree-Core Processing

A network of tree-ring chronologies was generated at 12 sites along a latitudinal gradient from southern Indiana to northern Michigan (Fig. 3.1, Table 3.1). Between one and six species are represented at each site for a total of 46 populations (stands) from nine species.

Details about site/species selection and field methods are described in Chapter 3. Cores were later sanded, the calendar dates of tree rings were established, ring widths were measured, and ring-width measurement series were standardized and detrended according to disciplinary standards (Stokes & Smiley 1996, Speer 2009). Again, further detail is provided in Chapter 3.

Growth-Climate Modeling

Modeling the relationship between tree growth and climate was conducted in the R statistical environment (R Core Team 2017). The climate variables considered in the modeling process included total monthly precipitation (Ppt) and minimum, mean, and maximum temperature (T_{min}, T_{mean}, and T_{max}), each averaged over the month. Variables were considered at the single-month scale throughout a window from May of the year preceding tree growth through September of the year of tree growth (Fritts 1976). The single-month scale was selected because pilot analysis revealed that single-month variables explained more variability than did variables spanning, two, three, and/or four months. Gridded 4 km × 4 km interpolations of these variables were obtained from the PRISM Climate Group (Daly et al. 2008).

The interval held in common by all tree-ring chronologies was split into two periods: the calibration period, 1903–1953, and the verification period, 1954–2004. Models were selected for each population over the calibration period. The function 'stepAIC' in the R package 'MASS' (Venables & Ripley 2002) was used to conduct forward-stepwise multiple regression (Chhin et al. 2008). This regression was conducted over three steps, with each step adding the single variable which lowered the Akaike Information Criterion (AIC) by the largest amount (Akaike

1974). I stopped at three steps, ensuring after each step that AIC went down, because it was found in pilot modeling that more than three variables in the final model resulted in over-fitting, i.e., though AIC typically continued to go down and adjusted r^2 to go up, the success of model verification over the 1954–2004 verification period tended to go down.

To be deemed reliable for projection of future growth, models had to pass three criteria over the verification period. First, the model's p-value had to be less than 0.05. Second, the reduction of error (RE) had to be greater than zero. This statistic was first used in meteorology for the verification of weather forecasting (Lorenz 1956), and it has been adopted extensively in the dendroclimatological literature (Fritts 1976, Cook et al. 1999). It involves comparing the predictive power of the selected model with the predictive power of the calibration-period mean. RE can theoretically range from $-\infty$ to 1; any value greater than zero indicates predictive skill. It can be found according to

$$RE = 1 - \left(\frac{\sum (x_i - \hat{x}_i)^2}{\sum (x_i - \bar{x}_c)^2} \right)$$

where x_i is the observed ring-width index (RWI) at year$_i$, $\hat{x}_i$ is the predicted RWI at that year, and $\bar{x}_c$ is the mean RWI of the calibration period. The final criterion was that the coefficient of efficiency (CE) also had to be greater than zero. CE was first used in hydrology (Nash & Sutcliffe 1971) and has also been adopted by dendroclimatologists (Cook et al. 1999). It has the same theoretical range and predictive-skill threshold as RE. It differs in that it compares the predictive power of the selected model with that of the verification-period mean according to

$$CE = 1 - \left(\frac{\sum (x_i - \hat{x}_i)^2}{\sum (x_i - \bar{x}_v)^2} \right)$$

Where $\bar{x}_v$ is the mean RWI of the verification period, and all other abbreviations are as stated previously. As soon as a model failed any of these criteria, the corresponding population was discarded from further analysis.

Future-Growth Projections

If a model passed the above three criteria, then that model was refit over the entire common interval, i.e., the calibration and verification periods were combined (Pederson et al. 2012). Corresponding climate data were then entered into the entire-interval model to simulate growth over the observational record (Brienen et al. 2010, Nitzsche et al. 2017).

Gridded, downscaled Coupled Model Intercomparison Project Phase 5 (CMIP5) projections of climate for the interval 2021–2099 were obtained for each study site from https://gdo-dcp.ucllnl.org/downscaled_cmip_projections/ for two climate-change scenarios, RCPs 4.5 and 8.5 (Taylor et al. 2012). RCP 4.5 represents the second-most benign scenario out of four, wherein atmospheric greenhouse gas concentrations stabilize by 2100. RCP 8.5 is the most severe scenario, wherein concentrations continue to increase even beyond 2100. The appropriate 1/8° × 1/8° grid was selected for each study site. All sites for which at least one growth-climate model was successfully verified fell within a downscaled grid except for the Martin's Bluff (MaB) site, for which the nearest available grid was selected. Downscaled projections from many CMIP5 global circulation models (GCMs) were available. I selected from a pool of 13 models which include the influence of the Great Lakes in their simulations (J. A. Andresen *pers. comm.*). I chose to forecast a wide range of potential future growth. Of the 13 potential GCMs, that which predicted the greatest amount of 21st-century warming and that

which predicted the least were selected (Moser et al. 2020). This was determined based on the median latitude and longitude of the tree-ring network. For the grid within which the median latitude/longitude fell, RCP 4.5 and 8.5 projections were obtained from each of the 13 potential GCMs. The projected mean annual temperature of this grid for 2021–2099 was compared among the GCMs under each RCP. For each RCP, the GCM MRI-CGCM3 predicted the least warming (Yukimoto et al. 2012) and the GCM GFDL-CM3 predicted the most (Griffies et al. 2011).

Projected climate from these two GCMs was compared across the different modeled scenarios and compared to the historic common interval. Rather than focusing on all examined variables, the variables which were consistently most important in the selected growth-climate models were examined. Differences in projected temperature and precipitation were visually compared with bar and box plots, respectively.

To project future growth, relevant projected variables from MRI-CGCM3 and GFDL-CM3 were entered into the models selected for each retained tree-ring chronology. The function 'predict' from the R package 'stats' was used to predict 2022–2099 RWI (R Core Team 2017). Projected RWI from each scenario (2 GCMs × 2 RCPs) were averaged over this interval and 95% confidence intervals of the mean were calculated. Comparisons of the mean of these four scenarios and of simulated RWI over the observational record were made for each population with ANOVA.

Results

Model Calibration and Verification

Of the 46 growth-climate models fit over the 1903–1953 calibration period, 27 were significant ($p < 0.05$) when fit to the 1954–2004 verification period (Table 4.1). The next two validation criteria were that RE and CE had to be > 0 over the verification period. Of the 27 models which made it to these steps, 14 passed each of these criteria (Table 4.1).

Model verification was generally more successful in the south of the gradient than in the north. Among 22 populations in the northern half of the gradient, there were only five successful verifications, three of which were *T. canadensis*. Validations were successful for 9/24 populations in the southern half of the gradient, from a mix of all six species that were sampled in the south.

Characteristics of Validated Models

For 9 of the 14 successfully validated models, the first variable to enter the model in stepwise regression over the calibration period was a current-summer maximum-temperature variable, whether in the month of June (5 populations), July (3), or August (1); these were all populations in the southern half of the study gradient; the correlation was always negative (Table 4.2). For the remaining 5 successfully validated populations, each in the northern half of the gradient, current-Jul_{Ppt} was the first variable in 2 populations (positive relationship), prior-$JulT_{Tmax}$ and prior-Aug_{Tmean} were each first in 1 (negative relationship), and prior-Nov_{Ppt} was first in 1 (positive relationship). Among the second and third variables to go in the model, frequent relationships were found with current-Jun or -Jul_{Tmax} (3 populations, relationships all negative),

with current-Jun or -Jul_{Ppt} (5 populations, all positive), and with T_{min}, T_{mean}, or T_{max} in the prior-October, November, or December (7 populations, all positive) (Table 4.2).

When the verified model was applied to the entire common interval, the three retained variables in combination explained between 14.7 and 48.3% of the variability of each population's growth (Table 4.2). Partial regression coefficients reveal the effect of retained variables in isolation. For example, the strongest growth-temperature relationship was between current-Jul_{Tmax} and *A. saccharum* RWI at Voorhees Audubon Sanctuary (Vrh). If all other variables were held constant, a 1 °C increase in Vrh Jul_{Tmax} would result in a .0571 decrease in *A. saccharum* RWI (Table 4.2). The strongest positive growth-temperature relationship was between current-Mar_{Tmin} *and T. canadensis* RWI at Martin's Bluff (MaB). There, a 1˚C increase in current-Mar_{Tmin} led to a 0.0315 increase in *T. canadensis* RWI. The effects of retained precipitation variables were always positive (Table 4.2). The maximum was a 0.00229 increase in RWI per mm increase of current-Jun_{Ppt} for *L. tulipifera* at Pioneer Mothers Memorial Forest (PMF).

Comparison of Historic and Projected Growth

The most consistently important variables to enter the retained models were summer temperature (June, July, or August) and precipitation (June or July). At all sites, June–August mean temperature was projected to increase significantly under all scenarios relative to the historic common interval. Projected increases in the mean range from 1.1 °C at PNC under MRI-CGCM3 for RCP 4.5 to 7.1 °C under GFDL-CM3 for RCP 8.5 at Petersons' Hemlock Grove (Fig. 4.1a). Under the GFDL-CM3 model, increases were more dramatic, even for RCP 4.5, than under

MRI-CGCM3 for RCP 8.5 (Fig. 4.1a). Projected temperature increases were significant throughout the gradient, but generally greater in the north. Regarding June–July total precipitation, it was generally projected to increase (Fig. 4.1b). This was true under both models, MRI-CGCM3 and GFDL-CM3. In the south of the gradient, projected increases were generally more dramatic under GFDL-CM3.

Future-Growth Projections

Growth over the rest of this century under both RCP 4.5 and 8.5 under both GCMs MRI-CGCM3 and GFDL-CM3 was generally projected to decline in relation to the historic common interval (Fig. 4.2). However, for some populations there would be no significant growth changes under the milder GCM, MRI-CGCM3. That is true for all three of the *T. canadensis* populations and for *A. saccharum* at Vrh (single-population one-way ANOVA p-values > 0.05). All ten other populations, except for one, would experience growth decline under MRI-CGCM3, at least for RCP 8.5. In some cases, this would be dramatic. *A. saccharum* at Maywood History Trail (Mwd) would decline by 13.1 and 16.4% under RCPs 4.5 and 8.5, respectively. *Carya ovata* at Mary Gray Bird Sanctuary (MGB) would decline by 8.13 and 9.91% (Fig. 4.2). The sole population projected to increase in growth under MRI-CGCM3 scenarios is *Q. alba* at Price Nature Center (PNC), where its growth would increase by 5.18 and 8.20% under RCPs 4.5 and 8.5, respectively.

Under GFDL-CM3 scenarios, growth would significantly decline for all but two populations, and the decline would generally be more dramatic than under the MRI-CGCM3 scenarios. Even for RCP 4.5, the decline under GFDL-CM3 would generally be more dramatic than either MRI-CGCM3 4.5 or MRI-CGCM3 8.5 (Fig. 4.2). For GFDL-CM3 under RCP 4.5, growth

declines would range from a non-significant 3.98% for *L. tulipifera* at PMF to 28.0% for *A. saccharum* at Mwd (Fig. 4.2). For GFDL-CM3 under RCP 8.5, declines would range from 4.47% for *L. tulipifera* at PMF ($p > 0.05$) to 34.2% for *A. saccharum* at Mwd. As under MRI-CGCM3, *Q. alba* growth at PNC would significantly increase under GFDL-CM3, by 11.8 and 12.1% under RCPs 4.5 and 8.5, respectively.

There was no latitudinal trend in future-growth projections. For example, the three populations projected to decline the most under GFDL-CM3 came from both the most northerly site (Mwd) and the third-most-southerly site (Vrh); the sole population projected to accelerate came from a mid-gradient site, PNC; the populations projected to face the mildest decline in growth came from the most southerly site, PMF. However, the lack of a clear trend may be confounded by differences among species. A different suite of species was sampled at each end of the gradient. Further, the maximum representation of any species was three populations, a number too small for the examination of within-species latitudinal trends.

Discussion

Model validation was relatively unsuccessful throughout the gradient, with 14/46 populations passing all three validation criteria. For the remaining 32 populations, it is not possible to project changes in growth with the present dataset. By contrast, calibrated growth-climate models were successfully verified for 3/5 populations in Australia (Nitzschke et al. 2017), 4/4 sites in Lithuania (Rimkus et al. 2019), 3/3 populations in Bangladesh (Rahman et al. 2018), 3/3 populations in northern Mexico (Pompa-Garcia et al. 2017), 33/33 populations in eastern boreal Canada, and 3/3 populations in subtropical China (Su et al. 2015). The low

verification rate in the present study may be due to the relatively benign climate of temperate eastern North America. Its humid climate leads to complacent (low-variability) tree-ring chronologies (Phipps 1982). In a gridded reconstruction of summer moisture based on composites of tree-ring chronologies available near each of 154 points throughout the continental United States, the lowest verification statistics were found for the upper Midwest and northern New England (Cook et al. 1999). The present finding that northerly populations had a lower model-verification success rate than did southerly ones supports that. Further, relatively low variability was also explained by growth-climate models derived from tree-ring chronologies in nearby Ontario: on the Bruce Peninsula and proximal islands (Buckley et al. 2004).

The finding in this study that summer precipitation and temperature variables were most important, being the first to enter the calibrated models in 13/14 successfully validated models, was consistent with the findings in Chapter 3 and with other published information on temperate tree growth in eastern North America. For example, LeBlanc et al. (2020) performed stepwise multiple regression to model ring-width-climate relationships for 45 *L. tulipifera* populations across eastern North America. For 35 populations, current-summer precipitation was the first or only variable to enter the model, and for 8 of 10 remaining populations a different summer precipitation or temperature variable was first to enter. Similar results were found for non-native *Pinus* hybrids growing in Michigan (Chhin 2015).

The only other classes of variables consistently retained in validated models were with current-Mar_{Temp}, and prior-Nov/Dec_{Temp}, and prior-Nov/Dec_{Ppt}. Relationships with these variables were positive, and it was hypothesized *a priori* that projected increases in these

variables could ameliorate projected exacerbation of summer moisture stress. However, even when these variables were selected in models, they tended to be selected second or third, and their influence tended to be relatively low (Table 4.2). Again, this was consistent with the modeling of LeBlanc et al. (2020). For 45 calibrated *L. tulipifera* growth-climate models, prior-Winter$_{Tmin}$ was included in 17, however it was the first variable to enter the model only twice. By contrast, in Chhin's (2015) and (2016) selection of growth-climate models for hybrid *Pinus* and hybrid *Populus* (aspen) growing in Michigan plantations, winter and spring temperature and precipitation tended to have more significant contributions to the models. Moving northward, Huang et al. (2013) found in eastern boreal Canada that climate variables outside of the growing season were frequently first to enter their calibrated models. Further, at these higher latitudes, growth was often positively related with temperature even during the growing season.

It was hypothesized *a priori* that projected reductions in 21st century tree growth would be greatest in the south of the gradient because the most southerly populations exhibited the strongest indications of summer moisture stress, i.e., the most strongly negative growth-temperature and strongly positive growth-precipitation relationships (Chapter 3). However, growth reductions were not projected to be greater in the south (Fig. 4.2). It should be reiterated that this question is confounded by the differing assemblage of species across the gradient. Another factor is that the projected warming of the GCMs selected for this study was greater in the north than in the south (Fig. 4.1a), as has been more widely predicted (Christensen et al. 2013). Further, projected summer moistening was greater in the south than in the north (Fig. 4.1b). Thus, climate change impacts on radial growth will not necessarily be

consistent with the expected trend of low-latitude/altitude populations suffering more than their conspecifics at higher latitudes/altitudes (Parmesan 2006). The opposite trend may even be found for some species, as predicted for *Pseudotsuga menziesii* (Douglas fir) in western North America (Chen et al. 2010).

A bright spot of the present study was that growth of one population, *Quercus alba* at Price Nature Center, was projected to increase under all climate change scenarios considered. This was because this population was relatively insensitive to summer temperature (Fig. 3.4a, Tables 3.4 and 4.2). It was more sensitive to summer precipitation and prior-fall temperature, two variables with which its growth was positively correlated and which were projected to increase under the climate projections selected. This unique set of growth-climate relationships could be due to site-level factors, however the other species sampled at this site, including the congeneric *Q. rubra*, did not share the insensitivity to summer temperature. It could also be due to adaptation to high temperatures. It is recommended that this be tested experimentally. If this population proved insensitive to experimental warming, it would be a good candidate for assisted gene flow (Aitken & Whitlock 2013).

By contrast, the other 13 populations for which future growth was projected are likely to experience lower growth for the rest of this century relative to historic observations under GCM GFDL-CM3 and 9/14 for MRI-CGCM3. This concerning result has been found for several other species/regions: *P. menziesii* in western North America (Chen et al. 2010), *Pinus contorta* (lodgepole pine) in Alberta (Chhin et al. 2008), *Mimosa acantholoba* in Mexico (Brienen et al. 2017), several lineages of both *Pinus nigra* × *P. densiflora* (hybrid pine) and *Populus* × *smithii* (hybrid aspen) in Michigan (Chhin 2015, 2016), three urban landscaping trees in Australia

(Nitzsche et al. 2017), and three species in Bangladesh (Rahman et al. 2018). By contrast, only two of three endangered conifer species studied in northern Mexico were projected to face growth declines, and the other to experience increased growth (Pompa-Garcia et al. 2017). Similarly, two conifers in Spain were projected to lose growth, the other to gain growth (Sanchez-Salguero et al. 2017). In subtropical China, one species was projected to lose growth, one to experience no change, and one to gain growth (Su et al. 2015). In Lithuania, several populations of *Pinus sylvestris* (Scots pine) were projected to experience radial growth increases (Rimkus et al. 2018). In four species of eastern boreal Canada growth increases were largely projected in the north of the region and little change in the south (Huang, et al. 2013). Tei et al. (2017) projected circumboreal future growth and found that growth was likely to increase across wide areas, such as in northern Eurasia and the west coast of Canada but likely to decrease over large areas elsewhere, such as interior Alaska and Canada. Charney et al. (2016) projected growth across North America and found it was likely to decrease in the interior west and Midwest and to increase in the far west, the southeast, and the far northeast.

It should be noted that the future growth projections presented here should be interpreted cautiously because the climate projections used in modeling future growth fall outside the range of climate variability used to calibrate the models (Chen et al. 2010). Further, there are a variety of other factors not considered in the models which will be influenced by global change, such as increasing erraticism of precipitation (Byun & Hamlet 2018), increased fire prevalence (Tang et al. 2015), conversion of snow to rain (Byun & Hamlet 2018), more rapid snowmelt (Suriano & Leathers 2017), successional maturation of eastern forests (Moser et al. 2020), nonnative insects and pathogens (Lovett et al. 2016), and a growing human population

(Moser et al. 2020). Further, modeling future growth is sensitive to the GCM selected for obtaining climate projections. By selecting two GCMs, one which is unusually mild in its warming projection and another which is unusually extreme, the present study attempts to model the full range of potential growth change in the absence of the effects of other changing variables.

Finally, CO_2 fertilization is a factor which could mitigate the negative consequences of summer moisture stress. As temperature increases or as precipitation decreases, trees must either close their stomata and cut off their CO_2 supply or leave their stomata open at the cost of heavy water loss. However, as atmospheric CO_2 concentrations continue to rise, the cost of keeping stomata closed more often could be offset. As discussed in Chapter 1, some evidence of growth enhancement due to CO_2 fertilization has been found (Lamarche et al. 1984, Bazzaz et al. 1990, Telewski et al. 1999, Wang et al. 2006, Cole et al. 2010, McMahon et al. 2010, Walker et al. 2019). In other cases, either no enhancement or only a temporary enhancement due to CO_2 fertilization was found (Salzer et al. 2009, Norby et al. 2010, Van der Sleen et al. 2015, Girardin et al. 2016). In a projection of future growth across North America. Charney et al. (2016) found that under RCP 8.5 it would take a 72% water-use efficiency increase, due to CO_2 fertilization, to offset growth declines. Despite the variables for which the present models did not account, the tree-ring based projections of the present study and other studies from the region (Chhin 2015, 2016; Charney et al. 2016) are consistent with projected range retraction (Walker et al. 2002, Prasad et al. 2020). Together, projections of reduced growth and range retraction suggest that land managers need to consider dramatic management strategies such as assisted colonization (Albrecht et al. 2012) and assisted gene flow (Aitken & Whitlock 2013).

To identify genotypes which are potentially resilient to a given location's future climate, systematic dendrochronological sampling is recommended for the region, followed by growth-climate modeling and projection of future growth under the climate of various locations (Chen et al. 2010).

Conclusion

The relationship between growth and climate was modeled for each of 46 tree populations from nine species across Indiana and Michigan. The models were calibrated on one half of available data. Verification was attempted on the other half of the data by comparing model-predicted growth with observations. Verification was successful for 14/46 populations. Growth of these 14 populations was forecast under ongoing climate change for the rest of this century according to projections for four climate-change scenarios.

Growth of one population was projected to increase by 5.18–12.1% depending on the scenario. Growth of the other 13 populations was generally projected to decline. Under the mildest scenario, only 4 of these 13 would decline significantly. However, under the second mildest 9 would decline significantly. Under the two scenarios with the most warming, declines would be significant in 12 populations, ranging from 4.79% in one *A. saccharum* population to 34.2% in a different population of that species. With large and widespread growth declines under all but the mildest warming scenario considered, significant management strategies should be considered.

APPENDIX

APPENDIX

Figures

Figure 4.1. Comparison of historic and projected June–August mean temperature (a) and June–July total precipitation (b). The number after each three-letter site code represents decimal degrees north latitude (Table 3.1). Climate projections are from global circulation models (GCMs) MRI-CGCM3 (Yukimoto et al. 2012) and GFDL-CM3 (Griffies et al. 2011) under representative concentration pathways (RCPs) 4.5 and 8.5.

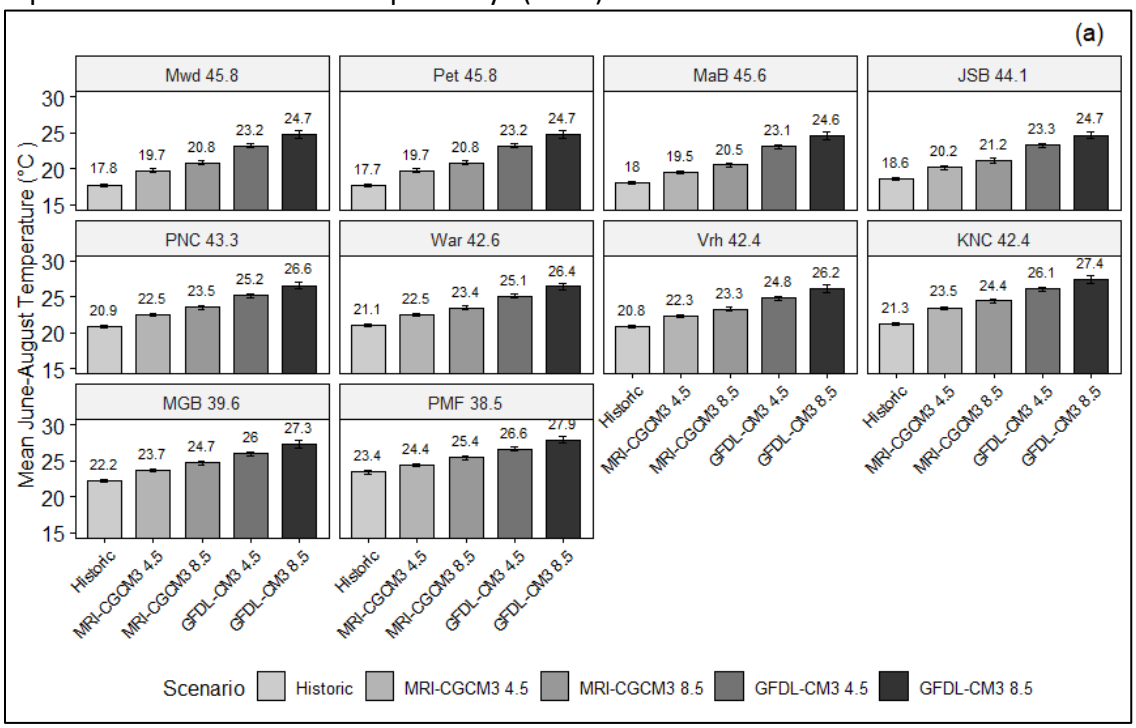

Figure 4.1 Cont'd

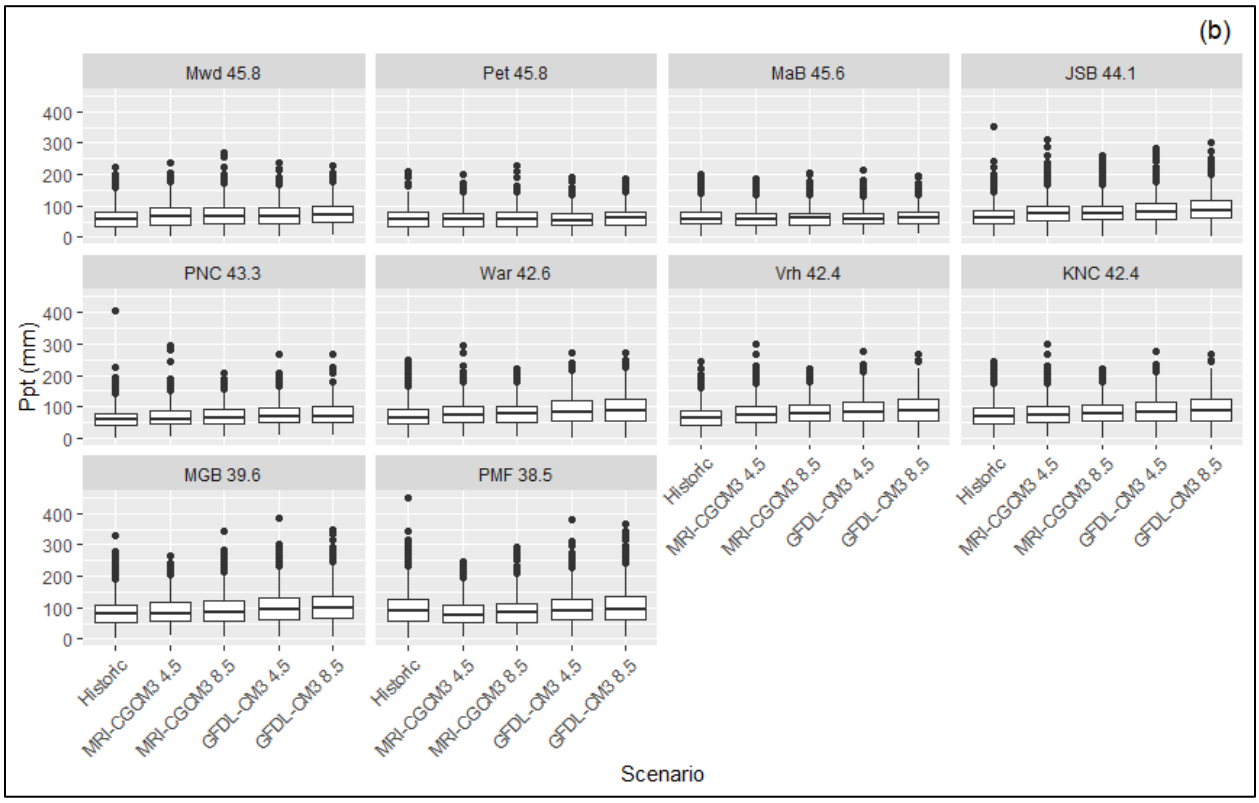

Figure 4.2. Mean forecasted ring-width indices (RWI) over years 2022-2099 under two representative concentration pathways (RCPs 4.5 and 8.5), under each of two GCMs, MRI-CGCM3 (Yukimoto et al. 2012) and GFDL-CM3 (Griffies et al. 2011), relative to simulated RWI over common interval 1903-2004. Historic and future RWI were simulated according to models fit over the 1903-1953 calibration period (Table 1). Note that RWI of all populations was standardized to a mean of 1 in the pre-modeling detrending process. Error bars represent 95% confidence intervals about the mean. Tree populations are arranged from north (left) to south (right); site abbreviations are in Table 3.1. Within each population, scenarios sharing a letter did not significantly differ in an ANOVA test ($p > 0.05$). Species codes: As = sugar maple *Acer saccharum*, Co = shagbark hickory *Carya ovata*, Fg = American beech *Fagus grandifolia*, Lt = tulip poplar *Liriodendron tulipifera*, Qa = white oak *Quercus alba*, Qr = red oak *Quercus rubra*, Tc = eastern hemlock *Tsuga canadensis*.

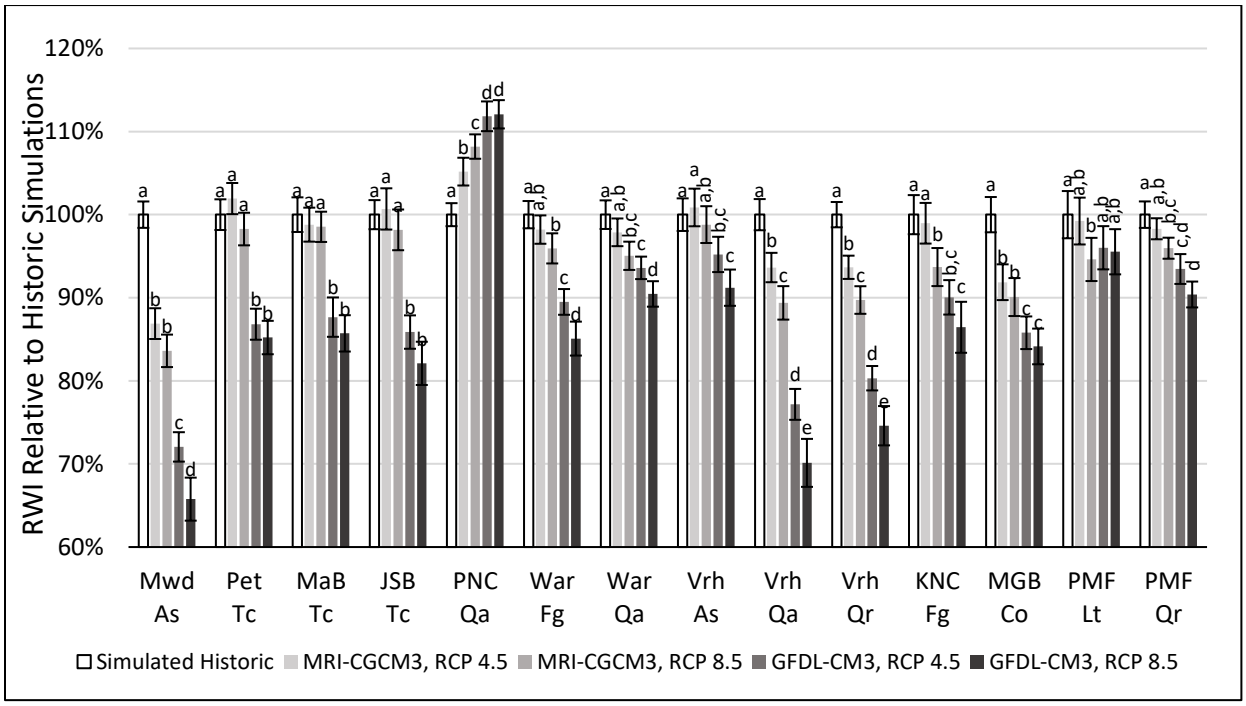

Tables

Table 4.1. Calibration and verification statistics and parameters for models relating climate and ring-width index. Data were split into calibration (1903-1953) and verification periods (1954-2004). Forward stepwise multiple regression established the three most explanatory variables over the calibration period. Models were then applied to the verification period and judged sequentially according to three criteria: p-value, reduction of error (RE), and coefficient of efficiency (CE). If a model failed any criterion it was then discarded and not judged by subsequent criteria. Parameters are listed in the order in which they entered the model. Climate variables are abbreviated with numbers corresponding to months (month 1 = Jan., 12 = Dec.), letters preceding months indicate whether the month occurred in the year prior to ring formation ("p") or in the year of ring formation (the current year, "c"). Specific climate variables are abbreviated as: 'Ppt' = total mm of precipitation and 'Tmean', 'Tmin', and 'Tmax' = mean, minimum, and maximum temperature (°C), each averaged over the month. RE and CE are explained in the Methods section above. Sites are arranged north to south (Table 3.1). Species codes: As = sugar maple *Acer saccharum*, Ba = yellow birch *Betula alleghaniensis*, Co = shagbark hickory *Carya ovata*, Fg = American beech *Fagus grandifolia*, Lt = tulip poplar *Liriodendron tulipifera*, Ps = white pine *Pinus strobus*, Qa = white oak *Quercus alba*, Qr = red oak *Quercus rubra*, Tc = eastern hemlock *Tsuga canadensis.*

Population	Model Parameters (Climate Variables)	Adj. r^2, 1903-1953	p-value, 1903-1953	Adj. r^2, 1954-2004	p-value, 1954-2004	RE	CE
HMC As	c7Ppt + p8Tmin + c3Ppt	0.389	8.12E-06	5.12E-04	0.397		
HMC Ba	c6Ppt + c7Ppt + p6Ppt	0.326	7.75E-05	0.0262	0.241		
HMC Ps	c2Tmax + p7Tmin + p8Tmin	0.325	7.80E-05	-0.0263	0.635		
HMC Qr	c3Ppt + p11Tmin + p6Tmax	0.236	1.29E-03	-0.0449	0.0177		
HMC Tc	p9Tmax + c4Tmax + p10Tmin	0.264	5.68E-04	0.0731	0.0879		
Mwd As	c7Ppt + p11Ppt + p8Tmin	0.256	7.22E-04	0.125	0.0260	0.0478	0.0200
Mwd Ba	c7Ppt + p8Ppt + c6Tmin	0.388	8.52E-06	0.128	0.0241	-0.174	

Table 4.1 Cont'd

Mwd Ps	c7Ppt + p9Ppt + p8Ppt	0.394	6.65E-06	0.0402	0.180		
Mwd Qr	c7Ppt + p8Ppt + p9Ppt	0.380	1.15E-05	.0305	0.220		
Pet Tc	p7Tmax + c6Ppt + c3Tmean	0.358	2.57E-05	0.316	1.06E-04	0.156	0.156
MAB As	c7Ppt + c6Ppt + p10Ppt	0.432	1.51E-06	0.140	0.0177	-0.438	
MaB Ba	c7Ppt + c6Tmin + p8Ppt	0.393	7.01E-06	0.158	0.0113	-0.281	
MaB Tc	p8Tmean + c3Tmin + p7Ppt	0.360	2.37E-05	0.325	7.92E-05	0.224	0.211
CoP Fg	c7Ppt + c2Ppt + p10Ppt	0.355	2.79E-05	0.118	0.031	-0.494	
CoP Ps	c7Tmax + p9Ppt + c5Tmin	0.353	2.98E-05	0.0550	0.131		
JSB As	c7Tmax + p12Tmax + c4Ppt	0.459	5.04E-07	0.0701	0.0942		
JSB Fg	c2Ppt + p12Tmax + c9Tmean	0.409	3.76E-06	-0.0430	0.816		
JSB Tc	p11Ppt + p7Tmin + p12Tmax	0.170	8.09E-03	0.118	0.0309	0.0891	0.0879
PNC As	c7Ppt + c2Ppt + p8Tmax	0.432	1.55E-06	-0.0131	0.508		
PNC Fg	c7Ppt + p7Ppt + c6Tmin	0.370	1.67E-05	0.0369	0.193		
PNC Qa	c7Ppt + p7Ppt + p11Tmin	0.446	8.59E-07	0.148	0.0144	0.146	0.136
PNC Qr	c7Ppt + c9Tmin + p10Tmin	0.378	1.21E-05	-0.0261	0.633		
War As	p12Tmax + c7Tmax + c5Tmean	0.444	9.55E-07	0.0971	0.0505		
War Fg	c8Tmax + c5Tmin + c6Tmax	0.460	4.78E-07	0.294	2.17E-04	0.0904	0.0890
War Lt	c6Tmax + p10Ppt + c4Tmin	0.249	8.74E-04	0.0960	0.0519		
War Qr	c6Tmax + p12Tmean + c8Tmax	0.408	4.31E-06	0.101	0.0457	-0.0821	

Table 4.1 Cont'd

Vrh As	c7Tmax + p12Tmean + c5Tmean	0.442	1.02E-06	0.188	4.98E-03	0.122	0.121
Vrh Co	p7Tmax + c7Tmax + c1Tmax	0.388	8.62E-06	-0.0396	0.779		
Vrh Qa	c7Tmax + p12Tmin + c6Tmax	0.458	5.25E-07	0.206	3.02E-03	0.111	0.108
Vrh Qr	c6Tmax + p12Tmin + c7Tmax	0.397	6.02E-06	0.268	5.01E-04	0.110	0.0975
KNC As	c7Tmax + p9Ppt + c8Ppt	0.453	6.53E-07	.0687	0.0972		
KNC Fg	c7Tmax + p5Tmax + c6Ppt	0.521	3.06E-08	0.343	4.27E-05	0.0643	0.0622
KNC Lt	c6Tmax + c7Ppt + c8Ppt	0.481	1.90E-07	0.219	2.13E-03	-0.0551	
KNC Qr	c6Tmax + p7Tmax + c8Ppt	0.420	2.50E-06	0.194	4.31E-03	-0.0890	
MGB As	c6Tmax + c7Ppt + p5Ppt	0.523	2.75E-08	0.127	0.0246	-0.436	
MGB Co	c6Tmax + c3Ppt + p10Tmin	0.516	3.78E-08	0.267	5.16E-04	0.191	0.190
MGB Fg	c6Tmax + c1Tmin + c4Tmin	0.572	2.27E-09	0.178	6.57E-03	-0.257	
MGB Lt	c7Tmax + c8Tmax + c2Ppt	0.481	1.93E-07	.0408	0.180		
MGB Qr	c6Tmax + c7Ppt + p12Tmax	0.592	7.45E-10	0.275	3.96E-04	-0.0332	
PMF As	c6Tmax + p8Tmax + p9Tmax	0.571	2.32E-09	0.107	0.0403	-0.643	
PMF Co	c6Tmax + c8Tmean + c7Ppt	0.590	8.13E-10	7.09E-04	0.396		
PMF Fg	c6Tmax + c6Ppt + c7Ppt	0.536	1.46E-08	0.122	0.0279	-0.327	
PMF Lt	c6Tmax + c6Ppt + p12Ppt	0.605	3.38E-10	0.262	6.00E-04	0.134	0.128
PMF Qa	c6Tmax + c7Ppt + c1Ppt	0.581	1.38E-09	0.242	1.08E-03	-0.130	
PMF Qr	c6Tmax + p6Tmax + c7Ppt	0.590	8.22E-10	0.277	3.80E-04	0.134	0.0951

Table 4.2. Model parameters and their coefficients when models established over the 1903–1953 calibration period were fit over the entire common interval, 1903–2004. Variables are listed in the order in which they entered the calibration-period model according to forward stepwise multiple regression. Climate variables are abbreviated with numbers corresponding to months (month 1 = Jan., 12 = Dec.), letters preceding months indicate whether the month occurred in the year prior to ring formation ("p") or in the year of ring formation (the current year, "c"). Specific climate variables are abbreviated as: 'Ppt' = total precipitation and 'Tmean', 'Tmin', and 'Tmax' = mean, minimum, and maximum temperature, each averaged over the month. Sites are arranged north (top) to south (Table 3.1). Species codes: As = sugar maple *Acer saccharum*, Co = shagbark hickory *Carya ovata*, Fg = American beech *Fagus grandifolia*, Lt = tulip poplar *Liriodendron tulipifera*, Qa = white oak *Quercus alba*, Qr = red oak *Quercus rubra*, Tc = eastern hemlock *Tsuga canadensis*.

Population	Model Parameters (Climate Variables)	Constant	Parameter 1 Coefficient	Parameter 2 Coefficient	Parameter 3 Coefficient	Adj. r^2
Mwd As	c7Ppt + p11Ppt + p8Tmin	1.43	8.26E-4	8.77E-4	-0.0466	0.147
Pet Tc	p7Tmax + c6Ppt + c3Tmean	2.18	-0.0462	7.75E-4	0.0277	0.279
MaB Tc	p8Tmean + c3Tmin + p7Ppt	2.06	-0.0473	0.0315	7.53E-4	0.324
JSB Tc	p11Ppt + p7Tmin + p12Tmax	1.52	1.49E-3	-0.0496	0.0235	0.159
PNC Qa	c7Ppt + p7Ppt + p11Tmin	0.816	1.83E-3	9.10E-4	0.0211	0.307
War Fg	c8Tmax + c5Tmin + c6Tmax	2.23	-0.0211	0.0270	-0.0324	0.338
War Qa	c6Tmax + p5Tmax + c7Ppt	1.72	-0.0402	0.0136	6.87E-4	0.359
Vrh As	c7Tmax + p12Tmean + c5Tmean	2.28	-0.0571	0.0239	0.0272	0.300
Vrh Qa	c7Tmax + p12Tmin + c6Tmax	2.86	-0.0338	0.0168	-0.0309	0.336
Vrh Qr	c6Tmax + p12Tmin + c7Tmax	2.45	-0.0312	9.16E-3	-0.0210	0.268
KNC Fg	c7Tmax + p5Tmax + c6Ppt	1.99	-0.0508	0.0150	1.86E-3	0.415
MGB Co	c6Tmax + c3Ppt + p10Tmin	2.42	-0.0569	5.53E-4	0.0184	0.384
PMF Lt	c6Tmax + c6Ppt + p12Ppt	1.73	-0.0359	2.29E-3	6.93E-4	0.400
PMF Qr	c6Tmax + p6Tmax + c7Ppt	1.77	-0.0401	0.0110	6.93E-4	0.483

CHAPTER FIVE

CONCLUDING REMARKS

In this dissertation, I used tree rings in Indiana and Michigan to better understand the climate of the era preceding instrumentally derived weather records, to compare relationships between growth and climate within and among tree species, and to project future tree growth under ongoing climate change.

It was found that even on humid South Manitou Island, Lake Michigan, in the humid eastern United States, severe drought was a common occurrence. Colleagues and I reconstructed 469 years of the moisture index Palmer Z Index over late-summer and found that 17% of years were at least one standard deviation (SD) drier than the mean; 2% were at least two SDs drier (Fig. 2.9b). Intense pluvials, which can have their own negative effects such as erosion and flooding, were also common, with 16% of years at least one SD wetter than the mean and 1% at least two SDs wetter. Extreme years occurred throughout the interval, but they were most common in the 20th century, with 22% of its years being one SD drier and 26% wetter than the mean. Further, all four of the driest years were in that century. Thus, climate change has already resulted in a more variable environment in northern Lake Michigan relative to historic conditions and led to droughts unmatched by anything from the preceding four centuries. Climate change is expected to bring warmer temperatures to the region, more erraticism in rainfall, and more variability in general. With many trees being ecological foundation species and with society relying on the products and services they provide, it is

important to understand how climate affects tree growth and whether this information can be valuable in projecting future growth.

A 12-site latitudinal gradient was established spanning southern Indiana to the Upper Peninsula of Michigan. Tree-core samples from 46 populations were taken at these sites from a mix of nine species. Relationships between ring widths and temperature/precipitation were quantified and compared within and among species. The dominant factors associated with tree growth were conditions in the summer, with negative growth-temperature and positive -precipitation relationships (Fig. 3.4). The strength of this relationship linearly decreased moving to the north. This was found across all species except *Tsuga canadensis*, however that species was still limited by summer conditions, but it was the conditions of the summer preceding the year of growth, unlike the other species (Tables 3.4 & 3.5).

It has been found in some tree-ring studies that the strength of growth-climate relationships has weakened in recent decades, rendering climate reconstructions and future-growth projections less reliable. I tested whether this had occurred in my study gradient by analyzing the strength of monthly growth-temperature and -precipitation relationships in overlapping 34-year windows. It was found that some growth-climate relationships did evolve but only in the months which were not significantly associated with growth (Fig. 3.6a & b). For the most influential months, the relationships were stable (Fig. 3.6c & d). Thus, tree rings are still recommended for reconstructing climate and projecting future growth in the Great Lakes Region.

In this study, growth was also commonly associated with spring temperatures (positively), winter temperature (positively), and winter precipitation (positively). Each of these

variables is expected to increase as climate change proceeds. Thus, even as climate change exacerbates summer moisture stress, which is so detrimental to tree growth, it may bring some benefit to tree growth through warmer, wetter winters and springs.

To project future growth, the same network of 46 tree-ring chronologies was used to establish parsimonious models between growth and climate. Forward stepwise multiple regression was used to select the most variability-explaining set of three variables over one half of the dataset. It was then attempted to verify the calibrated model on the other half of the dataset. This process tended to be unsuccessful (14 successes/46 attempts). This is likely due to the remote location of some of my sites, away from weather stations, and due to the relatively benign climate of the temperate east which leads to complacent tree growth. Nonetheless, future growth could be projected for the 14 successfully validated populations. This was done for the period 2022–2099 under two climate-change models, one which predicted relatively mild warming and one which predicted severe warming. Under the severe-warming model, growth was projected to decline significantly in 12/14 populations and to increase in one population. Under the mild scenario, growth was projected to decline in four populations, to increase in one, and to have no significant change in nine. This suggests that land managers need to prepare for severe imminent tree growth declines.

In future research, it is recommended that tree cores continue to be sampled from the major species in the Great Lakes Region. Researchers should carefully select sites that are nearby weather stations with long and consistent records. Using methods similar to those in this dissertation, models should be constructed that relate growth and climate, and these should be used to project future growth. When potentially climate-change-resilient populations

are identified, such as the *Quercus alba* population studied here at Price Nature Center, experimental warming under controlled conditions should be applied to seedlings from the site to test whether the growth-climate relationships observed were due to genetics or microsite. Populations for which climate-change resiliency is supported both through tree-ring-climate analysis and experimental warming should be considered candidates for use in assisted gene flow.

Another avenue of future research is sampling ancient trees, stumps, and wood in human-made structures to reconstruct climate. This will paint a clearer picture of what climate was like in the era before the keeping of instrumentally derived records. This is important to do soon because such wood is continuously lost to decay and fire.

Thank you for reading this dissertation. Now go out and hug a tree!

LITERATURE CITED

LITERATURE CITED

Aitken, S.N., Whitlock, M.C., 2013. Assisted Gene Flow to Facilitate Local Adaptation to Climate Change. Annual Review of Ecology, Evolution, and Systematics 44, 367–388.

Akaike, H., 1974. A new look at the statistical model identification. IEEE Transactions on Automatic Control 19, 716–723.

Albrecht, G.A., Brooke, C., Bennett, D.H., Garnett, S.T., 2013. The Ethics of Assisted Colonization in the Age of Anthropogenic Climate Change. Journal of Agricultural and Environmental Ethics 26, 827–845.

Andersen, B.J., 2005. The Historical Development of the Tension Zone Concept in the Great Lakes Region of North America. The Michigan Botanist 44, 127–138.

Anderson, D.G., Stahle, D.W., Cleaveland, M.K., 1995. Paleoclimate and the Potential Food Reserves of Mississippian Societies: A Case Study from the Savannah River Valley. American Antiquity 60, 258–286.

Andresen, J.A., 2012. Historical climate trends in Michigan and the Great Lakes region, in: Climate Change in the Great Lakes Region. Michigan State University Press, East Lansing, Michigan, USA 17–34.

Andresen, J.A., Winkler, J.A, 2009. Weather and Climate, in: Michigan Geography and Geology. Pearson Custom Publishing, Boston, Massachusetts, USA 288–311.

Au, T.F., Maxwell, J.T., Novick, K.A., Robeson, S.M., Warner, S.M., Lockwood, B.R., Phillips, R.P., Harley, G.L., Telewski, F.W., Therrell, M.D., Pederson, N., 2020. Demographic shifts in eastern US forests increase the impact of late-season drought on forest growth. Ecography 43, 1475–1486.

Babst, F., Poulter, B., Trouet, V., Tan, K., Neuwirth, B., Wilson, R., Carrer, M., Grabner, M., Tegel, W., Levanic, T., Panayotov, M., Urbinati, C., Bouriaud, O., Ciais, P., Frank, D., 2013. Site- and species-specific responses of forest growth to climate across the European continent. Global Ecology and Biogeography 22, 706–717.

Barber, V.A., Juday, G.P., Finney, B.P., 2000. Reduced growth of Alaskan white spruce in the twentieth century from temperature-induced drought stress. Nature 405, 668–673.

Bazzaz, F.A., Coleman, J.S., Morse, S.R., 1990. Growth responses of seven major co-occurring tree species of the northeastern United States to elevated CO_2. Canadian Journal of Forest Research 20, 1479–1484.

Biondi, F., Waikul, K., 2004. DENDROCLIM2002: A C++ program for statistical calibration of climate signals in tree-ring chronologies. Computers & Geosciences 30, 303–311.

Boisvert-Marsh, L., Périé, C., de Blois, S., 2014. Shifting with climate? Evidence for recent changes in tree species distribution at high latitudes. Ecosphere 5, 1–33.

Brienen, R.J.W., Lebrija-Trejos, E., Zuidema, P.A., Martínez-Ramos, M., 2010. Climate-growth analysis for a Mexican dry forest tree shows strong impact of sea surface temperatures and predicts future growth declines. Global Change Biology 16, 2001–2012.

Briffa, K.R., Schweingruber, F.H., Jones, P.D., Osborn, T.J., Shiyatov, S.G., Vaganov, E.A., 1998. Reduced sensitivity of recent tree-growth to temperature at high northern latitudes. Nature 391, 678–682.

Brubaker, L.B., 1980. Spatial Patterns of Tree Growth Anomalies in the Pacific Northwest. Ecology 61, 798–807.

Bruening, J.M., Tran, T.J., Bunn, A.G., Weiss, S.B., Salzer, M.W., 2017. Fine-scale modeling of bristlecone pine treeline position in the Great Basin, USA. Environmental Research Letters 12, 014008.

Brusca, R.C., Wiens, J.F., Meyer, W.M., Eble, J., Franklin, K., Overpeck, J.T., Moore, W., 2013. Dramatic response to climate change in the Southwest: Robert Whittaker's 1963 Arizona Mountain plant transect revisited. Ecology and Evolution 3, 3307–3319.

Buckley, B.M., Wilson, R.J.S., Kelly, P.E., Larson, D.W., Cook, E.R., 2004. Inferred summer precipitation for southern Ontario back to AD 610, as reconstructed from ring widths of Thuja occidentalis 34, 2541–2553.

Büntgen, U., Frank, D., Wilson, R., Carrer, M., Urbinati, C., Esper, J., 2008. Testing for tree-ring divergence in the European Alps. Global Change Biology 14, 2443–2453.

Buras, A., 2017. A comment on the expressed population signal. Dendrochronologia 44, 130–132.

Burnett, A.W., Kirby, M.E., Mullins, H.T., Patterson, W.P., 2003. Increasing Great Lake–Effect Snowfall during the Twentieth Century: A Regional Response to Global Warming? Journal of Climate 16, 3535–3542.

Burns, B.T., 1983. Simulated Anasazi Storage Behavior Using Crop Yields Reconstructed from Tree Rings, A.D. 652-1968. Dissertation, University of Arizona, Tucson, Arizona, USA.

Byun, K., Hamlet, A.F., 2018. Projected changes in future climate over the Midwest and Great Lakes region using downscaled CMIP5 ensembles. International Journal of Climatology 38, e531–e553.

Campbell, J.L., Socci, A.M., Templer, P.H., 2014. Increased nitrogen leaching following soil freezing is due to decreased root uptake in a northern hardwood forest. Global Change Biology 20, 2663–2673.

Carroll, A.L., Sillett, S.C., Kramer, R.D., 2014. Millennium-Scale Crossdating and Inter-Annual Climate Sensitivities of Standing California Redwoods. PLoS ONE 9, e102545.

Cedro, A., Cedro, B., 2015. Growth-climate relationships at yew and wild service trees on the eastern edge of their range in Europe. Forest Systems 24, e044.

Charney, N.D., Babst, F., Poulter, B., Record, S., Trouet, V.M., Frank, D., Enquist, B.J., Evans, M.E.K., 2016. Observed forest sensitivity to climate implies large changes in 21st century North American forest growth. Ecology Letters 19, 1119–1128.

Cheddadi, R., Araújo, M.B., Maiorano, L., Edwards, M., Guisan, A., Carré, M., Chevalier, M., Pearman, P.B., 2016. Temperature Range Shifts for Three European Tree Species over the Last 10,000 Years. Frontiers in Plant Science. 7, 1581.

Chen, I.-C., Hill, J.K., Ohlemüller, R., Roy, D.B., Thomas, C.D., 2011. Rapid Range Shifts of Species Associated with High Levels of Climate Warming. Science 333, 1024–1026.

Chen, P.-Y., Welsh, C., Hamann, A., 2010. Geographic variation in growth response of Douglas-fir to interannual climate variability and projected climate change. Global Change Biology 16, 3374–3385.

Chhin, S., 2016. Screening the Resilience of Short-Rotation Woody Crops to Climate Change. Geosciences 6, 7.

Chhin, S., 2015. Impact of future climate change on a genetic plantation of hybrid pine Botany 93, 397–404.

Chhin, S., Hogg, E.H. (Ted), Lieffers, V.J., Huang, S., 2008. Potential effects of climate change on the growth of lodgepole pine across diameter size classes and ecological regions. Forest Ecology and Management 256, 1692–1703.

Christensen, J.H., Kanikicharla, K.K., Aldrian, E., An, S.-I., de Castro, M., Dong, W., Goswami, P., Hall, A., Kanyanga, J.K., Kitoh, A., Kossin, J., Lau, N.-C., Renwick, J., Zhou, T., Abraham, L., Ambrizzi, T., Anderson, B., Arakawa, O., Arritt, R., Baldwin, M., Barlow, M., Barriopedro, D., Biasutti, M., Biner, S., Bromwich, D., Brown, J., Cai, W., Carvalho, L.V., Chang, P., Choi, J., Emanuel, K., Endo, H., Enfield, D.B., Evan, A., Giannini, A., Gillett, N., Hariharasubramanian, A., Huang, P., Jones, J., Karumuri, A., Katzfey, J., Kjellström, E., Knight, J., Knutson, T., Kulkarni, A., Kundeti, K.R., Lau, W.K., Lenderink, G., Mackellar, N.C., Meehl, G., Menéndez, C., Murakami, H., Nath, M.J., Neelin, J.D., van Oldenborgh, G.J., Polcher, J., Qian, Y., Ray, S., Reich, D., de Fonseca, B.R., Ruti, P., Screen, J., Sedláček, J., Solman, S., Stendel, M., Takayabu, I., Turner, J., Ummenhofer, C., Wang, B., Wang, C., Watterson, I., Wittenberg, A., Woollings, T., Yeh, S.-W., Zhang, C., Zhang, L., Zheng, X., Zou, L., Fyfe, J., Kwon, W.-T., 2013. Climate Phenomena and their Relevance for Future Regional Climate Change, in: Climate Change 2013: the Physical Science Basis: Working Group I Contribution to the Fifth Assessment Report of the Intergovernmental Panel on Climate Change. Cambridge University Press, Cambridge, United Kingdom and New York, NY, USA 1217–1308.

Cohen, J.G., Kost, M.A., Slaughter, B.S., Albert, D.A., 2014. A Field Guide to the Natural Communities of Michigan. Michigan State University Press, East Lansing, Michigan, USA, 196–199.

Cole, C.T., Anderson, J.E., Lindroth, R.L., Waller, D.M., 2010. Rising concentrations of atmospheric CO2 have increased growth in natural stands of quaking aspen (*Populus tremuloides*). Global Change Biology 16, 2186–2197.

Collins, M., Knutti, R., Arblaster, J., Dufresne, J.-L., Fichefet, T., Gao, X., Jr, W.J.G., Johns, T., Krinner, G., Shongwe, M., Weaver, A.J., Wehner, M., Allen, M.R., Andrews, T., Beyerle, U., Bitz, C.M., Bony, S., Booth, B.B.B., Brooks, H.E., Brovkin, V., Browne, O., Brutel-Vuilmet, C., Cane, M., Chadwick, R., Cook, E., Cook, K.H., Eby, M., Fasullo, J., Forest, C.E., Forster, P., Good, P., Goosse, H., Gregory, J.M., Hegerl, G.C., Hezel, P.J., Hodges, K.I., Holland, M.M., Huber, M., Joshi, M., Kharin, V., Kushnir, Y., Lawrence, D.M., Lee, R.W., Liddicoat, S., Lucas, C., Lucht, W., Marotzke, J., Massonnet, F., Matthews, H.D., Meinshausen, M., Morice, C., Otto, A., Patricola, C.M., Philippon, G., Rahmstorf, S., Riley, W.J., Saenko, O., Seager, R., Sedláček, J., Shaffrey, L.C., Shindell, D., Sillmann, J., Stevens, B., Stott, P.A., Webb, R., Zappa, G., Zickfeld, K., Joussaume, S., Mokssit, A., Taylor, K., Tett, S., 2013. Long-term Climate Change: Projections, Commitments and Irreversibility, in: Climate Change 2013: the Physical Science Basis: Working Group I Contribution to the Fifth Assessment Report of the Intergovernmental Panel on Climate Change. Cambridge University Press, Cambridge, United Kingdom and New York, NY, USA, 1029–1136.

Cook, E.R., 1985. A Time Series Analysis Approach to Tree Ring Standardization. Dissertation, University of Arizona, Tucson, Arizona, USA.

Cook, E.R., Cole, J., 1991. On predicting the response of forests in eastern North America to future climatic change. Climatic Change 19, 271–282.

Cook, E.R., Glitzenstein, J.S., Krusic, P.J., Harcombe, P.A., 2001. Identifying Functional Groups of Trees in West Gulf Coast Forests (USA): A Tree-Ring Approach. Ecological Applications 11, 883–903.

Cook, E.R., Meko, D.M., Stahle, D.W., Cleaveland, M.K., 1999. Drought Reconstructions for the Continental United States. Journal of Climate 12, 1145–1162.

Crimmins, S.M., Dobrowski, S.Z., Greenberg, J.A., Abatzoglou, J.T., Mynsberge, A.R., 2011. Changes in Climatic Water Balance Drive Downhill Shifts in Plant Species' Optimum Elevations. Science 331, 324–327.

Crouchet, S.E., Jensen, J., Schwartz, B.F. Schwinning, S., 2019. Tree mortality after a hot drought: distinguishing density-dependent and-independent drivers and why it matters. Frontiers in Forests and Global Change 2, 21.

Daly, C., Halbleib, M., Smith, J.I., Gibson, W.P., Doggett, M.K., Taylor, G.H., Curtis, J., Pasteris, P.P., 2008. Physiographically sensitive mapping of climatological temperature and precipitation across the conterminous United States. International Journal of Climatology 28, 2031–2064.

D'Arrigo, R., Wilson, R., Liepert, B., Cherubini, P., 2008. On the 'Divergence Problem' in Northern Forests: A review of the tree-ring evidence and possible causes. Global and Planetary Change 60, 289–305.

D'Arrigo, R.D., Kaufmann, R.K., Davi, N., Jacoby, G.C., Laskowski, C., Myneni, R.B., Cherubini, P., 2004. Thresholds for warming-induced growth decline at elevational tree line in the Yukon Territory, Canada. Global Biogeochemical Cycles 18.

Darwin, C., 1859. On the Origin of the Species by Means of Natural Selection, John Murray, London, United Kingdom.

Davis, M.B., 1983. Quaternary History of Deciduous Forests of Eastern North America and Europe. Annals of the Missouri Botanical Garden 70, 550–563.

Davis, M.B., Shaw, R.G., 2001. Range Shifts and Adaptive Responses to Quaternary Climate Change. Science 292, 673–679.

Dickmann, D.I., Leefers, L.A., 2016. The Forests of Michigan. University of Michigan Press, Ann Arbor, Michigan, USA, 1–30.

D'Orangeville, L., Duchesne, L., Houle, D., Kneeshaw, D., Côté, B., Pederson, N., 2016. Northeastern North America as a potential refugium for boreal forests in a warming climate. Science 352, 1452–1455.

D'Orangeville, L., Maxwell, J., Kneeshaw, D., Pederson, N., Duchesne, L., Logan, T., Houle, D., Arseneault, D., Beier, C.M., Bishop, D.A., Druckenbrod, D., Fraver, S., Girard, F., Halman, J., Hansen, C., Hart, J.L., Hartmann, H., Kaye, M., Leblanc, D., Manzoni, S., Ouimet, R., Rayback, S., Rollinson, C.R., Phillips, R.P., 2018. Drought timing and local climate determine the sensitivity of eastern temperate forests to drought. Global Change Biology 24, 2339–2351.

Douglass, A.E., 1935. Dating Pueblo Bonito and Other Ruins of the Southwest, National Geographic Society, Contributed Technical Papers, Pueblo Bonito Series 1, 1–74. Washington, D.C., USA.

Dulamsuren, C., Hauck, M., Kopp, G., Ruff, M., Leuschner, C., 2017. European beech responds to climate change with growth decline at lower, and growth increase at higher elevations in the center of its distribution range (SW Germany). Trees 31, 673–686.

Dye, A., 2019. Growth and climate response of four new *Tsuga canadensis* (L.) CARRIÈRE (eastern hemlock) tree-ring chronologies from Michigan's Upper Peninsula. The Great Lakes Botanist 58, 193–204.

Ford, T.W., 2014. Precipitation anomalies in Eastern-Central Iowa from 1640 – Present. Journal of Hydrology 519, 918–924.

Fritts, H.C, 1976. Tree Rings and Climate, Academic Press, London, UK, New York, New York, USA, and San Francisco, California, USA.

Fritts, H.C., 1965. Tree-ring evidence for climatic changes in western North America. Monthly Weather Review 93, 421–443.

Gamache, I., Payette, S., 2004. Height growth response of tree line black spruce to recent climate warming across the forest-tundra of eastern Canada. Journal of Ecology 92, 835–845.

Gao, L., Gou, X., Deng, Y., Liu, W., Yang, M., Zhao, Z., 2013. Climate–growth analysis of Qilian juniper across an altitudinal gradient in the central Qilian Mountains, northwest China. Trees 27, 379–388.

Gaul, D., Hertel, D., Borken, W., Matzner, E., Leuschner, C., 2008. Effects of experimental drought on the fine root system of mature Norway spruce. Forest Ecology and Management 256, 1151–1159.

Girardin, M.P., Bouriaud, O., Hogg, E.H., Kurz, W., Zimmermann, N.E., Metsaranta, J.M., de Jong, R., Frank, D.C., Esper, J., Büntgen, U., Guo, X.J., Bhatti, J., 2016. No growth stimulation of Canada's boreal forest under half-century of combined warming and CO_2 fertilization. Proceedings of the National Academy of Sciences USA 113, E8406–E8414.

Granda, E., Camarero, J.J., Gimeno, T.E., Martínez-Fernández, J., Valladares, F., 2013. Intensity and timing of warming and drought differentially affect growth patterns of co-occurring Mediterranean tree species. European Journal of Forest Research 132, 469–480.

Graumlich, L.J., 1993. Response of tree growth to climatic variation in the mixed conifer and deciduous forests of the upper Great Lakes region. Canadian Journal of Forest Research 23, 133–143.

Griffies, S.M., Winton, M., Donner, L.J., Horowitz, L.W., Downes, S.M., Farneti, R., Gnanadesikan, A., Hurlin, W.J., Lee, H.-C., Liang, Z., Palter, J.B., Samuels, B.L., Wittenberg, A.T., Wyman, B.L., Yin, J., Zadeh, N., 2011. The GFDL CM3 Coupled Climate Model: Characteristics of the Ocean and Sea Ice Simulations. Journal of Climate 24, 3520–3544.

Grissino-Mayer, H.D., 2001. Evaluating crossdating accuracy: a manual and tutorial for the computer program COFECHA. Tree-Ring Research, 57, 205–221.

Grissino-Mayer, H.D., 1996. A 2129-year reconstruction of precipitation for northwestern New Mexico, USA, in: Tree rings, Environment, and Humanity, Radiocarbon. Department of Geosciences, University of Arizona, Tucson, Arizona, USA, 191–204.

Harsch, M.A., Hulme, P.E., McGlone, M.S., Duncan, R.P., 2009. Are treelines advancing? A global meta-analysis of treeline response to climate warming. Ecology Letters 12, 1040–1049.

Hartmann, D.L., Tank, A.M.G.K., Rusticucci, M., Alexander, L.V., Brönnimann, S., Charabi, Y.A.R., Dentener, F.J., Dlugokencky, E.J., Easterling, D.R., Kaplan, A., Soden, B.J., Thorne, P.W., Wild, M., Zhai, P., 2013. Observations: Atmosphere and surface, in: Climate Change 2013: the Physical Science Basis: Working Group I Contribution to the Fifth Assessment Report of the Intergovernmental Panel on Climate Change. Cambridge University Press, Cambridge, United Kingdom and New York, NY, USA 159–254.

Harvey, J.E., Smiljanić, M., Scharnweber, T., Buras, A., Cedro, A., Cruz-García, R., Drobyshev, I., Janecka, K., Jansons, Ā., Kaczka, R., Klisz, M., Läänelaid, A., Matisons, R., Muffler, L., Sohar, K., Spyt, B., Stolz, J., Maaten, E. van der, Maaten-Theunissen, M. van der, Vitas, A., Weigel, R., Kreyling, J., Wilmking, M., 2020. Tree growth influenced by warming winter climate and summer moisture availability in northern temperate forests. Global Change Biology 26, 2505–2518.

Hayhoe, K., VanDorn, J., Croley, T., Schlegal, N., Wuebbles, D., 2010. Regional climate change projections for Chicago and the US Great Lakes. Journal of Great Lakes Research 36, 7–21.

Heberling, J.M., MacKenzie, C.M., Fridley, J.D., Kalisz, S., Primack, R.B., 2019. Phenological mismatch with trees reduces wildflower carbon budgets. Ecology Letters 22, 616–623.

Heim, R.R., 2002. A Review of Twentieth-Century Drought Indices Used in the United States. Bulletin of the American Meteorological Society 83, 1149–1166.

Hinckley, T.M., Dougherty, P.M., Lassoie, J.P., Roberts, J.E., Teskey, R.O., 1979. A Severe Drought: Impact on Tree Growth, Phenology, Net Photosynthetic Rate and Water Relations. The American Midland Naturalist 102, 307–316.

Holmes, R.L., 1983. Computer-Assisted Quality Control in Tree-Ring Dating and Measurement. Tree-Ring Bulletin 43, 69–78.

Housset, J.M., Girardin, M.P., Baconnet, M., Carcaillet, C., Bergeron, Y., 2015. Unexpected warming-induced growth decline in Thuja occidentalis at its northern limits in North America. Journal of Biogeography 42, 1233–1245.

Huang, J., Tardif, J.C., Bergeron, Y., Denneler, B., Berninger, F., Girardin, M.P., 2010. Radial growth response of four dominant boreal tree species to climate along a latitudinal gradient in the eastern Canadian boreal forest. Global Change Biology 16, 711–731.

Huang, J.-G., Bergeron, Y., Berninger, F., Zhai, L., Tardif, J.C., Denneler, B., 2013. Impact of Future Climate on Radial Growth of Four Major Boreal Tree Species in the Eastern Canadian Boreal Forest. PLOS ONE 8, e56758.

Hufkens, K., Friedl, M.A., Keenan, T.F., Sonnentag, O., Bailey, A., O'Keefe, J., Richardson, A.D., 2012. Ecological impacts of a widespread frost event following early spring leaf-out. Global Change Biology 18, 2365–2377.

Huo, Y., Gou, X., Liu, W., Li, J., Zhang, F., Fang, K., 2017. Climate–growth relationships of Schrenk spruce (Picea schrenkiana) along an altitudinal gradient in the western Tianshan mountains, northwest China. Trees 31, 429–439.

Hutchings, M.J., Robbirt, K.M., Roberts, D.L., Davy, A.J., 2018. Vulnerability of a specialized pollination mechanism to climate change revealed by a 356-year analysis. Botanical Journal of the Linnean Society 186, 498–509.

Jackson, S.T., Weng, C., 1999. Late Quaternary extinction of a tree species in eastern North America. Proceedings of the National Academy of Sciences USA 96, 13847–13852.

Jacoby, G.C., D'Arrigo, R.D., 1995. Tree ring width and density evidence of climatic and potential forest change in Alaska. Global Biogeochemical Cycles 9, 227–234.

Harman, J.R., 2009. Plant Geography, in: Michigan Geography and Geology. Pearson Custom Publishing, Boston, Massachusetts, USA 330–345.

Jump, A.S., Hunt, J.M., Peñuelas, J., 2006. Rapid climate change-related growth decline at the southern range edge of *Fagus sylvatica*. Global Change Biology 12, 2163–2174.

Kannenberg, S.A., Novick, K.A., Alexander, M.R., Maxwell, J.T., Moore, D.J., Phillips, R.P. and Anderegg, W.R.L., 2019. Linking drought legacy effects across scales: From leaves to tree rings to ecosystems. Global Change Biology 25, 2978–2992.

Kelly, A.E., Goulden, M.L., 2008. Rapid shifts in plant distribution with recent climate change. Proceedings of the National Academy of Sciences 105, 11823–11826.

Kelly, P.E., Cook, E.R., Larson, D.W., 1994. A 1397-year tree-ring chronology of *Thuja occidentalis* from cliff faces of the Niagara Escarpment, southern Ontario, Canada. Canadian Journal of Forest Research 24, 1049–1057.

Kelly, P.E., Larson, D.W., 2007. The Last Stand: A Journey Through the Ancient Cliff-face Forest of the Niagara Escarpment. Natural Heritage Books, Toronto, Ontario, Canada.

Kharuk, V., Im, S., Dvinskaya, M., 2010. Forest–tundra ecotone response to climate change in the Western Sayan Mountains, Siberia. Scandinavian Journal of Forest Research 25, 224–233.

Kirtman, B., Power, S.B., Adedoyin, A.J., Boer, G.J., Bojariu, R., Doblas-Reyes, F., Fiore, A.M., Kimoto, M., Meehl, G., Prather, M., Sarr, A., Schär, C., Sutton, R., van Oldenborgh, G.J., Vecchi, G., Wang, H.-J., Bindoff, N.L., Cameron-Smith, P., Clifton, O., Corti, S., Durack, P.J., Fichefet, T., García-Serrano, J., Ginoux, P., Guemas, V., Hawkins, E., Holland, M., Infanti, J., Ishii, M., Jacob, D., John, J., Klimont, Z., Knutson, T., Krinner, G., Lawrence, D., Lu, J., Murphy, D., Naik, V., Robock, A., Rodrigues, L., Sedláček, J., Slater, A., Smith, D., Stevenson, D.S., van Noije, T., Vavrus, S., Voulgarakis, A., Wild, O., Woollings, T., Young, P., Delecluse, P., Palmer, T., Shepherd, T., Zwiers, F., 2013. Near-Term Climate Change: Projections and Predictability, in: Climate Change 2013: the Physical Science Basis: Working Group I Contribution to the Fifth Assessment Report of the Intergovernmental Panel on Climate Change. Cambridge University Press, Cambridge, United Kingdom and New York, NY, USA 953–1028.

Knutson, T., Zeng, F., Wittenberg, A., 2014. Seasonal and annual mean precipitation extremes occurring during 2013: A U.S. focused analysis. Section 6 of: "Explaining extremes of 2013 from a climate perspective." Bulletin of the American Meteorological Society 95, S19–S23.

Kopp, C.W., Cleland, E.E., 2014. Shifts in plant species elevational range limits and abundances observed over nearly five decades in a western North America mountain range. Journal of Vegetation Science 25, 135–146.

Lamarche, V.C., Graybill, D.A., Fritts, H.C., Rose, M.R., 1984. Increasing Atmospheric Carbon Dioxide: Tree Ring Evidence for Growth Enhancement in Natural Vegetation. Science 225, 1019–1021.

Larson, E.R., Rawling, J.E., 2016. Developing new sources of proxy climate data from historical structures in the Lake Michigan-Huron Basin. Journal of Great Lakes Research 42, 328–335.

Larson, G.J., Kincare, K., 2009. Late Quaternary history of the eastern Mid-Continent region, USA, in: Michigan Geography and Geology. Pearson Custom Publishing, Boston, Massachusetts, 69–90.

Latte, N., Perin, J., Kint, V., Lebourgeois, F., Claessens, H., 2016. Major changes in growth rate and growth variability of beech (*Fagus sylvatica* L.) related to soil alteration and climate change in Belgium. Forests 7, 174.

LeBlanc, D., Maxwell, J., Pederson, N., Berland, A., Mandra, T., 2020. Radial growth responses of tulip poplar (Liriodendron tulipifera) to climate in the eastern United States. Ecosphere 11, e03203.

LeBlanc, D.C., Berland, A.M., 2019. Spatial variation in oak (Quercus spp.) radial growth responses to drought stress in eastern North America. Canadian Journal of Forest Research 49, 986–993.

Leefers, L.A., 2017. Statewide report: forest products industries' economic contributions to Michigan's economy - 2017 update. Michigan Department of Natural Resources Forest Resource Division. https://www.michigan.gov/documents/dnr/2016ForestProductsIndustriesContributions_535055_7.pdf

Legendre, P., Legendre, L.F.J., 1998. Numerical Ecology. Elsevier Scientific, New York, NY, USA.

Liang, E., Leuschner, C., Dulamsuren, C., Wagner, B., Hauck, M., 2016. Global warming-related tree growth decline and mortality on the north-eastern Tibetan plateau. Climatic Change 134, 163–176.

Littell, J.S., Peterson, D.L., Tjoelker, M., 2008. Douglas-fir growth in mountain ecosystems: water limits tree growth from stand to region. Ecological Monographs 78, 349–368.

Liu, H., Park Williams, A., Allen, C.D., Guo, D., Wu, X., Anenkhonov, O.A., Liang, E., Sandanov, D.V., Yin, Y., Qi, Z., Badmaeva, N.K., 2013. Rapid warming accelerates tree growth decline in semi-arid forests of Inner Asia. Global Change Biology 19, 2500–2510.

Lorenz, E. N., 1956: Empirical orthogonal functions and statistical weather prediction. Statistical Forecasting Scientific Rep. 1, Department of Meteorology, Massachusetts Institute of Technology, Cambridge, Massachusetts, USA.

Lovett, G.M., Weiss, M., Liebhold, A.M., Holmes, T.P., Leung, B., Lambert, K.F., Orwig, D.A., Campbell, F.T., Rosenthal, J., McCullough, D.G., Wildova, R., Ayres, M.P., Canham, C.D., Foster, D.R., LaDeau, S.L., Weldy, T., 2016. Nonnative forest insects and pathogens in the United States: Impacts and policy options. Ecological Applications 26, 1437–1455.

Lovis, W.A., Mainfort, R.C., Noble, V.E., 1976. Archaeological inventory and evaluation of Sleeping Bear Dunes National Lakeshore. Archaeological Survey Report Number 5. Michigan State University Museum, East Lansing, Michigan, USA.

Lovis, W.A., Monaghan, G.W., Arbogast, A.F., 2017. Site20LU115, Sleeping Bear Dunes National Lakeshore: synthesis of archaeological and environmental data recovery. Report submitted to National Park Service, Midwest Archaeological Center, Lincoln, Nebraska, USA (Contract P15AC01378).

Lovis, W.A., Monaghan, G.W., Arbogast, A.F., 2020. Reconstructing the precontact Late Woodland archaeology of site 20LU115 and the landscape history of Sleeping Bear Point, Great Lakes, USA. The Journal of Island and Coastal Archaeology 15, 1–21.

MacArthur, R.H., 1972. Geographical Ecology: Patterns in the Distribution of Species, Harper & Row, New York, New York, USA.

Marchin, R., Zeng, H., Hoffmann, W., 2010. Drought-deciduous behavior reduces nutrient losses from temperate deciduous trees under severe drought. Oecologia 163, 845–854.

Marquardt, P.E., Miranda, B.R., Telewski, F.W., 2019. Shifts in Climate–Growth Relationships of Sky Island Pines. Forests 10, 1011.

Martin-Benito, D., Pederson, N., 2015. Convergence in drought stress, but a divergence of climatic drivers across a latitudinal gradient in a temperate broadleaf forest. Journal of Biogeography 42, 925–937.

Masson-Delmotte, V., Schulz, M., Abe-Ouchi, A., Beer, J., Ganopolski, A., Fidel, J., Rouco, G., Jansen, E., Lambeck, K., Luterbacher, J., Naish, T., Ramesh, R., Rojas, M., Shao, X., Anchukaitis, K., Arblaster, J., Bartlein, P.J., Benito, G., Clark, P., Comiso, J.C., Crowley, T., Deckker, P.D., de Vernal, A., Delmonte, B., DiNezio, P., Dowsett, H.J., Edwards, R.L., Fischer, H., Fleitmann, D., Foster, G., Fröhlich, C., Hall, A., Hargreaves, J., Haywood, A., Hollis, C., Krinner, G., Landais, A., Li, C., Lunt, D., Mahowald, N., McGregor, S., Meehl, G., Mitrovica, J.X., Moberg, A., Mudelsee, M., Muhs, D.R., Mulitza, S., Müller, S., Overland, J., Parrenin, F., Pearson, P., Robock, A., Rohling, E., Salzmann, U., Savarino, J., Sedláček, J., Shindell, D., Smerdon, J., Solomina, O., Tarasov, P., Vinther, B., Waelbroeck, C., Wolf, D., Yokoyama, Y., Yoshimori, M., Zachos, J., Zwartz, D., Gupta, A.K., Rahimzadeh, F., Raynaud, D., Wanner, H., 2013. Information from Paleoclimate Archives, in: Climate Change 2013: the Physical Science Basis: Working Group I Contribution to the Fifth Assessment Report of the Intergovernmental Panel on Climate Change. Cambridge University Press, Cambridge, United Kingdom and New York, NY, USA 383–464.

Maxwell, J.T., Harley, G.L., 2017. Increased tree-ring network density reveals more precise estimations of sub-regional hydroclimate variability and climate dynamics in the Midwest, USA. Climate Dynamics 49, 1479–1493.

Maxwell, J.T., Harley, G.L., Matheus, T.J., 2015. Dendroclimatic reconstructions from multiple co-occurring species: a case study from an old-growth deciduous forest in Indiana, USA. International Journal of Climatology 35, 860–870.

Maxwell, J.T., Harley, G.L., Matheus, T.J., Strange, B.M., Van Aken, K., Au, T.F., Bregy, J.C., 2020. Sampling density and date along with species selection influence spatial representation of tree-ring reconstructions. Climate of the Past 16, 1901–1916.

Maxwell, J.T., Harley, G.L., Robeson, S.M., 2016. On the declining relationship between tree growth and climate in the Midwest United States: the fading drought signal. Climatic Change 138, 127–142.

Maxwell, R.S., Hessl, A.E., Cook, E.R., Buckley, B.M., 2012. A Multicentury Reconstruction of May Precipitation for the Mid-Atlantic Region Using Juniperus virginiana Tree Rings. Journal of Climate 25, 1045–1056.

Maxwell, R.S., Hessl, A.E., Cook, E.R., Pederson, N., 2011. A multispecies tree ring reconstruction of Potomac River streamflow (950–2001). Water Resources Research 47, W05512.

McMahon, S.M., Parker, G.G., Miller, D.R., 2010. Evidence for a recent increase in forest growth. Proceedings of the National Academy of Sciences 107, 3611–3615.

Medvigy, D., Beaulieu, C., 2012. Trends in Daily Solar Radiation and Precipitation Coefficients of

Variation since 1984. Journal of Climate 25, 1330–1339.
Mishra, V., Cherkauer, K.A., 2010. Retrospective droughts in the crop growing season: Implications to corn and soybean yield in the Midwestern United States. Agricultural and Forest Meteorology 150, 1030–1045.

Montgomery, K., 2006. Variation in Temperature With Altitude and Latitude. Journal of Geography 105, 133–135.

Morice, C.P., Kennedy, J.J., Rayner, N.A., Jones, P.D., 2012. Quantifying uncertainties in global and regional temperature change using an ensemble of observational estimates: The HadCRUT4 data set. Journal of Geophysical Research: Atmospheres 117.

Moser, W.K., Butler-Leopold, P., Hausman, C., Iverson, L., Ontl, T., Brand, L., Matthews, S., Peters, M., Prasad, A., 2020. The impact of climate change on forest systems in the northern United States: Projections and implications for forest management, in: Achieving sustainable management of boreal and temperate forests. Burleigh and Dodds Science Publishing, Cambridge, UK, 239–290.

Nash, J.E., Sutcliffe, J.V., 1970. River flow forecasting through conceptual models part I — A discussion of principles. Journal of Hydrology 10, 282–290.

Natalini, F., Alejano, R., Vázquez-Piqué, J., Pardos, M., Calama, R., Büntgen, U., 2016. Spatiotemporal variability of stone pine (*Pinus pinea* L.) growth response to climate across the Iberian Peninsula. Dendrochronologia 40, 72–84.

Neukom, R., Barboza, L.A., Erb, M.P., Shi, F., Emile-Geay, J., Evans, M.N., Franke, J., Kaufman, D.S., Lücke, L., Rehfeld, K., Schurer, A., Zhu, F., Brönnimann, S., Hakim, G.J., Henley, B.J., Ljungqvist, F.C., McKay, N., Valler, V., von Gunten, L., PAGES 2k Consortium, 2019. Consistent multidecadal variability in global temperature reconstructions and simulations over the Common Era. Nature Geoscience 12, 643–649.

Nitschke, C.R., Nichols, S., Allen, K., Dobbs, C., Livesley, S.J., Baker, P.J., Lynch, Y., 2017. The influence of climate and drought on urban tree growth in southeast Australia and the implications for future growth under climate change. Landscape and Urban Planning 167, 275–287.

NOAA National Centers for Environmental information (2012a) State of the climate: National overview for March 2012. www.ncdc.noaa.gov/sotc/national/201203 (accessed 2 Mar 2020)

NOAA National Centers for Environmental information (2012b) State of the climate: National overview for August 2012. www.ncdc.noaa.gov/sotc/national/201208 (accessed 2 Mar 2020)

NOAA National Centers for Environmental information (2015) State of the climate: National overview for February 2015. www.ncdc.noaa.gov/sotc/national/201502 (accessed 2 Mar 2020).

NOAA National Centers for Environmental information (2017a) State of the climate: National overview for February 2017. www.ncdc.noaa.gov/sotc/national/201702 (accessed 2 Mar 2020).

NOAA National Centers for Environmental information (2017b) State of the climate: National overview for September 2017 www.ncdc.noaa.gov/sotc/national/201709 (accessed 2 Mar 2020).

Norby, R.J., Warren, J.M., Iversen, C.M., Medlyn, B.E., McMurtrie, R.E., 2010. CO2 enhancement of forest productivity constrained by limited nitrogen availability. Proceedings of the National Academy of Sciences 107, 19368–19373.

Osborn, T.J., Biffa, K.R., Jones, P.D., 1997. Adjusting variance for sample-size in tree-ring chronologies and other regional-mean timeseries. Dendrochronologia 15, 89–99.

Panek, J.A., Goldstein, A.H., 2001. Response of stomatal conductance to drought in ponderosa pine: implications for carbon and ozone uptake. Tree Physiology 21, 337–344.

Parmesan, C., 2006. Ecological and Evolutionary Responses to Recent Climate Change. Annual Review of Ecology, Evolution, and Systematics 37, 637–669.

Pataki, D.E., Oren, R., 2003. Species differences in stomatal control of water loss at the canopy scale in a mature bottomland deciduous forest. Advances in Water Resources 26, 1267–1278.

Pederson, N., Bell, A.R., Cook, E.R., Lall, U., Devineni, N., Seager, R., Eggleston, K., Vranes, K.P., 2013. Is an Epic Pluvial Masking the Water Insecurity of the Greater New York City Region? Journal of Climate 26, 1339–1354.

Pederson, N., Bell, A.R., Knight, T.A., Leland, C., Malcomb, N., Anchukaitis, K.J., Tackett, K., Scheff, J., Brice, A., Catron, B., Blozan, W., Riddle, J., 2012. A long-term perspective on a modern drought in the American Southeast. Environmental Research Letters. 7, 014034.

Pederson, N., Cook, E.R., Jacoby, G.C., Peteet, D.M., Griffin, K.L., 2004. The influence of winter temperatures on the annual radial growth of six northern range margin tree species. Dendrochronologia 22, 7–29.

Pederson, Neil, Tackett, K., McEwan, R.W., Clark, S., Cooper, A., Brosi, G., Eaton, R., Stockwell, R.D., 2012. Long-term drought sensitivity of trees in second-growth forests in a humid

region. Canadian Journal of Forest Research. 42:1837–1850.
Penskar, M.R., Derosier, A.L. 2012. Assisting the Michigan wildlife action plan: Tools and information for incorporating plants. Final report to NatureServe. Michigan Natural Features Inventory Report No. 2012-, Lansing, Michigan, USA.

Peterson, D.W., Peterson, D.L., 1994. Effects of climate on radial growth of subalpine conifers in the North Cascade Mountains. Canadian Journal Forest Research 24, 1921–1932.

Phipps, R.L., 1982. Comments on Interpretation on Climatic Information from Tree Rings, Eastern North America. Tree-Ring Bulletin 42, 11–22.

Pompa-García, M., Sanchez-Salguero, R., Camarero, J., 2017. Observed and projected impacts of climate on radial growth of three endangered conifers in northern Mexico indicate high vulnerability of drought-sensitive species from mesic habitats. Dendrochronologia 45, 145–155.

Ponocná, T., Spyt, B., Kaczka, R., Büntgen, U., Treml, V., 2016. Growth trends and climate responses of Norway spruce along elevational gradients in East-Central Europe. Trees 30, 1633–1646.

Prasad, A., Pedlar, J., Peters, M., McKenney, D., Iverson, L., Matthews, S., Adams, B., 2020. Combining US and Canadian forest inventories to assess habitat suitability and migration potential of 25 tree species under climate change. Diversity and Distributions 26, 1142–1159.

Pretzsch, H., Biber, P., Schütze, G., Uhl, E., Rötzer, T., 2014. Forest stand growth dynamics in Central Europe have accelerated since 1870. Nature Communications 5, 4967.

Pyke, G.H., Thomson, J.D., Inouye, D.W., Miller, T.J., 2016. Effects of climate change on phenologies and distributions of bumble bees and the plants they visit. Ecosphere 7, e01267.

Quiring, S.M., 2004. Growing-season moisture variability in the eastern USA during the last 800 years. Climate Research 27, 9–17.

R Core Team, R.C., 2017. R: a language and environment for statistical computing. Vienna, Austria: R Foundation for Statistical Computing.

Rahman, M., Islam, M., Bräuning, A., 2018. Tree radial growth is projected to decline in South Asian moist forest trees under climate change. Global and Planetary Change 170, 106–119.

Rasmussen, K.K., 2007. Dendroecological analysis of a rare sub-canopy tree: Effects of climate, latitude, habitat conditions and forest history. Dendrochronologia 25, 3–17.

Rimkus, E., Edvardsson, J., Kazys, J., Pukiene, R., Lukošiūnaitė, S., Linkevičienė, R., Corona, C., 2019. Scots pine radial growth response to climate and future projections at peat and mineral soils in the boreo-nemoral zone. Theoretical and Applied Climatology 136, 639–650.

Robakowski, P., Li, Y., Reich, P.B., 2012. Local ecotypic and species range-related adaptation influence photosynthetic temperature optima in deciduous broadleaved trees. Plant Ecology 213, 113–125.

Rocky Mountain Tree-Ring Research, Inc. & the Tree Ring Laboratory of Lamont-Doherty Earth Observatory and Columbia University, 2013. Eastern OLDLIST: A database of maximum tree ages for Eastern North America. https://www.ldeo.columbia.edu/~adk/oldlisteast/.

Rodriguez-Cabal, M.A., Barrios-Garcia, M.N., Amico, G.C., Aizen, M.A., Sanders, N.J., 2013. Node-by-node disassembly of a mutualistic interaction web driven by species introductions. Proceedings of the National Academy of Sciences 110, 16503–16507.

Saladyga, T., Maxwell, R.S., 2015. Temporal variability in climate response of eastern hemlock in the Central Appalachian Region. Southeastern Geographer 55, 143–163.

Salzer, M.W., Hughes, M.K., Bunn, A.G., Kipfmueller, K.F., 2009. Recent unprecedented tree-ring growth in bristlecone pine at the highest elevations and possible causes. Proceedings of the National Academy of Sciences 106, 20348–20353.

Sánchez-Salguero, R., Camarero, J.J., Gutiérrez, E., Rouco, F.G., Gazol, A., Sangüesa-Barreda, G., Andreu-Hayles, L., Linares, J.C., Seftigen, K., 2017. Assessing forest vulnerability to climate warming using a process-based model of tree growth: bad prospects for rear-edges. Global Change Biology 23, 2705–2719.

Schaberg, P.G., Shane, J.B., Cali, P.F., Donnelly, J.R., Strimbeck, G.R., 1998. Photosynthetic capacity of red spruce during winter. Tree Physiology 18, 271–276.

Schneider, L., Esper, J., Timonen, M., Büntgen, U., 2014. Detection and evaluation of an early divergence problem in northern Fennoscandian tree-ring data. Oikos 123, 559–566.

Schroeder, A.H., 1968. Shifting for survival in the Spanish Southwest. New Mexico Historical Review 43, 291–310.

Scott, R.W., Huff, F.A., 1996. Impacts of the Great Lakes on regional climate conditions. Journal of Great Lakes Research 22, 845–863.

Siefert, A., Lesser, M.R., Fridley, J.D., 2015. How do climate and dispersal traits limit ranges of tree species along latitudinal and elevational gradients? Global Ecology and

Biogeography 24, 581–593.
Silva, L.C.R., Sun, G., Zhu-Barker, X., Liang, Q., Wu, N., Horwath, W.R., 2016. Tree growth acceleration and expansion of alpine forests: The synergistic effect of atmospheric and edaphic change. Science Advances 2, e1501302.

Speer, J.H., 2010. Fundamentals of Tree-ring Research. University of Arizona Press, Tucson, Arizona, USA.
Stahle, D.W., Cleaveland, M.K., Blanton, D.B., Therrell, M.D., Gay, D.A., 1998. The lost colony and Jamestown droughts. Science 280, 564–567.

Stahle, D.W., Cook, E.R., Cleaveland, M.K., Therrell, M.D., Meko, D.M., Grissino-Mayer, H.D., Watson, E., Luckman, B.H., 2000. Tree-ring data document 16th century megadrought over North America. Eos, Transactions American Geophysical Union 81, 121–125.

Stine, A.R., Huybers, P., 2014. Arctic tree rings as recorders of variations in light availability. Nature Communications 5, 3836.

Stokes, M.A., 1996. An Introduction to Tree-ring Dating. University of Arizona Press, Tucson, Arizona, USA.

Sturm, M., Racine, C., Tape, K., 2001. Increasing shrub abundance in the Arctic. Nature 411, 546–547.

Su, H., Axmacher, J.C., Yang, B., Sang, W., 2015. Differential radial growth response of three coexisting dominant tree species to local and large-scale climate variability in a subtropical evergreen broad-leaved forest of China. Ecological Research 30, 745–754.

Suriano, Z.J., Leathers, D.J., 2017. Spatio-temporal variability of Great Lakes basin snow cover ablation events. Hydrological Processes 31, 4229–4237.

Suriano, Z.J., Robinson, D.A., Leathers, D.J., 2019. Changing snow depth in the Great Lakes basin (USA): Implications and trends. Anthropocene 26, 100208.

Tang, Y., Zhong, S., Luo, L., Bian, X., Heilman, W.E., Winkler, J., 2015. The Potential Impact of Regional Climate Change on Fire Weather in the United States. Annals of the Association of American Geographers 105, 1–21.

Taylor, K.E., Stouffer, R.J., Meehl, G.A., 2012. An Overview of CMIP5 and the Experiment Design. Bulletin of the American Meteorological Society 93, 485–498.

Tei, S., Sugimoto, A., Yonenobu, H., Matsuura, Y., Osawa, A., Sato, H., Fujinuma, J., Maximov, T., 2017. Tree-ring analysis and modeling approaches yield contrary response of circumboreal forest productivity to climate change. Global Change Biology 23, 5179–

5188.
Telewski, F.W., Swanson, R.T., Strain, B.R., Burns, J.M., 1999. Wood properties and ring width responses to long-term atmospheric CO2 enrichment in field-grown loblolly pine (*Pinus taeda* L.). Plant, Cell & Environment 22, 213–219.

Tierney, G.L., Fahey, T.J., Groffman, P.M., Hardy, J.P., Fitzhugh, R.D., Driscoll, C.T., 2001. Soil freezing alters fine root dynamics in a northern hardwood forest. Biogeochemistry 56, 175–190.

Vaganov, E.A., Hughes, M.K., Kirdyanov, A.V., Schweingruber, F.H., Silkin, P.P., 1999. Influence of snowfall and melt timing on tree growth in subarctic Eurasia. Nature 400, 149–151.

van der Sleen, P., Groenendijk, P., Vlam, M., Anten, N.P.R., Boom, A., Bongers, F., Pons, T.L., Terburg, G., Zuidema, P.A., 2015. No growth stimulation of tropical trees by 150 years of CO 2 fertilization but water-use efficiency increased. Nature Geoscience 8, 24–28.

Venables, W.N., Ripley, B.D., 2013. Modern Applied Statistics with S-PLUS. Springer Science & Business Media.

Walker, A.P., De Kauwe, M.G., Medlyn, B.E., Zaehle, S., Iversen, C.M., Asao, S., Guenet, B., Harper, A., Hickler, T., Hungate, B.A., Jain, A.K., Luo, Y., Lu, X., Lu, M., Luus, K., Megonigal, J.P., Oren, R., Ryan, E., Shu, S., Talhelm, A., Wang, Y.-P., Warren, J.M., Werner, C., Xia, J., Yang, B., Zak, D.R., Norby, R.J., 2019. Decadal biomass increment in early secondary succession woody ecosystems is increased by CO_2 enrichment. Nature Communications 10, 454.

Walker, K.V., Davis, M.B., Sugita, S., 2002. Climate Change and Shifts in Potential Tree Species Range Limits in the Great Lakes Region. Journal of Great Lakes Research 28, 555–567.

Wang, G.G., Chhin, S., Bauerle, W.L. 2006. Effect of natural atmospheric CO_2 fertilization suggested by open-grown white spruce in a dry environment. Global Change Biology 12, 601–610.

Wang, T., Hamann, A., Yanchuk, A., O'Neill, G.A., Aitken, S.N., 2006. Use of response functions in selecting lodgepole pine populations for future climates. Global Change Biology 12, 2404–2416.

Warner, S.M., Jeffries, S.J., Lovis, W.A., Arbogast A.F., Telewski, F.W. 2021. Tree ring-reconstructed late summer moisture conditions, 1546 to present, northern Lake Michigan, USA. Climate Research 83, 43–56.

Whittaker, R.H., Niering, W.A., 1964. Vegetation of the Santa Catalina Mountains, Arizona. I. Ecological Classification and Distribution of Species. Journal of the Arizona Academy of Science 3, 9–34.

Wibbe, M.L., Blanke, M.M., Lenz, F., 1994. Respiration of apple trees between leaf fall and leaf emergence. Environmental and Experimental Botany 34, 25–30.

Wigley, T.M.L., Briffa, K.R., Jones, P.D., 1984. On the Average Value of Correlated Time Series, with Applications in Dendroclimatology and Hydrometeorology. Journal of Applied Meteorology and Climatology 23, 201–213.

Williams, J.W., Jackson, S.T., 2007. Novel climates, no-analog communities, and ecological surprises. Frontiers in Ecology and the Environment 5, 475–482.

Willis, C.G., Ruhfel, B., Primack, R.B., Miller-Rushing, A.J., Davis, C.C., 2008. Phylogenetic patterns of species loss in Thoreau's woods are driven by climate change. Proceedings of the National Academy of Sciences 105, 17029–17033.

Wolter, K., Hoerling, M., Eischeid, J.K., van Oldenborgh, G.J., Quan, X.-W., Walsh, J.E., Chase, T.N., Dole, R.M., 2015. How Unusual was the Cold Winter of 2013/14 in the Upper Midwest? Bulletin of the American Meteorological Society 96, S10–S14.

Woodhouse, C.A., Overpeck, J.T., 1998. 2000 years of drought variability in the central United States. Bulletin of the American Meteorological Society 79, 2693–2714.

Wu, X., Li, X., Liu, H., Ciais, P., Li, Y., Xu, C., Babst, F., Guo, W., Hao, B., Wang, P., Huang, Y., Liu, S., Tian, Y., He, B., Zhang, C., 2019. Uneven winter snow influence on tree growth across temperate China. Global Change Biology 25, 144–154.

Yamaguchi, D.K., 1991. A simple method for cross-dating increment cores from living trees. Canadian Journal of Forest Research 21, 414–416.

Yukimoto, S., Adachi, Y., Hosaka, M., Sakami, T., Yoshimura, H., Hirabara, M., Tanaka, T.Y., Shindo, E., Tsujino, H., Deushi, M., Mizuta, R., Yabu, S., Obata, A., Nakano, H., Koshiro, T., Ose, T., Kitoh, A., 2012. A New Global Climate Model of the Meteorological Research Institute: MRI-CGCM3 —Model Description and Basic Performance—. Journal of the Meteorological Society of Japan. Ser. II 90A, 23–64.

Zhang, T., 2005. Influence of the seasonal snow cover on the ground thermal regime: An overview. Reviews of Geophysics 43, RG4002.